Development of antiviral strategies against positive-sense single stranded RNA viruses

Inaugural Dissertation

for
the doctoral degree of
Dr. rer. nat.

from the Faculty of Biology
University of Duisburg-Essen
Germany

Submitted by

Denisa Bojkova

Born in Bojnice, Slovakia

June 2020

DOI: 10.17185/duepublico/73307
URN: urn:nbn:de:hbz:464-20201203-084939-3

The experiments underlying the present work were conducted at the Institute of Virology at Essen University Hospital and at the Institute of Medical Virology at University Hospital Frankfurt am Main.

1. Examiner: Prof. Dr. Sandra Ciesek

2. Examiner: Prof. Dr. Matthias Gunzer

3. Examiner: Prof. Dr. Manfred Schubert-Zsilavecz

Chair of the Board of Examiners: Prof. Dr. Ulf Dittmer

Date of the oral examination: 02.09.2020

“It takes all the running you can do just to keep in the same place.”

Red Queen

Table of contents

Summary

Infectious diseases caused by viral pathogens remain a major global health threat. Undoubtedly, great progress has been achieved in this regard by the development of highly efficient direct acting antivirals (DAAs). However, there is no clinically approved antiviral treatment for the majority of viral infections. Additionally, the inhibition of viral replication is not always sufficient to prevent a progression of a disease caused by the infection. In the present work we addressed challenges in the development of antiviral therapies against two positive-sense single stranded RNA viruses ((+)ssRNA), hepatitis C virus (HCV) and severe acute respiratory syndrome coronavirus 2 (SARS-CoV-2). While there are currently no antiviral regimens approved for clinical use against SARS-CoV-2, HCV infection can be nowadays efficiently cured by DAA treatment. However, several studies reported an acceleration of recurrent hepatocellular carcinoma in HCV-positive patients who underwent DAA therapy. On that account, we focused our first study on the identification of phenotypic changes driven by direct acting antivirals in hepatoma cells. We demonstrated that the treatment of liver-derived cells with sofosbuvir (SOF), a nucleoside analogue and a backbone of DAA therapy against HCV, activated the EGFR signalling pathway. The serine/threonine kinase profiling revealed several other kinases downstream of EGFR, also activated during SOF treatment. Our findings imply that SOF may have an impact on liver-related pathological processes via the promotion of EGFR signalling and its downstream pathways. Notably, the administration of EGFR inhibitor, erlotinib, during SOF treatment could prevent this effect. In our second study we established a human cell culture model for SARS-CoV-2 infection which allowed us to perform a comprehensive analysis of host translatome and proteome during the infection. We identified several components of translation, splicing and metabolism to be remarkably altered during the course of viral infection. By applying inhibitors we proved that these pathways represent druggable targets for antiviral therapy against SARS-CoV-2. Globally, our work can contribute to efforts to develop highly efficient therapies against two (+)ssRNA viruses which are currently affecting millions of people worldwide. Our findings provide a rationale for the development of a host-targeted therapy in combination with canonical pathogen-directed drugs as antiviral strategy able to clear viruses as well as resolve underlying diseases. Lastly, we rapidly identified novel host targets which may accelerate the drug discovery against the current pandemic.

Zusammenfassung

Virale Infektionserkrankungen stellen eine große globale Gesundheitsgefahr dar und die Entwicklung hochpotenter direkt wirkender antiviraler Substanzen (*direct acting antivirals*, DAA) bedeutet einen großen Fortschritt in deren Bekämpfung. Für die meisten Virusinfektionen ist bislang jedoch keine klinisch zugelassene antivirale Behandlung verfügbar. Darüber hinaus ist die Inhibierung der viralen Replikation oft nicht ausreichend, um das Fortschreiten der Erkrankung zu verhindern. In der vorliegenden Arbeit werden Herausforderungen in der Entwicklung antiviraler Behandlungsmöglichkeiten für zwei positiv strangorientierte einzelsträngige RNA-Viren (*positive-sense single stranded RNA viruses*, (+)ssRNA-Viren), Hepatitis C Virus (HCV) und *severe acute respiratory syndrome coronavirus 2* (SARS-CoV-2), thematisiert. Während es für SARS-CoV-2 aktuell keine klinisch zugelassene antivirale Therapie gibt, kann eine HCV-Infektion heutzutage durch die Behandlung mit DAAs effektiv geheilt werden. Mehrere Studien berichten jedoch von einem Anstieg bei wiederkehrenden hepatozellulären Karzinomen bei HCV-positiven Patienten, die mit DAAs behandelt wurden. Aus diesem Grund haben wir uns in unserer ersten Studie darauf konzentriert, phänotypische Veränderungen, die durch DAAs in Hepatomazellen ausgelöst werden, zu identifizieren. Wir konnten zeigen, dass die Behandlung von aus der Leber stammenden Zellen mit Sofosbuvir (SOF), einem Nukleosidanalogon und Rückgrat der DAA-Behandlung von HCV, den EGFR-Signalweg aktiviert. Die Analyse von Serin/Threonin-Kinasen legte offen, dass einige weitere Kinasen, die EGFR nachgeschaltet sind, ebenfalls während der SOF-Behandlung aktiviert werden. Unsere Ergebnisse lassen vermuten, dass SOF durch die Aktivierung von EGFR und dessen nachgeschalteten Signalwegen einen Einfluss auf pathologische Entwicklungen in der Leber haben könnte. Die Verabreichung des EGFR-Inhibitors Erlotinib während einer SOF-Behandlung könnte diesen Effekt verhindern. In unserer zweiten Studie haben wir ein Zellkulturmodell für SARS-CoV-2 etabliert, welches eine umfassende Analyse von Wirts-Translatom und Proteom während der Infektion von humanen Zielzellen ermöglicht hat. Wir konnten zeigen, dass sich verschiedene Komponenten des Spleißens, der Translation und des Stoffwechsels im Verlauf der Virusinfektion auffallend verändert haben. Durch die Anwendung von Inhibitoren haben wir bewiesen, dass diese Signalwege therapeutische Angriffspunkte für die antivirale Behandlung von SARS-CoV-2 sind. Generell kann unsere Arbeit zu den Bemühungen beitragen, hochwirksame Therapien

gegen zwei (+)ssRNA Viren, die aktuell Millionen Menschen weltweit betreffen, zu entwickeln. Unsere Erkenntnisse bilden eine Grundlage für die Entwicklung einer personalisierten Behandlung in Kombination mit antiviralen Medikamenten, so dass die Therapie sowohl das Virus neutralisiert als auch die zu Grunde liegende Erkrankung heilt. Darüber hinaus ist es uns gelungen, neuartige Angriffspunkte im Wirt zu identifizieren, die die Suche nach einem Medikament gegen die aktuelle Pandemie vorantreiben könnten.

1 Introduction

1.1 Medical importance and strategies in design of antiviral agents

Viral infections account for a considerable amount of human diseases, with substantial costs in mortality, morbidity and economic terms. Over the past decades, the administration of effective vaccines has led to the eradication of the smallpox virus and dramatically decreased the number of infections with polio, measles, mumps and rubella worldwide [1]. Despite the fact that the most effective way to combat viral infections is a vaccine, several viral pathogens have so far proven to be intractable to the vaccine approach. Particularly for viruses causing chronic infections, such as human immunodeficiency virus (HIV) and hepatitis C virus (HCV), an antiviral treatment remains the only option in limiting or resolving the disease manifestation [2,3].

The development of active antiviral agents is of high relevance for emerging viruses. The majority of such viruses normally exists in the animal population, however, in rare cases they are able to cross the species barrier and develop infections in humans. This represents a serious global health threat with epidemic and pandemic potential in immunologically naïve human populations [4]. For vaccine development a genetic and phenotypic characterization of emerging viruses is required which strongly depends on the establishment of a cell culture system for virus replication and production. This lengthy process of generating a vaccine during an epidemic or pandemic of emerging viruses emphasizes the use of antiviral agents for disease control [5,6].

The first step in the designing of antiviral agents is to identify the structure and function of the molecular targets and their function in the virus life cycle that the antiviral drug is supposed to act on. [7,8]. The viral replication cycle can be broken down into a common set of steps as depicted in Fig. 1. In general, the viral life cycle starts with attachment and entry into target cells, which is followed by uncoating of the viral genome allowing for gene expression and genome replication. Then the new viral particles are assembled, maturated and released [9–13]. In principle, each of these stages has been already pursued as target for drug inhibition either at viral or cellular proteins [7].

Targeting viral proteins is a very attractive strategy since the resulting compounds possess high specificity for their viral target and thereby exhibit lower toxicity for the

host [14]. On the other hand, their high selectivity for a specific virus narrows down the possible spectrum of antiviral effects and increases the likelihood of virus drug-resistance development. Since many viruses exploit the same cellular pathways, targeting host proteins offers antiviral compounds with a broader spectrum of antiviral activity with lower chance of resistance development [15]. However, such regimens possess a higher likelihood of toxicity or side effects since they might affect essential pathways in the host cell. Since both approaches for designing antiviral agents have their advantages and drawbacks, both strategies are worth exploring given the enormously diverse nature of viral infections [16].

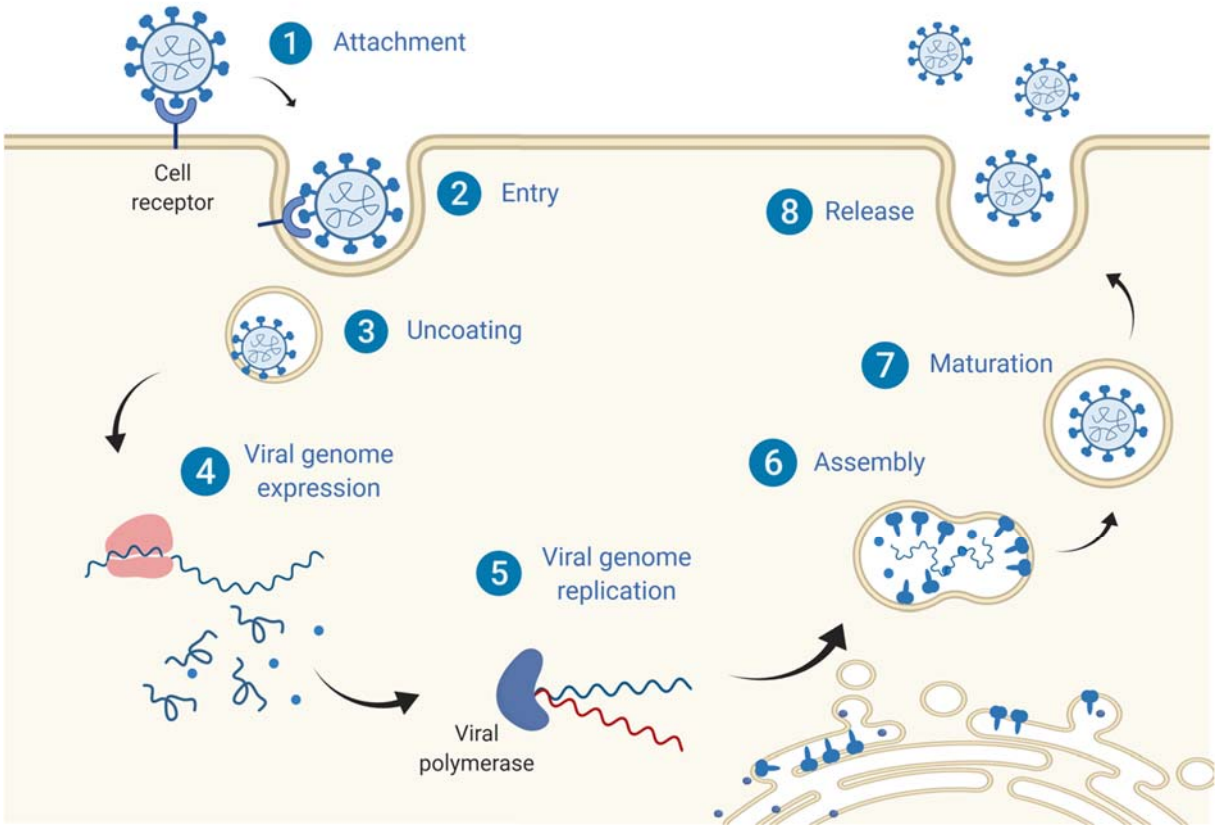

Fig. 1 General scheme of the viral life cycle. (1-2) Virus glycoproteins recognize and bind host receptor resulting in internalization of viral particle into cytoplasm of host cell. (3) Subsequently, viral genome is released by uncoating. (4) Viral proteins, which are essential for virus replication and formation of new viral particles, are expressed by host translation machinery. (5) Simultaneously, viral genome replication takes place. (6-8) Next, new viral particles are assembled and maturated. (8) As a final step viral progeny is released from host cell.

1.1.1 Direct acting antivirals

Most of the antiviral drugs currently approved are designed to target viral proteins. Direct virus-targeting antivirals or direct acting antivirals (DAAs) proved to be very successful in clinical use to resolve viral infections [7,17]. In general, DAAs are considered very safe for clinical use since the majority of the targeted viral proteins have no human homologs [7,18,19]. The major limitation of DAAs is their low genetic barrier to resistance since their mode of action results in selective pressure facilitating mutations, which in consequence make the virus refractory to the treatment [20–22]. The most potent viral protein inhibitors are targeting proteins that facilitate crucial steps of virus replication such as viral glycoproteins, viral proteases, integrases and polymerases. In the next chapters, some of the currently clinically approved DAAs and their targets will be further discussed.

1.1.1.1 Inhibitors of viral glycoproteins

Viral glycoproteins have a definite role in the pathogenesis of viruses. They facilitate the attachment to cell-surface receptors and thereby mediate the entry process [23]. Since the inhibition of viral attachment and entry prevents all subsequent steps in virus infection these stages represent attractive targets for DAAs. Especially in the case of HIV, targeting the entry process is of high interest, since it prevents the integration of the viral genome into the host cell DNA and the establishment of latent viral reservoirs [24]. Currently, one antiviral drug directly interfering with virus glycoproteins has been approved for clinical use. Enfuvirtide is a peptide which binds to gp41 of HIV-1 to block the membrane fusion and entry [25]. Importantly, enfuvirtide is not approved for HIV-2 treatment due to the lack of activity [26].

Other inhibitors, which recognize and bind viral glycoproteins, used in clinical practice are neutralizing antibodies. The advantages of neutralizing antibodies as therapeutics are their highly durable potency combined with negligible toxicity [27]. However, after the establishment of a viral infection they exhibit minimal antiviral effect. Other main drawbacks include the generation of neutralization-resistant virus mutants, the high cost of production and storage [28]. Therefore, there are only a few antibodies approved for clinical use today, such as for example VariZIG for varicella-zoster virus (VZV) and palivizumab for respiratory syncytial virus (RSV) [7,29].

The influenza virus (both A and B) utilizes its viral glycoprotein, neuraminidase, for a unique strategy of releasing newly formed virus particles from the host cells [30]. Therefore, direct inhibitors of neuraminidase, zanamivir and oseltamivir (effective against influenza A and to a much lesser extent against influenza B), prevent influenza infections by disrupting virus release rather than virus entry [31].

1.1.1.2 Inhibitors of viral proteases and integrase

Another group of DAAs targets proteins which help viruses to execute one or several steps of the viral life cycle [13]. These proteins, such as viral proteases and integrases, represent an important target in combating viral infections [7].

Viral proteases of RNA viruses carry out the proteolysis to release the viral proteins from polyprotein precursor [32]. As a result, viral proteins can subsequently function in replication/transcription and maturation of new viral particles [33,34]. Numerous inhibitors of viral proteases that are in clinical use were developed against HCV NS3/4A protease. Boceprevir and telaprevir were the first two approved DAAs for the treatment of HCV that could bind the active site of the protease domain of NS3 [35,36]. However, they were soon withdrawn from the market due to their restricted activity (only genotype 1), low genetic barriers to resistance and severe adverse side effects [37]. Further development resulted in NS3/4A protease inhibitors such as paritaprevir, glecaprevir, grazoprevir and voxilaprevir with improved antiviral potency, which are up to date widely utilized for treating HCV [38]. During HIV-1 infection, viral protease is responsible for the production of all viral enzymes and structural proteins necessary to produce mature, virulent virions [39]. There are numerous protease inhibitors currently approved to treat HIV-1 infections, such as for example darunavir, fosamprenavir, lopinavir and saquinavir. All HIV-1 protease inhibitors share close chemical structures derived from its natural peptide substrate, which results in the cross-resistance of HIV-1 protease. Therefore, they are only applied in combination with other anti-HIV drugs to avoid drug resistance [7,19,40].

Another group of DAAs targets integrase, a protein facilitating a crucial step of HIV-1 infection. HIV-1 integrase is a viral specific enzyme that is responsible for the insertion of viral DNA into the host chromosome [41]. Currently, raltegravir, dolutegravir and bictegravir are recommended as part of antiretroviral therapy due to their lasting viral suppression and excellent tolerability with minimal toxicity [42–44].

1.1.1.3 Inhibitors of viral polymerase

Almost all viruses encode their own polymerases to execute the central step of their life cycle - replication. Thus, targeting polymerases for the development of antivirals has been considered as an attractive possibility to obtain inhibitors against a broad spectrum of viruses. There are two major classes of polymerase inhibitors: (i) nucleoside and nucleotide substrate analogues and (ii) non-nucleoside (allosteric) inhibitors [45].

Nucleoside/nucleotide analogues (NAs) play an essential role in direct acting antivirals targeting viral polymerases. NAs mimic the structure of naturally occurring nucleosides and thereby compete with them to bind to the active site of a polymerase. Due to specific modifications in their structure, their incorporation into viral RNA/DNA leads to a disruption of viral replication [46,47]. Currently, there are over 30 approved NAs that are applied as antiviral agents for therapy of HIV, herpesvirus infections and viral hepatitis [7,48].

Non-nucleoside inhibitors bind to the allosteric site of viral polymerase and thereby prevent a structural shift of the viral polymerase domains. This results in the abolishment of the catalytic activity of polymerase. In comparison to NAs, they do not require metabolic activation [49]. Up to date, there is one approved allosteric inhibitor of NS5B polymerase, dasabuvir, for the treatment of HCV [50]. In the case of HIV-1, allosteric inhibitors are directed against reverse transcriptase. Currently, there are five approved anti-HIV-1 non-nucleoside reverse transcriptase inhibitors (NNRTIs): nevirapine, delavirdine, efavirenz, etravirine and rilpivirine [51].

1.1.2 Host-targeting antivirals

Viruses as obligatory intracellular parasites are unable to complete their replication cycle without the help of the host cell proteins. Therefore, targeting such cellular proteins represents an attractive strategy for antiviral therapies [52]. However, knowledge on cellular proteins and pathways exploited by viruses is still very limited. The identification of novel host factors by employing techniques such as genome scale RNA interference, transcriptional and proteomic profiling, represents a great opportunity to generate broad knowledge on host–virus interactions which should serve as rationale for drug development [53,54]. Host-targeting antivirals (HTA) may display broad antiviral activity and are rarely associated with development of resistance

[15]. Additionally, clearance of viral infections causing chronic diseases or severe acute infections by direct virus-targeting antivirals may not prevent the progression of the underlying disease [55–57]. Therefore, employment of host-target therapy both able to interfere with host cell factors that are necessary for viral replication or persistence and to balance immune response at sites of pathology may represent a preferable strategy.

1.1.2.1 Inhibitors of host factors

HTA can interfere with viral infections by several mechanisms: one common mechanism relies on the inhibition of host factors required for the establishment of productive or persistent viral replication. One of these essential host factors for each virus is a cellular viral entry receptor. To date, only one cellular viral entry receptor inhibitor is approved for clinical use. Maraviroc targets CCR5, the major co-receptor required for HIV-1/2 infection of CD4-positive cells [58]. It is worth mentioning that during early infection, HIV-1/2 predominately uses CCR5 for virus entry, whereas CXCR4 is exploited at late stages of disease [59]. Therefore, the use of maraviroc requires the phenotypic identification of CCR5/CXCR4-dependent viruses [60]. Recently, another promising entry inhibitor underwent the second phase of clinical trials [61]: Bulevertide is a peptide binding to the cell surface molecule sodium taurocholate co-transporting polypeptide (NTCP), entry factor for hepatitis B (HBV) as well as hepatitis D virus (HDV) [62]. Importantly, the treatment was associated with improvement of liver stiffness [61].

1.1.2.2 Enhancers of immune response

Interferons (IFNs) are crucial part of the innate immune response to viral infections [63]. In response to the presence of virus in a host cell, IFNs induce the expression of numerous IFN-stimulated genes (ISGs), whose protein products inhibit different steps of virus life cycle [64]. Several recombinant IFNs-alpha (IFNs-α) have been licensed for the treatment of viral infections [7]. Due to the ability of IFN-α to restrict viral infections it is used in certain instances as a primary antiviral therapy, particularly in the absence of an effective antiviral drug or vaccination [65]. Currently, IFN-α based regimens are used for therapy of HBV and HDV infection [66]. The administration of IFN-α for HCV infections has been minimized, since new effective DAAs have entered

the market [50]. A major limitation of IFN-α -based therapies is the high frequency of side effects such as influenza-like symptoms with fever and fatigue, depression, bone marrow suppression and exacerbated autoimmunity [67].

Another group of enhancers of immune response are toll-like-receptor (TLR) agonists [68]. TLR play an important role in the recognition of viral pathogen and the activation of signalling cascade resulting in cytokines production [69]. Imiquimod is a TLR7 agonist approved for topical treatment of external genital and perianal warts which are frequently caused by human papillomaviruses (HPVs) [70].

1.2 Positive-sense single stranded RNA viruses

Despite the simple common structure consisting of nucleic acid encased in a protein shell, viruses display an impressive diversity of lifestyles accompanied by a profound complexity of functions. The Baltimore classification divides viral families into seven different groups according to their genome (RNA/DNA) and strategy of replication [71]. The viruses possessing single stranded RNA, which functions directly as messenger RNA (mRNA), belong to the group of so-called positive-sense single stranded RNA viruses ((+)ssRNA). Upon infection of the target cell, (+)ssRNA viruses first translate their genomes into single or several polyproteins encoding for a replication complex containing RNA-dependent RNA polymerase (RdRp). Unlike other RNA viruses, (+)ssRNA viruses do not carry their own polymerase in the capsid. Thus, viral RNA replication cannot begin until the genomic RNA is translated to produce polymerase. The replication of the viral genome occurs through negative sense RNA intermediate in cytoplasm. The formation of the new viral particles is located on intracellular membranes in association with membrane rearrangements [72–74]. The group of (+)ssRNA viruses includes families such as *Flaviridae*, *Coronaviridae* and *Picornaviridae* which consist of a great number of human pathogens. Despite their common replication strategy, these families highly differ in their size, cell tropism and pathogenesis [72,75]. In the next chapters, two members of (+)ssRNA viruses, HCV and the newly discovered severe acute respiratory syndrome coronavirus 2 (SARS-CoV-2) will be discussed in the context of therapy development.

1.2.1 Hepatitis C virus (HCV)

HCV is the prototype member of genus *Hepacivirus* in the *Flaviviridae* family of viruses [76]. The HCV genome consists of approximately 9,600 nucleotides and encodes for three structural (core, E1, E2), viroporin (p7) and six non-structural proteins (NS2, NS3, NS4A, NS4B, NS5A and NS5B) [77,78]. The viral particle is formed by a nucleocapsid, comprising the core protein and viral genome and an envelope consisting of two different virus entry glycoproteins E1 and E2. There are seven identified genotypes (1–7) with approximately 30% nucleotide sequence divergence among them. One of the most pronounced features of HCV is its strict cell tropism, meaning, that the productive viral infection exclusively occurs in hepatocytes [2,78,79].

1.2.1.1 Pathogenesis of HCV

HCV is one of the main contributors to chronic liver diseases worldwide with currently 70 million people being infected [80]. After exposure to HCV, the infection progresses first with an acute phase. However, only less than 25% of cases are clinically apparent. Symptoms, if present, manifest 2–26 weeks after HCV exposure, and the acute illness lasts 2–12 weeks. After primary (acute) infection the disease progression can have two possible courses (Fig. 2a). About 15-45% of all cases account for individuals able to spontaneously clear the virus. However, the majority of infected people will develop chronic infection. Around 15–30% of individuals with chronic HCV infection will develop complications, including cirrhosis and hepatocellular carcinoma (HCC), within 20–30 years. Additionally, the disease progression can be further accelerated by factors such as higher age of acquisition, diabetes, high alcohol consumption, HIV/HBV co-infection, and immunosuppression [80–82].

As depicted in Fig. 2b, the development of HCV-induced HCC is a stepwise process. It starts with a primary acute infection which progresses into a chronic disease. During chronic infection, HCV presence triggers increased levels of reactive oxygen species (ROS) and persistent inflammation [83,84]. This results in prolonged liver damage at metabolic and genetic levels leading to cell death. Consequently, inflammation-mediated liver damage prompts repeated hepatocellular regeneration favouring chromosomal instability and irreversible genetic and/or epigenetic changes. This ongoing hepatocellular turnover may select for pro-neoplastic clones that eventually progress into the formation of HCC. Additionally, HCV infection activates hepatic stellate cells (HSCs) to produce excess extracellular matrix (ECM) causing fibrosis. Importantly, an increasing risk of HCC development in HCV-infected patients is tightly correlated with the severity of liver fibrosis [85–87].

Besides the indirect effect of HCV infection on the development of a pro-oncogenic environment, numerous studies suggest that HCV proteins trigger proliferative signalling. Overexpression of HCV proteins in cell culture showed that at least four HCV proteins (core, NS3, NS5A, and NS5B) seem to deregulate potentially oncogenic signalling pathways [88–91]. Additionally, HCV core, NS3 and NS5B seem to impair the function of tumour suppressor retinoblastoma protein (pRb) [92–94]. In an HCV core-transgenic mouse model, the presence of HCV core protein activated transforming growth factor beta (TGF-β), which has been shown to promote cell invasion and metastasis as well as stimulation of fibrogenesis [95]

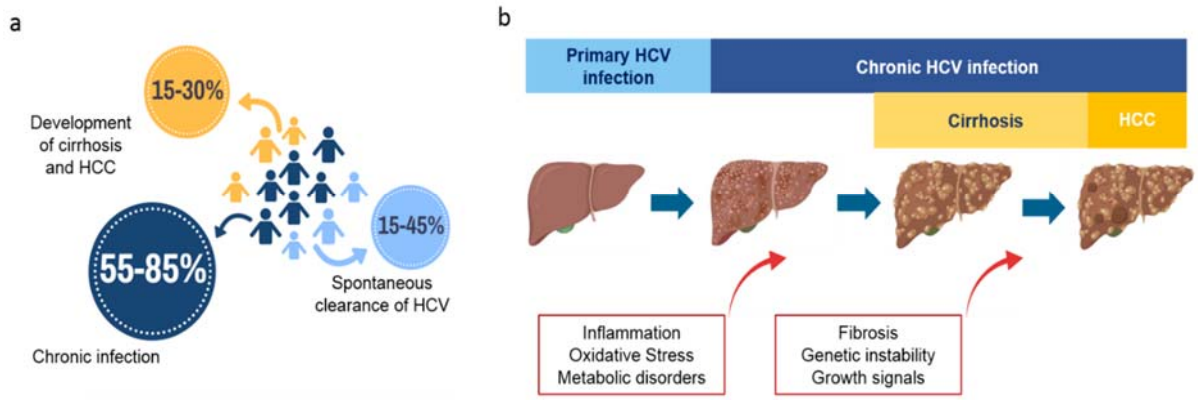

Fig. 2 Course of disease in individuals infected with HCV. (a) Distribution of disease outcome among infected individuals according to World Health Organization (WHO). (b) Progression and development of cirrhosis and HCC in chronically HCV infected patients.

1.2.1.2 Advances in HCV therapy and remaining challenges

HCV was identified in 1989 by Houghton and colleagues in serum from a patient with post-transfusion non-A, non-B hepatitis [76]. As shown in the timeline of major advances in HCV research and therapy (Fig. 3), the first therapy approved for clinical use was IFN-α2 monotherapy. However, this therapy yielded sustained virological response (SVR) only in about 8% of patients [96]. This was later improved by conjugation of IFN-α to polyethylene glycol (pegIFN-α2), which prolonged its half-life from about 2.3 h to almost 50 h, and by its co-administration together with ribavirin [97]. This combination achieved SVR in approximately 80% of patients infected with HCV genotypes 2 and 3, but only 40–50% of patients infected with HCV genotype 1 [98]. Besides a significant remaining number of patients not responding to this treatment, the combination of pegIFN-α2 and the nucleoside analogue ribavirin also exhibited pronounced side-effects [99].

One major obstacle in the development of a novel antiviral therapy was the inability of patient virus isolates to replicate in cell culture models [100]. This has changed after the introduction of the first self-replicating construct consisting of NS3-NS5B viral sequence from strain Con1 (genotype 1b) functioning as replicon system in Huh-7 hepatoma cell line [101]. This achievement has allowed to characterize the HCV replication complex and provide an experimental system for biochemical and structural research. The next major milestone in HCV research was the introduction of a cell

culture system able to produce infectious virus particles. This has facilitated the studying of the complete lifecycle of HCV in hepatoma cell lines [102]. These and many other breakthroughs contributed to the development of DAAs which have been designated to completely change the landscape of HCV therapy [50,103]. Nowadays, a combination of different classes of DAAs is the gold standard for the treatment of HCV, achieving over 90% rates of SVR for most viral genotypes, with shorter treatment durations and fewer side effects [104,105].

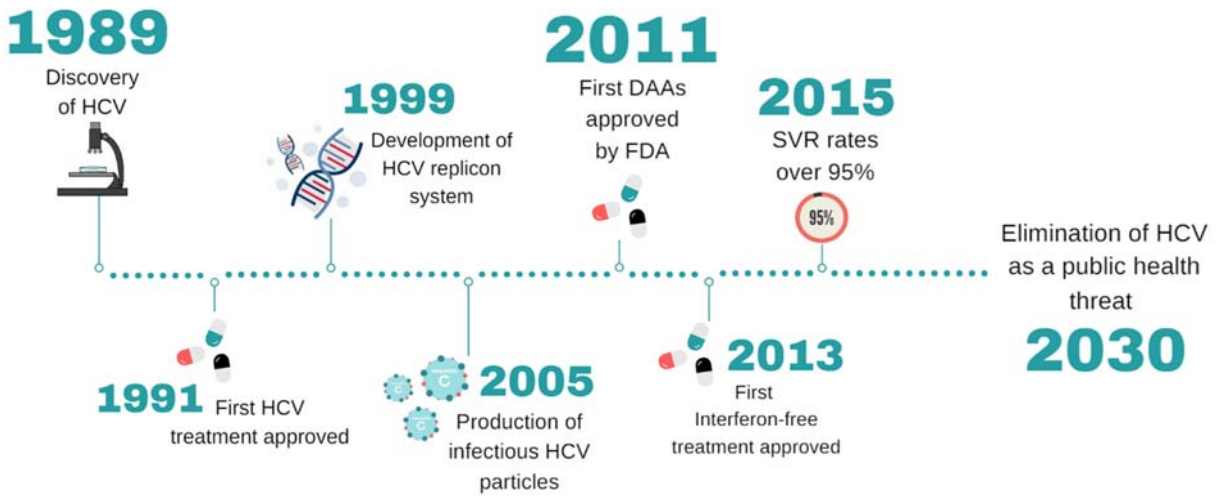

Fig. 3 Timeline of main advances in HCV research and therapy. From the discovery of HCV (1989), it took two decades of enormous effort in basic and translational research (1999, 2005, 2011 and 2013) to develop and introduce an antiviral therapy allowing to cure HCV infection in over 95% of patients (2015). In 2017, the WHO established the target to eliminate chronic HCV infection by the year 2030.

As shown in Fig. 4, there are three main classes of DAAs based on their target protein. The first group of DAAs targets protease activity of NS3 in complex with NS4A which plays a central role in the processing of viral polyprotein. Currently, a second generation of protease inhibitors is already available, with improved efficacy and higher barrier to resistance [106]. The second group inhibits multifunctional protein NS5A, which is essential for viral RNA replication as well as for viral assembly [107,108]. The third group targeting NS5B RNA polymerase consists of two inhibitors with distinct mode of action. The first is SOF, a nucleoside analogue, which is a backbone in the majority of currently applied HCV treatment combinations. This is based on its activity against most genotypes, high genetic barrier to resistance and safety profile [109]. The second class represents non-nucleoside inhibitor, Dasabuvir, which blocks conformational changes required for polymerase activity. However, compared to Sofosbuvir, Dasabuvir targets poorly conserved sequence thereby having a lower barrier to resistance as well as poor pan-genotypic activity [110].

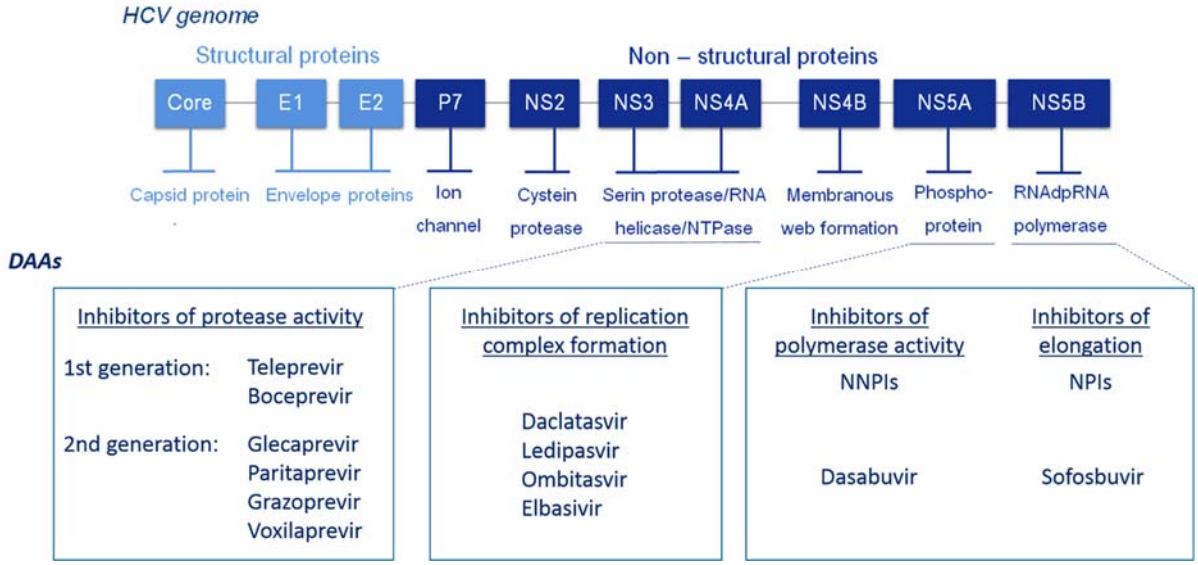

Fig. 4 Overview of direct acting antivirals and their targets. All available DAAs are active against HCV non-structural proteins, whose functions are crucial for HCV gene expression (NS3/NS4A), replication (NS5A and NS5A) and assembly of viral particles (NS5A).

Even though HCV has become a curable disease, several challenges remain. One issue are the costs for DAA therapies, which are still too high in low income countries with significantly high prevalence of HCV-positive patients. Fortunately, this is slowly changing by increasing availability of low-cost generic DAAs in those countries [111]. The most urgent challenge is the high number of HCV-infected people unaware of their infection. In fact, the rate of diagnosed HCV-positive patients is estimated to be below 50% in selected countries [112]. National screening guidelines are needed to overcome this issue. Another important challenge represents optimizing DAA regimens to limit resistance development. The selection of multi-resistant strains is expected and can possibly lead to a number of patients without treatment options in the future [110]. Since chronic HCV infection is one of the leading causes for liver cancer and exhibits a high prevalence, it is expected that the number of patients developing HCC will remain high [113,114]. Furthermore, DAA-based HCV clearance does not completely eliminate the risk of liver cancer in patients with HCC history [115]. The last important step towards the eradication of HCV as health burden remains the development of an effective vaccine.

1.2.2 Severe acute respiratory syndrome coronavirus 2 (SARS-CoV-2)

In December 2019, a previously unknown coronavirus was isolated from bronchoalveolar-lavage fluid of a patient with severe pneumonia in Wuhan, China [116]. The novel virus, initially named 2019-nCoV and currently called severe acute respiratory syndrome coronavirus-2 (SARS-CoV-2), was designated as causative agent of Coronavirus Disease 2019 (COVID-19) [117]. Despite the effort to prevent the transmission of SARS-CoV-2, the virus has spread throughout mainland China to 188 countries and was declared a pandemic by WHO in March 2020 [118]. As of 25th of May 2020, the viral infection has resulted in 5,428,605 confirmed cases and 345,375 deaths worldwide [118].

1.2.2.1 Molecular virology of SARS-CoV-2

SARS-CoV-2 belongs to the genus betacoronavirus in the family *Coronaviridae*, together with SARS-CoV and Middle East respiratory syndrome coronavirus (MERS-CoV) with 80% and 50% homology, respectively, [116,119] and it is closely related to bat-origin SARS-like coronavirus (bat-SL-CoV-ZC45) and pangolin coronavirus (Pangolin-CoV) with around 90% identity [120,121]. Therefore, bats and pangolins are very likely to be natural reservoirs of SARS-CoV-2. However, in contrast to SARS-CoV and MERS-CoV the intermediate host is yet to be known [122,123].

All coronaviruses possess large, positive-sense RNA genome of an approx. size of 30 kb. Two-thirds of the viral RNA are translated into two large polyproteins (pp1a, pp1ab) from two open reading frames (ORFs), ORF1a and ORF1b, as depicted in Fig. 5. Both ORFs together encode for 16 non-structural proteins (nsp) [124]. The polyproteins are cleaved into single proteins by two viral proteases, a papain-like protease (PLpro, nsp3) and a main/3C-like protease (3CLpro, nsp5) [124,125]. The RNA replication complex consists of RNA dependent RNA polymerase (RdRp, nsp12) and two co-factors, nsp7 and nsp8 [126]. The amplification of the viral genome occurs through negative-sense RNA intermediates, which serve as the templates for the synthesis of positive-sense genomic RNA and subgenomic RNAs (sgRNAs). sgRNAs encode the four structural proteins - spike (S), envelope (E), membrane (M) and nucleocapsid (N) protein - as well as several accessory proteins. SARS-CoV-2 is known to encode six accessory proteins (3a, 6, 7a, 7b, 8, and 10), each of unknown or poorly understood function [127]. Entry of SARS-CoV-2 is mediated via interaction of the viral spike (S)

protein with the cellular receptor angiotensin converting enzyme 2 (ACE2) [128]. This interaction depends on proteolytic activation of S protein. By now one cellular proteases, transmembrane serine protease 2 (TMPRSS2) was described to mediate this cleavage [129,130].

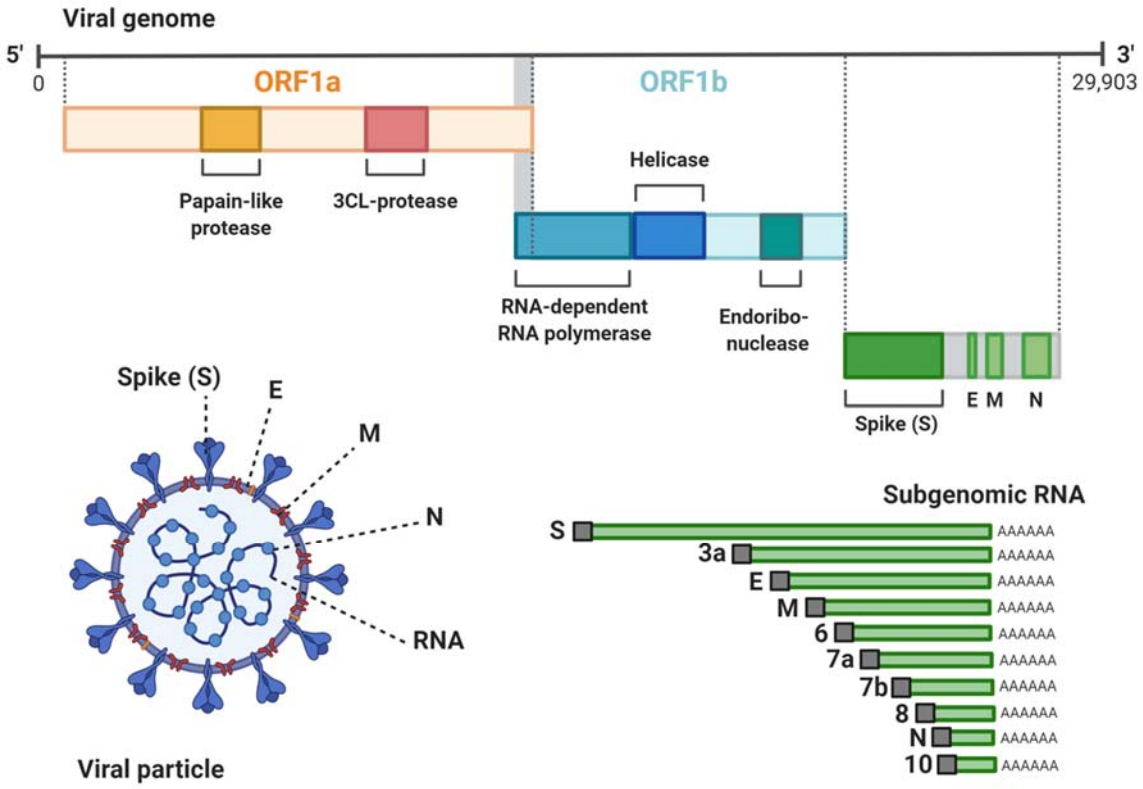

Fig. 5 Organization of SARS-CoV-2 genome and virion structure. The full-length genome contains ORF1a and ORF1b. The unique feature of coronaviruses is the transcription of subgenomic RNAs, which are translated into structural proteins. They then serve to form new viral particles.

1.2.2.2 Clinical and epidemiological features of COVID-19

Although the majority of the earliest cases of COVID-19 were linked to a seafood market in Wuhan assuming zoonotic or environmental exposures, it is now clear that SARS-CoV-2 is transmitted from human to human [131,132]. COVID-19 is

characterized most frequently by a respiratory infection which can progress to pneumonia, severe lung damage and death [116,133–135]. The symptoms of COVID-19 infection appear after an incubation period which varies from 2 to 14 days. The most common symptoms at onset of COVID-19 are fever, cough and fatigue with less frequent symptoms being diarrhoea, nausea and vomiting [136]. The progression of the disease and the development of acute respiratory distress syndrome (ARDS) has been shown to strongly depend on the age and underlying co-morbidities of infected patients [131,134,135]. The clinical features of COVID-19 in risk groups are very similar to SARS and MERS, since all three coronaviruses induce excessive and aberrant non-effective host immune responses associated with severe lung pathology [137–140].

Basic epidemiological characteristics of COVID-19 in comparison to SARS and MERS are depicted in Table 1. Current numbers estimate the case fatality rate (CFR) of COVID-19 to be around 3.4%. This is significantly lower in comparison to infections caused by SARS-CoV and MERS-CoV, 9.6-11% and 34.4% respectively. The differences in the severity of COVID-19, SARS and MERS are further highlighted by the hospitalization rates: 19% of COVID-19 patients versus most cases of SARS and MERS patients [141,142].

Table 1 Epidemiological characteristics of emerging coronaviruses.

The table highlights differences among highly pathogenic coronaviruses. Data was acquired from WHO.

Disease	COVID-19	SARS	MERS
Disease Causing Pathogen	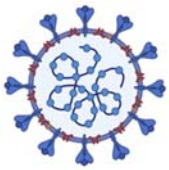 SARS-CoV-2	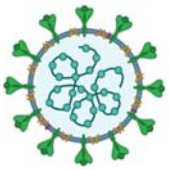 SARS-CoV	 MERS-CoV
R_0 Basic Reproductive Number	2.0 - 2.5	3	0.3 - 0.8
CFR Case Fatality Rate	~3.4%	9.6 - 11%	34.4%
Incubation Time	4 - 14 days	2 - 7 days	6 days
Hospitalization Rate	~19%	Most cases	Most cases
Annual Infected (global)	~ 5 mil (ongoing)	8098 (in 2003)	420

1.2.2.3 COVID-19 and current treatment options

The rapid spread of SARS-CoV-2 has resulted in an urgent need for effective therapeutic strategies. Currently, there are several drugs tested in clinical trials for their efficiency, however, the mainstay of clinical management is largely symptomatic treatment with organ support for seriously ill patients.

To date, many potential substances able to directly or indirectly target the viral life cycle have been suggested by *in silico* predictions or *in vitro* antiviral assays. The most promising candidates, currently under clinical investigation, are summarized in Fig. 6. Nafamostat and camostat are both inhibitors of TMPRSS2, which is required for priming of S protein to allow the binding of virus to its host receptor, ACE2 [130]. Both drugs are approved for treatment of pancreatitis in Japan and therefore can be immediately repurposed for treatment of COVID-19 [143,144].

Chloroquine and hydroxychloroquine are traditionally used as antimalarial drugs. Both drugs are currently investigated for their effects against COVID-19 in clinical trials since they showed promising antiviral effects *in vitro* [145,146]. They appear to block viral entry into cells by inhibiting glycosylation of host receptors, proteolytic processing, and

endosomal acidification [147]. However, their benefit for treatment of COVID-19 remains controversial [148].

Lopinavir and ritonavir were investigated as inhibitors of the main protease, 3CLpro of SARS-CoV and MERS-CoV [149]. Based on the clinical experience with treatment of SARS and MERS, there are several clinical trials applying lopinavir and ritonavir against COVID-19 [150]. However, in a randomized, controlled, open-label trial involving severely ill COVID-19 patients, no benefits of these medicaments were observed [151].

Currently, the most promising antiviral drug applied for COVID-19 therapy is remdesivir. It is a prodrug of an adenosine analogue, whose active form can incorporate into nascent viral RNA causing pre-mature RNA synthesis termination. Remdesivir originally showed antiviral potential against Ebola virus [152]. Its potent activity against SARS-CoV-2 was demonstrated *in vitro* as well as in clinical use [145,153]. At the moment, numerous clinical trials are addressing its benefit for mildly and severely ill COVID-19 patients.

Similarly, favipiravir and ribavirin, two different nucleotide analogues preventing viral RNA replication with broad effect against RNA viruses, are currently applied for treatment of COVID-19 [154]. Favipiravir is a medicament approved for the treatment of the influenza virus in Japan [155]. Antiviral effects of both, favipiravir and ribavirin against SARS-CoV-2 have been shown *in-vitro*, however only in high doses [145].

Nitazoxanide is an anthelminthic agent which has demonstrated antiviral activity against SARS-CoV-2 *in vitro* [145]. In studies with MERS-CoV, its antiviral effect was purposed to be mediated by blocking maturation of the viral nucleocapsid and thereby preventing the production of the infectious viral particles [156]. However, currently ongoing clinical trials have to support evidence on its effectivity in COVID-19 patients.

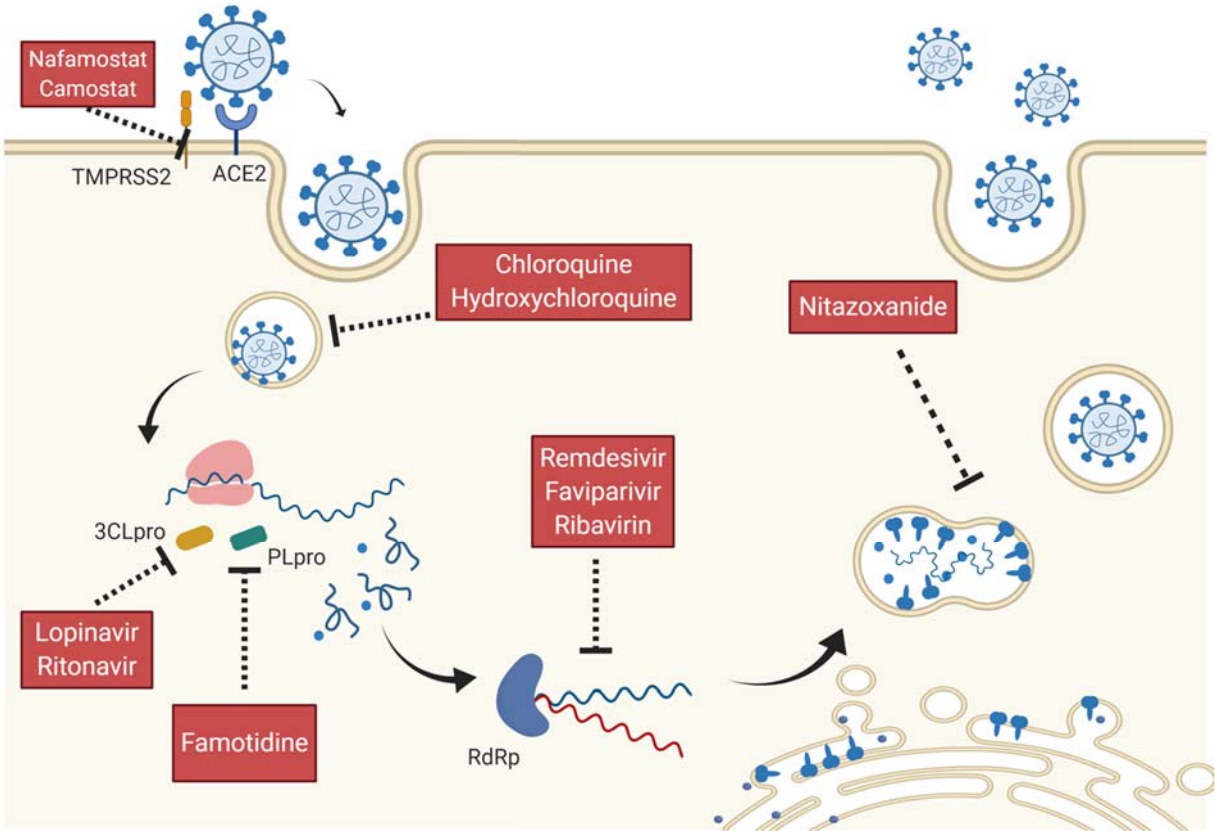

Fig. 6 Potential inhibitors of SARS-CoV-2. Scheme depicts currently clinically tested drugs for treatment of COVID-19 patients and the respective stages of the SARS-CoV-2 life cycle which they supposedly interfere with.

1.3 Aims and scope

The development of DAAs represents an important strategy in clearance of viral infections. Indeed, enormous progress has been made in the past decades to develop and introduce highly specific and efficient DAAs in clinical use, especially for HIV-1 and HCV. However, clinical experience has shown that simple inhibition of viral replication and clearance of viral infection is not always enough to eliminate the risk of disease progression in severely ill patients. This is of particular interest in the context of treatment of chronic HCV infection, where concerns have been raised regarding the impact of DAAs on the development of HCC in chronically HCV-infected patients. On that account, we aimed to identify and characterize phenotypic changes driven by DAAs in liver-derived cells in our first study. Our findings showed drug-induced cellular signalling and processes which could contribute to better understanding the ongoing risk of HCC relapse despite the clearance of viral infection [157].

These findings further highlighted that there is an urgent need for antiviral strategies able to clear viruses as well as resolve underlying diseases. One of these strategies could be the employment of HTAs. The currently emerged SARS-CoV-2 which is able to cause severe pneumonia in infected patients, represents a perfect example where such a strategy could be of high benefit. However, detailed knowledge of virus-host interaction, which is required for such an approach, is still missing. Therefore, the aim of our second study was to establish and characterize a human cell culture model for SARS-CoV-2 infection allowing for the proteomic analysis of cellular infection profile. Additionally, this system was applied for rapid screening of substances able to interfere with identified cellular pathways [158].

2 Results

In the context of this doctoral work, the following manuscripts were published:

2.1 Study 1: Sofosbuvir activates EGFR-dependent pathways in hepatoma cells with implications for liver-related pathological processes

cells

MDPI

Article

Sofosbuvir Activates EGFR-Dependent Pathways in Hepatoma Cells with Implications for Liver-Related Pathological Processes

Denisa Bojkova [1,2], Sandra Westhaus [1,2], Rui Costa [1], Lejla Timmer [1], Nora Funkenberg [1], Marek Korencak [3], Hendrik Streeck [3], Florian Vondran [4,5], Ruth Broering [6], Stefan Heinrichs [7], Karl S Lang [8] and Sandra Ciesek [1,2,5,*]

1 Institute of Virology, University Hospital Essen, University Duisburg-Essen, 45147 Essen, Germany; denisa.bojkova@kgu.de (D.B.); sandra.westhaus@kgu.de (S.W.); rcosta@sund.ku.dk (R.C.); lejla.timmer@uk-essen.de (L.T.); nora.funkenberg@googlemail.com (N.F.)
2 Institute of Medical Virology, University Hospital, Goethe University Frankfurt am Main, 60590 Frankfurt, Germany
3 Institute for HIV research, University Hospital Essen, University Duisburg-Essen, 45147 Essen, Germany; marek.korencak@uk-essen.de (M.K.); hendrik.streeck@uk-essen.de (H.S.)
4 Clinic for General, Abdominal and Transplant Surgery, Hannover Medical School, 30625 Hannover, Germany; vondran.florian@mh-hannover.de
5 German Center for Infection Research (DZIF), 45147 Essen, Germany
6 Department of Gastroenterology and Hepatology, University Hospital Essen, University Duisburg-Essen, 45147 Essen, Germany; ruth.broering@uni-due.de
7 Institute for Transfusion Medicine, University Hospital Essen, University Duisburg-Essen, 45147 Essen, Germany; stefan.heinrichs@uk-essen.de
8 Institute of Immunology, University Hospital Essen, University Duisburg-Essen, 45147 Essen, Germany; KarlSebastian.Lang@uk-essen.de
* Correspondence: sandra.ciesek@kgu.de; Tel.: +49-69-63015219

Received: 9 March 2020; Accepted: 13 April 2020; Published: 17 April 2020

Abstract: Direct acting antivirals (DAAs) revolutionized the therapy of chronic hepatitis C infection. However, unexpected high recurrence rates of hepatocellular carcinoma (HCC) after DAA treatment became an issue in patients with advanced cirrhosis and fibrosis. In this study, we aimed to investigate an impact of DAA treatment on the molecular changes related to HCC development and progression in hepatoma cell lines and primary human hepatocytes. We found that treatment with sofosbuvir (SOF), a backbone of DAA therapy, caused an increase in EGFR expression and phosphorylation. As a result, enhanced translocation of EGFR into the nucleus and transactivation of factors associated with cell cycle progression, B-MYB and Cyclin D1, was detected. Serine/threonine kinase profiling identified additional pathways, especially the MAPK pathway, also activated during SOF treatment. Importantly, the blocking of EGFR kinase activity by erlotinib during SOF treatment prevented all downstream events. Altogether, our findings suggest that SOF may have an impact on pathological processes in the liver via the induction of EGFR signaling. Notably, zidovudine, another nucleoside analogue, exerted a similar cell phenotype, suggesting that the observed effects may be induced by additional members of this drug class.

Keywords: direct-acting antivirals; HCV; HCC recurrence; nucleotide analogue; EGFR pathway

1. Introduction

With approximately 71 million chronically infected patients, hepatitis C virus (HCV) represents one of the leading etiologies for the development of hepatocellular carcinoma (HCC) worldwide [1,2].

Recently introduced direct acting antivirals (DAAs) have dramatically improved the treatment of chronic HCV infection. Nowadays, DAAs allow a sustained virological response to be achieved in more than 95% of patients without major side effects [3–5]. Even though these new drugs represent a huge breakthrough for a majority of chronically HCV-infected patients, the benefit of interferon-(IFN)-free therapies for a subset of patients has recently been questioned by several groups. Two studies showed an increase in the recurrence rates of HCC (27% and 29%) after DAA treatment in patients who had been successfully treated for HCC prior to the start of DAA therapy and were disease free for different periods of time [6,7]. Moreover, the recurrent tumors exhibited signs of microvascular invasion and were characterized by a more aggressive phenotype with faster progression to advanced stages [8]. Further studies have confirmed the increase in the recurrence/occurrence of HCC after DAA treatment, whereas others have refuted these results [9–13].

Despite these contradictory reports, several mechanisms for the high rate of tumor relapses and de novo tumors after DAA therapy have been proposed. A decrease of inflammation signals followed by a reduction of immune surveillance could allow tumor clones to progress without immediate recognition and elimination by the immune system [7]. Indeed, several research groups showed that the clearance of HCV with DAA treatment changed the innate immunity [14–16]. Other studies indicated a potential effect of IFN-free therapy on angiogenesis [17,18]. They observed an increase in the serum concentrations of vascular endothelial growth factor (VEGF) and angiopoietin-2, growth factors responsible for vascular remodeling in tumors, during DAA treatment and this increase correlated with a higher risk of HCC relapse and de novo occurrence [17,18]. All these studies provide a possible rationale for the involvement of DAA treatment in the modification of the local immune status, cytokine signaling network, and pro-angiogenesis molecules. However, the underlying modified cellular pathways have not yet been elucidated.

In light of these results, we aimed to investigate how DAAs modulate relevant molecular pathways and protein expression involved in liver pathological processes in liver-derived cell lines. Our analysis revealed an altered cell phenotype following sofosbuvir treatment, which was characterized by changes in the cell cycle distribution, expression of cell cycle-regulating factors, and proliferation. Further investigation identified the activation of epidermal growth factor receptor (EGFR) signaling by its phosphorylation and translocation into the nucleus as a driver of these alterations.

2. Materials and Methods

2.1. Cell Culture and Compounds

HepG2, HuH-6, Huh-7, and HEK293 cells were maintained in Dulbecco's modified Eagle medium (DMEM, Thermo Fisher Scientific, Schwerte, Germany) containing 10% (*v/v*) fetal bovine serum (Biochrom, Cambridge, UK) and 10,000 U penicillin/streptomycin, 1% (*v/v*) L-glutamine, and 1% (*v/v*) non-essential amino-acids (Thermo Fisher Scientific, Schwerte, Germany). Primary human hepatocytes (PHHs) were isolated as previously described [19,20]. PHHs were maintained in William's Medium E (PAN Biotech, Aidenbach, Germany) containing 10% (*v/v*) fetal bovine serum (Biochrom, Cambridge, UK) and 10,000 U penicillin/streptomycin, 1% (*v/v*) L-glutamine, 1% (*v/v*) non-essential amino-acids, 5mmol/L Hepes (Thermo Fisher Scientific, Schwerte, Germany), 2% (*v/v*) dimethyl sulfoxide (DMSO, Roth, Karlsruhe, Germany), 5 µg/mL insulin, and 0.05 mmol/L hydrocortisone (Sigma Aldrich, Munich, Germany). Sofosbuvir, daclatasvir, simeprevir, erlotinib, doramapimod, zidovudine, and tenofovir (Selleckchem, Munich, Germany) were dissolved in DMSO (Roth, Karlsruhe, Germany) and diluted in DMEM at the final concentration depicted in each figure.

2.2. Cell Cycle Analysis by DNA Staining

Cells were fixed and permeabilized with BD Cytofix/Cytoperm™ (BD Bioscience, San Jose, CA, USA) and stained with CytoPhase™ Violet (BioLegend, London, UK). DNA content was measured by

flow cytometry using BD FACS Canto II (Backman Coulter, Krefeld, Germany). Cell cycle distribution was determined by FCS Express 6 (De Novo Software, Glendale, CA, USA).

2.3. Measurement of Apoptosis, Proliferation, and Cytotoxicity

Apoptosis was detected through double staining of the membrane alteration (phosphatidylserine flip) with Annexin V and live versus dead status of cells with Zombie Violet according to the manufacturer's protocol (BioLegend, London, UK). Flow cytometry using BD FACS Canto II (Backman Coulter, Krefeld, Germany) was applied to define the Annexin V+/Zombie Violet- population as early apoptotic cells and Annexin V+/Zombie Violet+ as late apoptotic cells. Cell proliferation was assayed by trypan blue exclusion of cells counted by phase microscopy. Cytotoxicity of different DAAs was determined using the Rotitest® Vital (Roth, Karlsruhe, Germany) according to the manufacturer's instructions.

2.4. Immunoblot Analysis

Whole cell lysates were prepared with M-PER™ Mammalian Protein Extraction Reagent containing protease and phosphatase inhibition cocktail (Thermo Fisher Scientific, Schwerte, Germany). Nuclear and cytoplasm fractions were obtained with NE-PER™ Nuclear and Cytoplasmic Extraction Reagent (Thermo Fisher Scientific, Schwerte, Germany). Proteins were separated by SDS-PAGE (Bio-Rad, Munich, Germany) and transferred to PVDF membrane. Immunoblot analysis was performed using the following antibodies: Anti-B-MYB, anti-EGFR, anti-pEGFR, anti-CyclinD1, anti-β-tubulin, anti-LaminB1 (Abcam, Cambridge, UK), p38, p-p38 (CST, Frankfurt am Main, Germany), and anti-β-actin (Sigma-Aldrich, Munich, Germany). Proteins were visualized using peroxidase-coupled secondary antibodies anti-rabbit (Sigma-Aldrich, Munich, Germany) or anti-mouse (Dianova, Hamburg, Germany) and an enhanced chemiluminescence system (GE Healthcare, Buckinghamshire, UK). Immunoblots were analyzed by Gel analyzer plugin in ImageJ 1.50i and the values of target proteins were normalized to a housekeeping gene.

2.5. Serine/Threonine Kinase Profiling

Serine/threonine kinase (STK) activity profiles were determined with the serine/threonine PamChip® peptide microarray system (PamGene International B.V., BJ's-Hertogenbosch, Netherlands). Each microarray contains a porous matrix probed with covalently attached 144 STK-specific conserved peptides of phosphomotifs, enabling constant flow-through of the lysates containing activated or inactivated kinases in the presence of ATP, and thus facilitating the phosphorylation of peptides. Subsequently, the phosphorylation is detected using fluorescently labelled antibodies. Preparation of the samples, phosphorylation measurement, and data analysis were performed according to the manufacturer´s protocol (www.pamgene.com). Briefly, cells were lysed with M-PER™ containing protease and phosphatase inhibition cocktail and stored at −80 °C till the measurement. The measurement was performed on a PamStation®12 system utilizing the evolve protocol (1300STKlysv09.PS12Protocol, PamGene). For the detection, 0.5 µg of protein lysate was applied. Quantification of the peptides' phosphorylation was conducted using Bionavigator software (PamGene). Since one peptide can be phosphorylated by several kinases and kinases can usually phosphorylate several peptides, PamGene developed a tool, Upstream kinase analysis, to identify the most likely activated kinases. The Upstream kinase analysis is based on the comparison of phosphorylated peptides on an array with databases of documented interactions, such as HPRD, PhosphoSitePlus as well as the in-silico predictions database PhosphoNET. Based on a specificity and significance score, the analysis classifies kinases according to a median final score (MFS) and median kinase statistics (MKS). The resulting list of kinases is based on the final score [MFS+MKS]. Final scores were clustered using the heatmaps2 function of the gplots package of the R suite. Briefly, distances were calculated using Pearson correlation and cell line clustering was calculated via UPGMA. Scripts are available upon request.

2.6. Statistics

All experiments were performed under similar conditions. The respective number of independent experiments is depicted in each figure legend. Prism 6 software (GraphPad software, San Diego, CA, USA) was used to plot the graphical representation and to perform statistical analysis. Statistical significance was calculated by one-way ANOVA, two-way ANOVA, or an unpaired/paired *t*-test as described in the figure legends (ns—not significant, * $p < 0.05$, ** $p < 0.01$, *** $p < 0.005$).

3. Results

3.1. Cell Cycle Distribution after DAA Treatment in Hepatoma Cell Lines

First, we tested whether therapeutic concentrations of different DAAs [21–23] exhibited cytotoxicity in our hepatoma cell model, HepG2 cells. For that purpose, HepG2 cells were treated for four consecutive days with DAAs from each major drug class: Sofosbuvir (SOF, NS5B polymerase inhibitor), daclatasvir (DCV, NS5A protein inhibitor), and simeprevir (SMV, NS3-4A protease inhibitor). Drug-containing cell culture medium was replaced daily. The investigated drug concentrations, which included the maximum concentrations of each drug detected in patient plasma, did not cause toxic effects in hepatoma cells (Figure 1a).

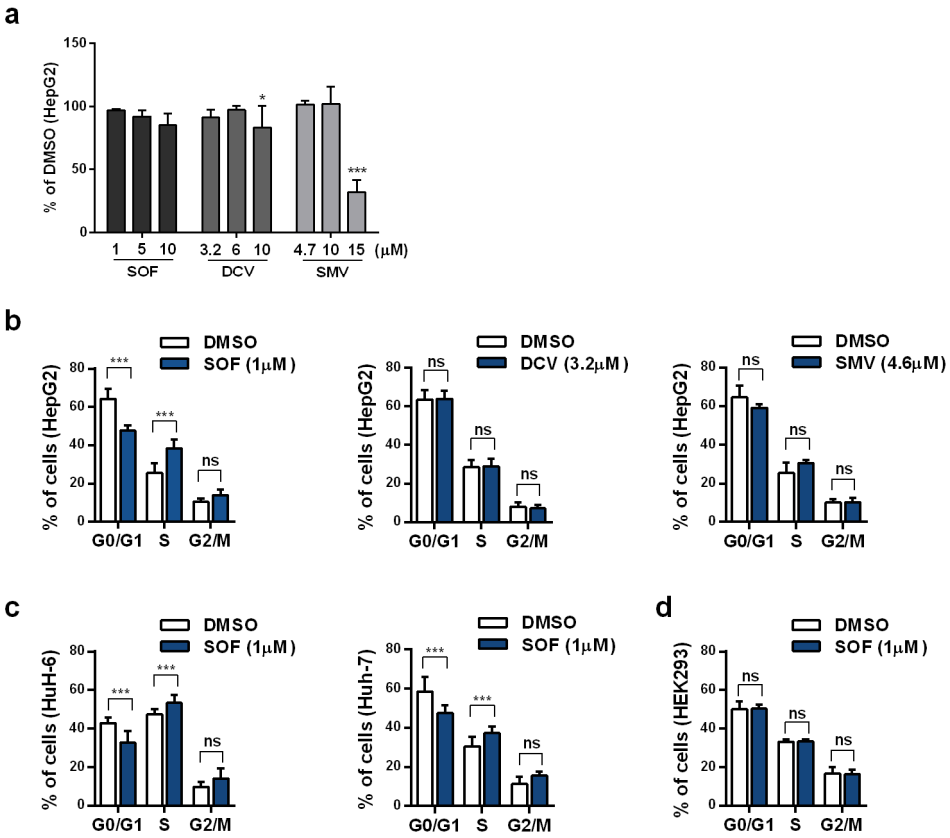

Figure 1. Cell cycle distribution after DAA treatment. (**a**) Cytotoxicity of an increasing concentration of each DAA in HepG2 cells was detected by Rotitest® Vital. Bar graph displays the absorbance as a fold change in relation to DMSO. Cell cycle distribution was evaluated by flow cytometric analysis of DNA content in HepG2 cells treated with SOF, DCV, or SMV (**b**); HuH-6 and Huh-7 cells (**c**); and HEK293 cells (**d**) treated with SOF for four consecutive days. Data are displayed as the percentage of cells in each phase. All shown data represent mean + s.d. from three independent experiments. Statistical significance was determined through two-way ANOVA (**a**–**d**). ns: not significant; * $p \leq 0.05$; *** $p \leq 0.005$.

Next, we tested if different DAAs have any impact on the cell cycle distribution of hepatoma cells. As shown in Figure 1b, SOF treatment led to a significant decrease in the percentage of cells in G0/G1 phase from 64.2% to 47.6% while the percentage of cells in S and G2/M phase increased from 25.5% to 38.4% and from 10.3% to 14.0%, respectively. The same effect of SOF on the cell cycle was confirmed in two additional hepatoma cell lines, HuH-6 and Huh-7 (Figure 1c). No effect on the cell cycle distribution by DCV or SMV was detected. SOF as a prodrug requires metabolic activation to its active triphosphate (TP) form to exhibit its effect [21]. In this context, hepatocytes possess the strongest ability to convert SOF to its active metabolite whereas non-hepatic cells do not support this conversion [24]. Here, we confirmed that in non-hepatic cells, HEK293 (Figure 1d), SOF treatment did not detectably alter the cell cycle distribution.

3.2. Sofosbuvir Induces Pro-Survival Changes in Hepatoma Cells

An increase in the proportion of cells in S phase following SOF treatment could suggest DNA damage with ongoing DNA repair mechanisms. SOF is an uridine nucleotide analogue (NA) able to incorporate into the HCV RNA chain and thereby block viral replication [21]. Interestingly, a number of HCV NAs failed in phase II mainly due to off-target effects impairing mitochondrial protein synthesis [25]. Crucially, our monitoring of mitochondrial respiration during SOF treatment did not reveal any impairment (Figure S1a,c).

As a response to DNA damage, cells are prompted to apoptosis or survival [26]. In order to elucidate the additional molecular events accompanying cell cycle distribution changes caused by SOF, we investigated the induction of apoptosis (Figure 2a) and proliferation rates (Figure 2b). No increase in the proportion of apoptotic cells was detected. Whereas, the proliferation rate after SOF therapy was higher compared to the vehicle control. Together, these data suggest that cells were directed towards survival. Interestingly, the rates of glycolysis and glycolytic capacity (Figure S1b,d) had an upward trend accompanying rising concentrations of SOF, which might be a reaction to an increased demand of metabolites resulting from enhanced proliferation. Additionally, SOF (Figure S2a) had no effect on the proliferation of HEK293 cells, which further points to the active triphosphate form of SOF as the driver of alterations in hepatoma cells. DCV and SMV did not alter the proliferation rates (Figure S2b).

Next, we evaluated the expression of cell cycle-regulating factors, Myb-related protein B (B-MYB) and Cyclin D1, which are responsible for G1/S transition [27,28]. Additionally, B-MYB is also required for the expression of late cell cycle genes [28]. As depicted in Figure 2c, both proteins were increased in SOF-treated cells. In contrast, the B-MYB and Cyclin D1 protein levels did not change after DCV or SMV treatment (Figure 2d). Moreover, SOF had no effect on B-MYB expression in HEK293 cells (Figure S2c).

In summary, SOF, but not DCV or SMV, altered the expression of cell cycle-regulating factors, accompanied by a shift in the cell cycle distribution. Moreover, an observed increase in proliferation and no signs of apoptosis indicate a pro-survival reprogramming of the cells treated with SOF. We also confirmed the obligatory SOF metabolic activation in the induction of cell fate reprogramming given that the non-hepatic cell line HEK293 did not support molecular changes resulting from exposure to SOF.

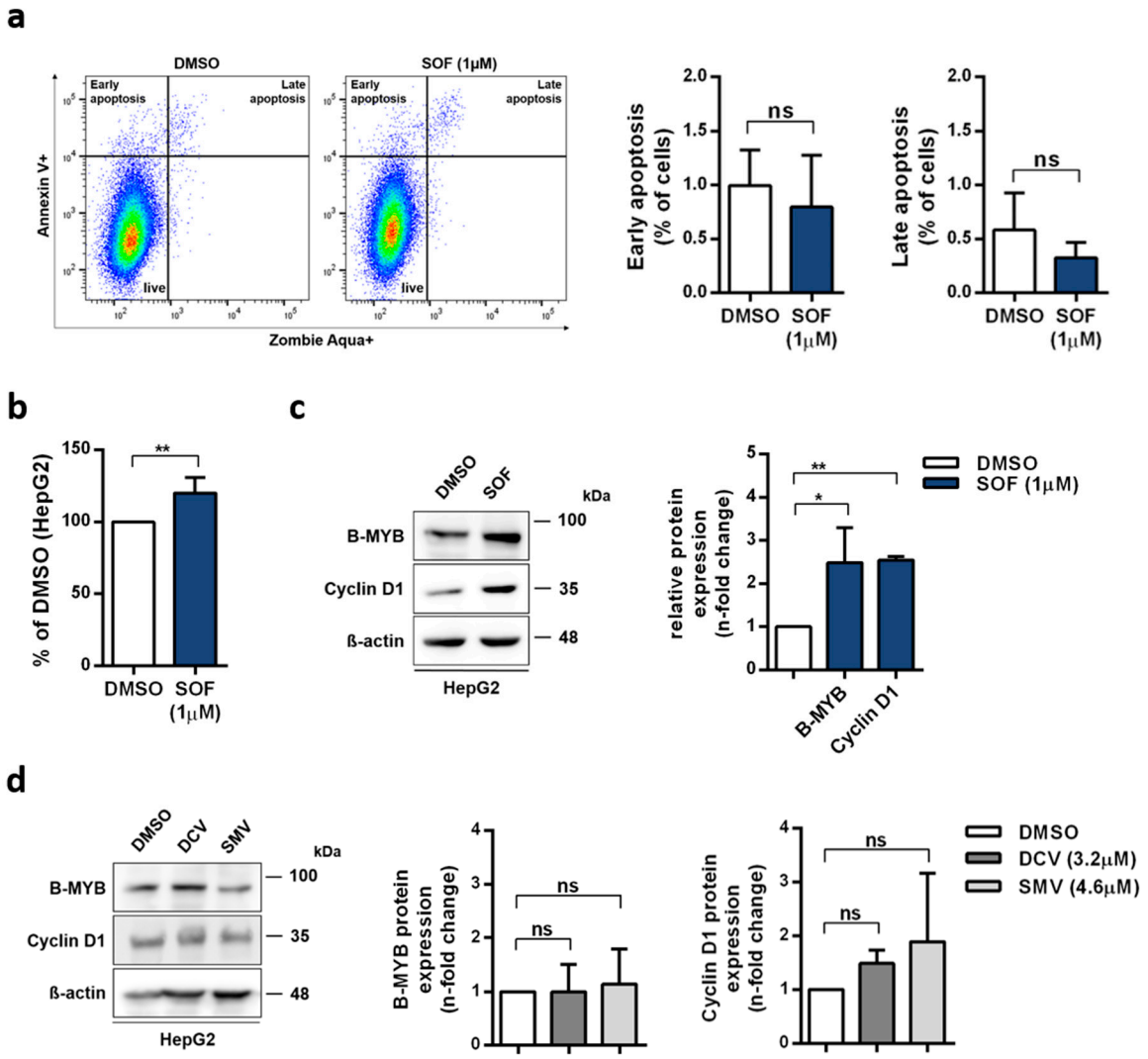

Figure 2. Impact of SOF treatment on cell cycle progression (**a**) Proportion of apoptotic cells was determined with Annexin V and live/dead cells staining in HepG2 cells incubated with SOF at day five. (**b**) Proliferation rates of SOF-treated cells were evaluated by trypan blue exclusion and displayed in relation to the vehicle control DMSO. (**c**,**d**) B-MYB and Cyclin D1 protein expression after SOF (**c**) and DCV or SMV (**d**) treatment were analyzed by immunoblot. One representative immunoblot is shown. Bar graph displays relative protein expression as fold change in relation to DMSO. All shown data represent mean + s.d. from three (a, b, c B-MYB, d) and two (d CyclinD1) independent experiments. Statistical significance was determined through one-way ANOVA (**c**,**d**) and unpaired *t*-test (**a**,**b**). ns: not significant; * $p \leq 0.05$; ** $p \leq 0.01$.

3.3. SOF Induces Activation of EGFR in Hepatoma Cells

The expression of cell cycle-regulating factors like B-MYB and Cyclin D1 is strongly regulated at many different levels. Interestingly, one common upstream regulator of these two proteins is epidermal growth factor receptor (EGFR) [29,30]. On this account, we aimed to examine whether SOF treatment also influences EGFR expression. The SOF-treated HepG2 cells (Figure 3a) displayed an increased expression of the EGFR protein, which, in contrast, was not observed in HEK293 cells (Figure 3b). Additionally, we examined whether the elevated expression of EGFR and its downstream target B-MYB also occurs in primary human hepatocytes (PHHs) after SOF treatment. As demonstrated in Figure 3c, both EGFR and B-MYB protein levels increased in the presence of SOF.

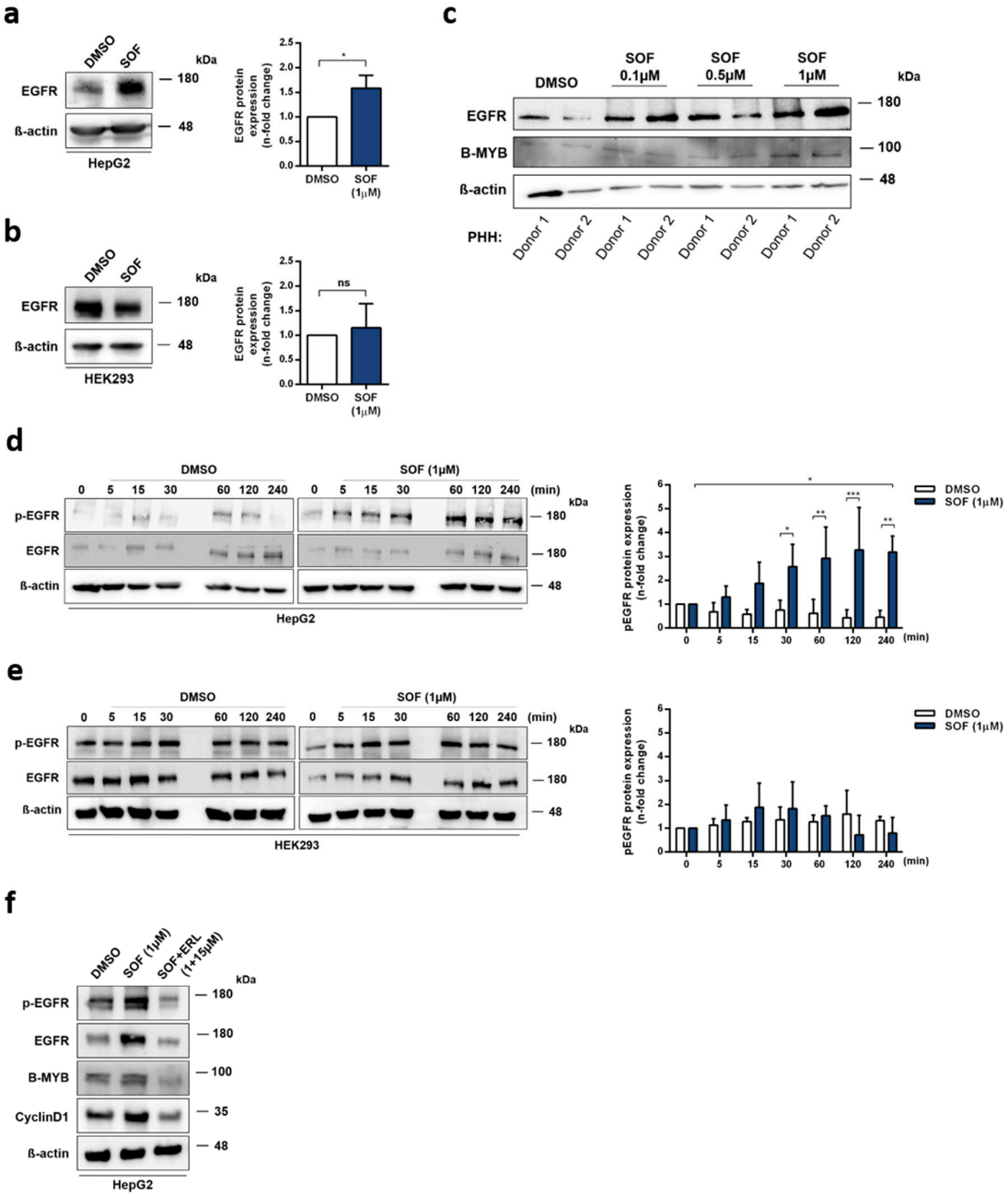

Figure 3. Sofosbuvir increases the expression and activation of EGFR. (**a**,**b**) EGFR protein levels after SOF treatment were identified by immunoblot analysis. One representative immunoblot is displayed. EGFR expression is presented in the bar graphs as a fold change relative to the DMSO control (mean + s.d. from three biological replicates). (**c**) PHHs were incubated with rising concentrations of SOF for four days. EGFR and B-MYB protein levels were evaluated by immunoblot analysis. One representative immunoblot of two independent experiment is displayed. (**d**) HepG2 and (**e**) HEK-293 cells were starved for 24 h prior to SOF treatment. Protein levels of the phosphorylated form of EGFR (pEGFR) were assessed at the depicted time points by immunoblot analysis. One representative immunoblot is presented. pEGFR expression is shown as a fold change in relation to time point 0 (mean + s.d. from three biological replicates). (**f**) EGFR, pEGFR, B-MYB, and Cyclin D1 protein levels after treatment with SOF and SOF in combination with the EGFR inhibitor, erlotinib (ERL), were identified by immunoblot analysis. One representative immunoblot of two independent experiments is shown. Statistical significance was determined through an unpaired *t*-test (**a**,**b**), paired *t*-test (d, time point 0 vs. 240 min), and two-way ANOVA (**d**,**e**). ns: not significant; * $p \leq 0.05$; ** $p \leq 0.01$; *** $p \leq 0.005$.

Transactivation of B-MYB and Cyclin D1 expression driven by EGFR activation requires, as a first step, the phosphorylation of EGFR [29,30]. To verify that EGFR is increasingly phosphorylated in SOF-treated cells, HepG2 and HEK293 cells were starved for 24 h and subsequently treated with SOF or the vehicle control for different periods of time (0–240min). Figure 3d documents a time-dependent increase in the phosphorylation of EGFR after SOF treatment whereas the DMSO control did not exhibit increased phosphorylation. In HEK293 cells (Figure 3e), SOF had no effect on EGFR phosphorylation.

To further study the functional relevance of EGFR activation after SOF treatment, we utilized an EGFR inhibitor, erlotinib (ERL), together with SOF. As shown in Figure 3f, the addition of ERL led to a reduced expression of EGFR, pEGFR, B-MYB, and Cyclin D1. Moreover, we confirmed that the presence of ERL induced apoptosis (Figure S3a) and prevented an SOF-related increase in proliferation (Figure S3b).

In summary, SOF specifically altered the expression and activation of EGFR in liver-derived cells, which in turn led to an increased expression of its downstream targets. These events could be prevented by the employment of an EGFR inhibitor during SOF treatment.

3.4. Activity-Based Kinases Profiling in Hepatoma Cells Reveals Pathways Activated by SOF Treatment

Phosphorylation of EGFR as a receptor tyrosine kinase leads to a downstream signal transduction, resulting in the activation of a wide range of pathways and the expression of a significant number of genes. Since the majority of phosphoproteome results from serine/threonine phosphorylation [31], we aimed to identify serine/threonine kinases (STKs) activated upon SOF treatment. As depicted in Figure 4a, we utilized high-throughput STK PamChip® array based on the measurement of peptide phosphorylation. Figure 4b displays the STK profiles of the most likely activated kinases after SOF treatment versus the control in HepG2, HuH-6, and HEK293 cells. The exact value of the final score for each kinase is depicted in Table S1. We could clearly observe the activation of several STK in the hepatoma cell lines HepG2 and HuH-6, whereas in non-hepatic HEK293 cells, SOF treatment had no impact on STK activation. This further highlights the active form of SOF as being responsible for the phenotype alteration observed in hepatoma cells.

To further reveal the interactions between activated STK in HepG2 cells and analyze their influence on biological processes, the highest ranked kinases (final score >2) were subjected to pathway analysis by GeneGo (Figure 4c) and STRING v11 (Figure 4d). Expectedly, the most enriched pathway regarding biological processes was protein kinase activity. Biological process terms, such as the cellular response to stress, positive regulation of the cell cycle, and negative regulation of apoptosis, were highly enriched with the activated kinase list as input. Additionally, we observed enrichment of pathways, such as the mitogen-activated protein kinase (MAPK) cascade, Akt1 activation, and cAMP response element-binding protein (CREB) phosphorylation, which are downstream in the EGFR signaling network. On this account, we evaluated the expression of the phosphorylated form of Akt, c-Raf, and MEK1/2 (Figure S4). We could show an increase in the phosphorylation of both Akt and MEK1/2 after SOF treatment, which further confirms the activation of EGFR downstream signaling after SOF treatment.

Taken together, high-throughput STK profiling after SOF treatment in different cell lines revealed the activation of several signaling pathways downstream of EGFR and further confirmed the role of the active SOF TP form in the establishment of an altered cell phenotype.

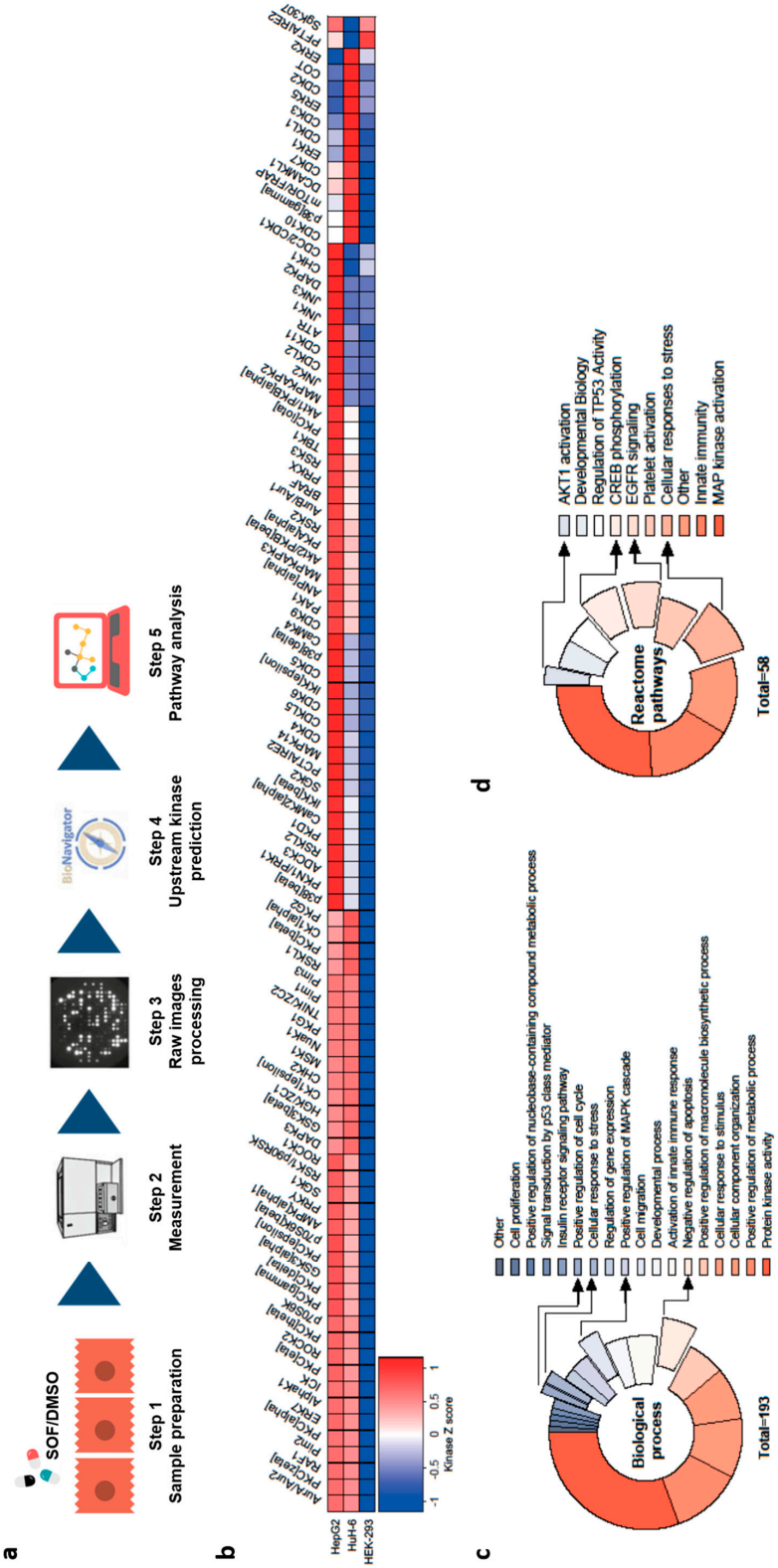

Figure 4. Kinases activation profiling after SOF treatment. (**a**) Representation of STK kinase activation profiling. (**b**) Heatmap of kinases with the highest probability of activation in HepG2, HuH-6, and HEK293 cells after SOF treatment sorted from high (red) to low (blue) kinase Z score. (**c**,**d**) Pathway analysis of top activated kinases in HepG2 cells (final score >2) based on their enrichment in specific biological processes (GeneGo, corrected p value $< 10^{-4}$) (**c**) or reactome pathways (STRING, false discovery rate $< 10^{-4}$) (**d**). Displayed data represent three independent experiments.

3.5. Regulation and Nuclear Translocation of SOF-Activated EGFR

In the context of downstream EGFR signaling, positive regulation of the MAPK cascade appeared to be activated after SOF treatment. Interestingly, one member of this cascade, p38 (MAPK14), is also able to act upstream of EGFR and initiate its phosphorylation and internalization as a response to stress [32]. This can be prevented by utilizing p38 inhibitors [33]. Therefore, we were interested if SOF acts as a stress inducer recognized by p38, which in consequence activates EGFR. On this account, we applied both a p38 inhibitor, doramapimod (DOR), and an EGFR inhibitor, erlotinib (ERL), during SOF treatment and evaluated the activation of both p38 and EGFR (Figure 5a).

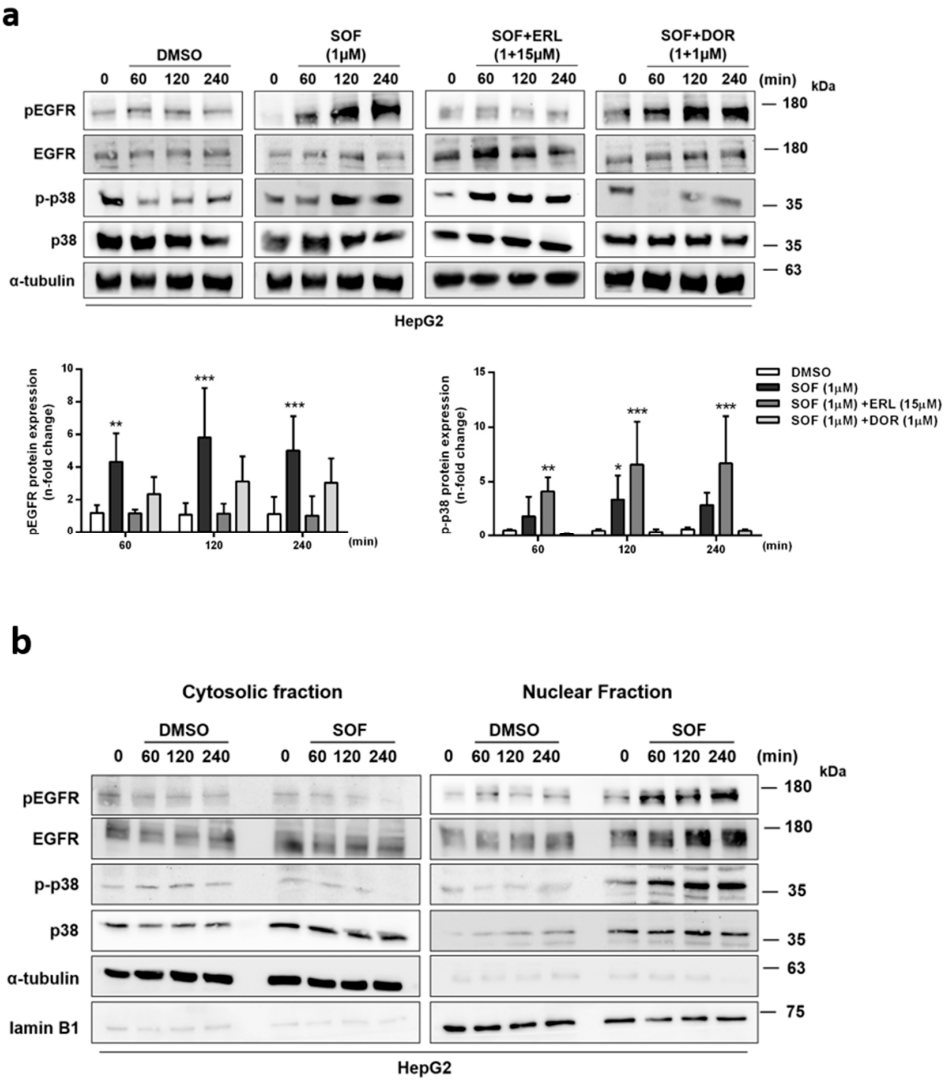

Figure 5. Regulation of EGFR phosphorylation and nuclear translocation during SOF treatment. (**a**) HepG2 cells were starved for 24 h and subsequently treated with SOF alone or in combination with pEGFR inhibitor (ERL) or p-p38 inhibitor (DOR). The protein level of target proteins was assessed at depicted time points by immunoblot analysis. One representative immunoblot is presented. Bar graphs display the relative quantification of pEGFR and p-p38 shown as fold change in relation to time point 0 (mean + s.d. from three independent experiments). Statistical significance was determined through two-way ANOVA (DMSO vs. treatment). * $p \leq 0.05$; ** $p \leq 0.01$; *** $p \leq 0.005$. (**b**) The expression of target proteins in the cytoplasm and nucleus after SOF treatment at different time points was detected by immunoblot an lysis. One representative immunoblot of three (EGFR, pEGFR) and two (p-p38, p38) independent experiments is shown.

We could confirm that p38 is indeed activated during SOF treatment. The addition of ERL to the SOF treatment led to the inhibition of EGFR phosphorylation. However, p38 phosphorylation was still induced, which could be explained by the pro-apoptotic effect of ERL [34]. DOR in combination with SOF effectively blocked p38 phosphorylation. In contrast, no inhibitory effect on EGFR phosphorylation was observed, but the EGFR phosphorylation exhibited rather an increasing tendency over time just as was observed with the SOF treatment only. These results suggest that p38 activation is not crucial for the induction of EGFR phosphorylation observed during SOF treatment.

One interesting feature of EGFR in addition to its traditional well-described signaling pathway is its ability to translocate into the nucleus, where it is responsible for transcriptional regulation of genes involved in cell cycle regulation, proliferation, and DNA repair [35]. Additional kinases, as well as p38, were reported to similarly undergo nuclear translocation [36]. To investigate if EGFR and p38 translocation also occur during SOF treatment, we evaluated the level of both proteins in the cytoplasm and the nucleus. As demonstrated in Figure 5b, the levels of the phosphorylated forms of both proteins were increased in the nuclear fraction after exposure to SOF.

In summary, our data suggest a p38-independent mechanism of EGFR activation during SOF treatment. We also confirmed EGFR nuclear translocation upon SOF treatment. Additionally, the same event was also observed for p38.

3.6. Role of Other Nucleoside Analogues in EGFR Activation

Since SOF belongs to a broad group of nucleotide analogues (NAs), we further investigated if the altered phenotype in hepatoma cells can also be detected with other nucleoside analogues. On this account, we utilized zidovudine (AZT) and tenofovir (TDF), which are both widely used in clinical practice. As shown in Figure 6a, both drugs decreased the cell viability of HepG2 cells even at the lowest concentration. This was also mirrored in the cell cycle distribution (Figure 6b), apoptosis induction (Figure 6c), and proliferation (Figure 6d). Compared to SOF, both AZT and TDF displayed a stronger effect on the cell cycle distribution, with a reduction of cells in G0/G1 phase and an increase in S phase. In case of TDF, an increase in G2/M phase was also observed. Additionally, both AZT and TDF increased the rates of early apoptosis. In the case of TDF, this observation also correlates with reduced proliferation rates. Interestingly, we observed that AZT but not TDF led to an increased expression of EGFR (Figure 6e). As depicted in Figure 6f, this was in line with the high levels of EGFR phosphorylation induced upon AZT treatment.

Altogether, we showed that NAs were able to cause alteration of the cell cycle in hepatoma cells; however, the outcome differed between them. Whereas AZT induced changes comparable to SOF, increased expression, and phosphorylation of EGFR, TDF manifested its effect on cells by an induction of apoptosis and a decrease in cell proliferation without any signs of EGFR activation.

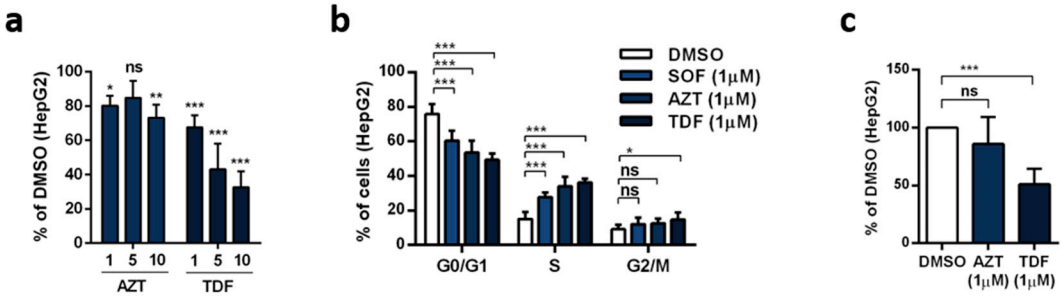

Figure 6. *Cont.*

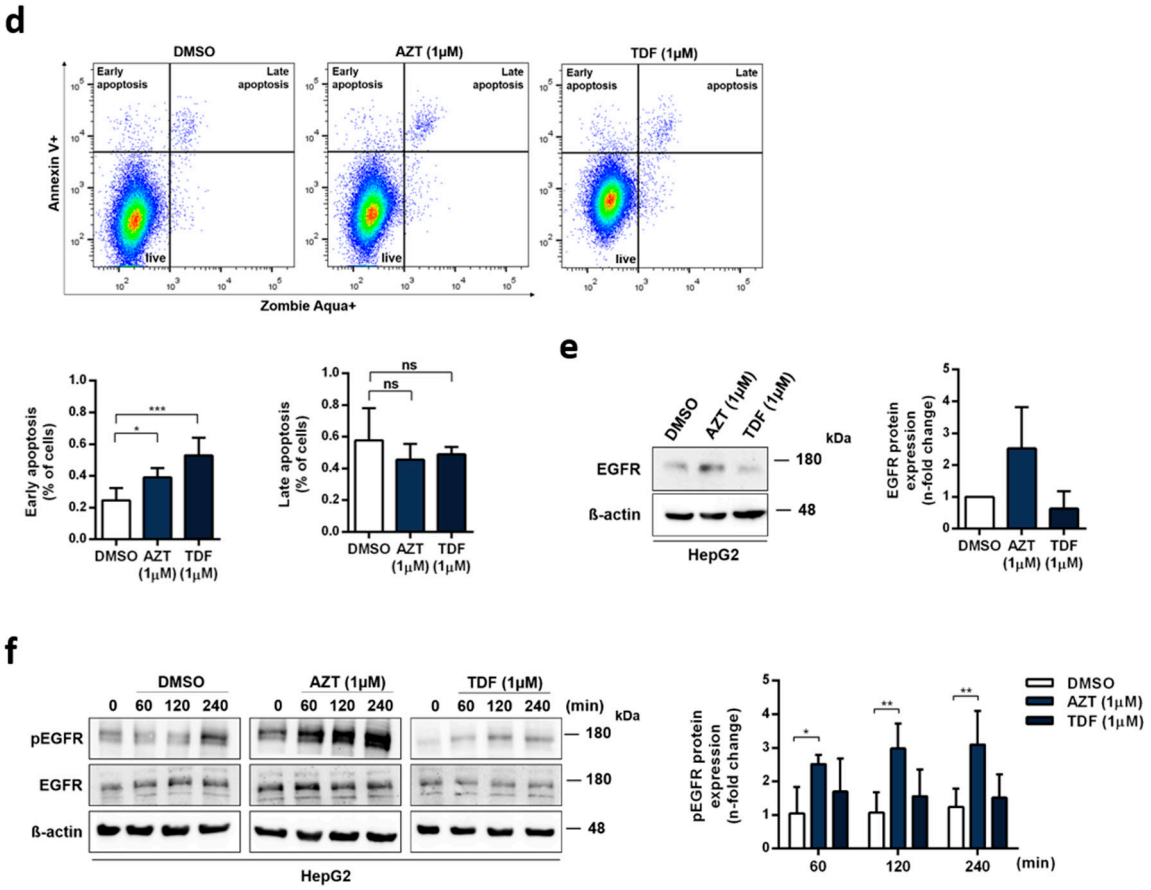

Figure 6. Effect of different nucleotide analogues on alteration in the cell phenotype and activation of EGFR. (**a**) Cytotoxicity of zidovudine (AZT) and tenofovir (TDF) in HepG2 cells was detected by Rotitest® Vital. Bar graph displays absorbance as a fold change in relation to DMSO. (**b**) Cell cycle analysis of HepG2 cells treated with AZT and TDF. (**c**) Apoptosis induction was evaluated with Annexin V and live/dead cell staining by flow cytometry. (**d**) Proliferation rates were determined by trypan blue exclusion and displayed in relation to DMSO. (**e**) EGFR expression after four days of continuous treatment with AZT and TDF. One representative immunoblot is shown. Bar graph presents relative quantification of EGFR as a fold change compared to DMSO. (**f**) Activation of EGFR after AZT and TDF therapy was evaluated by immunoblot analysis at different time points. One representative immunoblot is depicted. pEGFR expression is shown as a fold change in relation to time point 0. All graphs present mean + s.d. from three independent experiments. Statistical significance was determined through one-way ANOVA (**a**,**c**,**d**) and two-way ANOVA (**b**,**f**). ns: not significant; * $p \leq 0.05$; ** $p \leq 0.01$; *** $p \leq 0.005$.

4. Discussion

The introduction of a novel highly effective therapy with DAA able to clear HCV infection in over 95% of patients has raised expectations of reducing liver cancer in chronically HCV-infected patients [3,4]. Despite data supporting an improvement of liver function after DAA therapy [5], several other reports presented findings questioning the impact of IFN-free treatment on the risk of HCC development [6,7]. These studies have reported a higher number of tumor relapses in patients who underwent successful HCC treatment and were disease free before starting DAA therapy than expected [6,7,37]. In our study, we hypothesized that DAA treatment might introduce certain cellular signaling processes facilitating tumor progression in individual patients with pre-existing pro-oncogenic changes in liver tissue. The screening of phenotype changes among different DAA demonstrated an SOF-driven pro-survival alteration, which was not observed with the two other drugs, DCV and SMV.

SOF is a prodrug of an uridine nucleotide analogue with pan-genotypic activity, which is used as a backbone in DAA-based therapies [21]. NAs exert their cytotoxicity mainly by interfering with host DNA replication, resulting in a DNA damage response, which at a molecular level decides the cell fate: Survival or apoptosis. The outcome is based on the imbalance between pro-survival and pro-apoptotic factors [38]. An observed increase in proliferation rates and no induction of apoptosis after SOF treatment indicated that the cells were destined to survive and proliferate rather than initiate apoptosis. Other evidence for a pro-survival reprogramming of the hepatoma cells was the elevated expression of B-MYB and Cyclin D1 after SOF exposure. Both proteins are required for progression through the cell cycle, and their responsibility for the high proliferation capacity of tumor cells in multiple cancers is well documented [39–41]. Together with their pro-survival role during the DNA damage response [40,42], it further suggests an active involvement in cell survival following treatment with SOF.

NAs play an important role in antiviral therapies because of their potency and high barrier to resistance. Interestingly, a number of HCV NAs failed in phase II mainly due to off-target effects impairing mitochondrial protein synthesis [25]. However, mitochondrial respiration did not appear to be impaired by SOF. Based on our results and previous findings, SOF also seems to be a poor substrate for mitochondrial RNA polymerase [43]. Therefore, off-target incorporation of SOF affecting mitochondrial respiration seems unlikely. The question of how/if SOF induces a DNA damage response remains open. Interestingly, increasing SOF concentrations were associated with a non-significant upward trend in glycolysis and glycolytic capacity, which may reflect an increased demand of metabolites in response to enhanced proliferation or positive feedback in nucleotide anabolism, given both glycose-6-phosphate and phosphoenolpyruvate are precursors of nucleotide synthesis.

EGFR is a very well-studied receptor tyrosine kinase, which mediates extremely complex signal transduction [31]. Besides the traditional cytoplasmic pathway leading to the activation of pathways responsible for cell cycle progression, proliferation, and resistance to apoptosis, EGFR possesses the ability to translocate into the nucleus in response to ligand stimulation or stress inducers [29,30,44]. Based on the origin of the stimulation, nuclear EGFR acts as a transcription enhancer of a subset of genes, of which B-MYB and Cyclin D1 exhibited elevated expression after exposure to SOF. On this account, we first confirmed the increase in the phosphorylation of EGFR in response to SOF stimulation, which in turn led to an enhanced expression of EGFR after a four-day exposure to the drug. This is consistent with previous findings showing that prolonged activation of EGFR enhances EGFR transcription through proteins downstream in the EGFR signaling pathway [45,46]. Next, by introducing an EGFR inhibitor during SOF treatment, we reversed the pro-survival outcome mediated by EGFR activation and directed cells towards apoptosis. By detecting an increase of phosphorylated EGFR in the nucleus, we validated our proposed model: As a result of the active TP form of SOF in hepatoma cells, EGFR is activated and translocated into the nucleus, where it enhances the transcription of pro-survival genes.

Phosphorylation of EGFR results in a signal transduction network with diverse outcomes, where none of the signaling pathways act separately but in a highly inter-linked way. Therefore, we assumed that the activation of EGFR during SOF treatment with its subsequent nuclear translocation is not a separate event, but it can involve an entire signaling network. To untangle this network, we utilized global kinase activity profiling. Based on the identified kinome activation, we elucidated the biological processes and reactome pathways activated during SOF exposure. We confirmed the activation of biological processes as positive regulation of the cell cycle, cell proliferation, and negative regulation of apoptosis. In addition, we observed the activation of several pathways located downstream of EGFR signaling, such as AKT1 activation and CREB phosphorylation, whose role in promoting cell survival by directly inactivating components of the cell death machinery was shown previously [41,47,48]. Moreover, both of these pathways are involved in VEGF expression [49,50], the key angiogenic factor, whose elevated expression was previously shown to occur after DAA treatment [16–18]. Therefore, the contribution of SOF treatment to angiogenesis should be closely examined in the future.

The MAPK cascade was another highly enriched pathway. The MAPK cascade can be activated in an EGFR-dependent manner but also independently of EGFR as a response to various stress stimuli. We confirmed that p38, a member of the MAPK cascade, is indeed activated during SOF treatment and translocated into the nucleus. Interestingly, the role of p38 in the regulation of EGFR in response to stress stimuli was shown by several groups [32,33,51]. However, we could demonstrate that the inhibition of p38 had no effect on the increased activation of EGFR observed during the exposure of cells to SOF, which excludes p38 as a driver of EGFR activation in this context.

Lastly, we explored the possibility of other commonly used NAs exhibiting the same effect on hepatoma cells as SOF. Both AZT and TNF showed a strong effect on the cell cycle; however, only AZT treatment led to increased EGFR expression and its activation. This difference could be explained by the much more pronounced cytotoxic effect of TNF in human cancer cells in comparison to AZT [52], which we also observed in hepatoma cells. AZT is a thymidine analogue able to incorporate into the DNA of host cells, causing a DNA damage response [53]. Additionally, S phase arrest with an increase in Cyclin D1 expression in response to AZT was documented [54]. Interestingly, in the vaginal epithelium of mice, long-term treatment with AZT was correlated with elevated proliferation of the vaginal epithelial basal layer accompanied by the expression of pre-neoplastic markers [55]. Based on our results, the activation of EGFR and its downstream signaling pathway after SOF and AZT treatment could represent a novel putative mechanism of NAs' toxicity.

Although the molecular mechanisms of HCV-induced hepatocarcinogenesis have not been fully elucidated, in HCV-infected patients, most occurrences of HCC develop only after the establishment of cirrhosis [56]. Therefore, the progression of cirrhosis represents a major risk for HCC development. Several studies implicated the role of overexpression and activation of EGFR in the progression of cirrhosis [57,58]. In fact, elevated levels of EGFR were reported in 68% of HCC and correlated with poor patient outcome [59]. In the context of HCV infection, EGFR is crucial for HCV entry [60]. Moreover, HCV was shown to activate the EGFR during entry and also specifically through its NS3/4A protease during infection [61,62]. Recent research demonstrated an HCV-induced epigenetic signature, which persists after DAA-mediated eradication of HCV. These epigenetic changes were associated with pathways contributing to HCC development [63,64]. Importantly, one of these studies showed that the inhibition of EGFR kinase activity reverted HCV-induced epigenetic signatures [64]. Therefore, EGFR activation seemed to be an important player in facilitating an HCV-induced tumorigenic environment. On this account, we showed that SOF treatment activates EGFR-dependent signaling pathways and thereby could represent an additional factor contributing to the risk of HCC development.

Based on the restricted availability of liver tissue from cirrhotic HCV-infected patients before, during, and after DAA treatment, our study was performed only in the setting of a cell culture system. The limitations of liver biopsies, such as invasiveness, sampling error, and inter-observer variability, are the main reasons why non-invasive technics are preferable for the monitoring of cirrhosis and fibrosis. In this context, the observed drug-induced alteration in the cell phenotype in vitro might not completely recapitulate the in vivo setting. However, we could show an increase in the expression of EGFR and its downstream target B-MYB in freshly isolated primary human hepatocytes, which more closely resemble liver tissue characteristics.

In conclusion, we could show that SOF treatment leads to an increased EGFR-dependent pathway activation, resulting in cell cycle progression, cell survival, and proliferation. Since ongoing activation of the EGFR signaling pathway and its downstream targets is involved in several liver-related pathologic processes, the impact of SOF on them should be further studied.

Supplementary Materials: The following are available online at http://www.mdpi.com/2073-4409/9/4/1003/s1, Figure S1: Sofosbuvir treatment does not impair mitochondrial respiration, Figure S2: Non-hepatic cells HEK-293 and other DAA do not support SOF-induced phenotype, Figure S3: Application of Erlotinib during SOF treatment induces apoptosis and inhibits proliferation. Figure S4 Activation of EGFR downstream signaling targets after SOF treatment. Tab S1 Predicted activated STK kinases after SOF treatment.

Author Contributions: "Conceptualization, S.C. and D.B.; methodology, D.B. and S.C..; software, D.B. and R.C.; validation, D.B., S.W. and R.C.; formal analysis, D.B and R.C.; investigation, D.B., S.W., R.C., L.T., N.F. and M.K.; resources, H.S., S.H., F.V., R.B., K.S.L. and S.C.; data curation, D.B, S.W., R.C, S.C.; writing—original draft preparation, D.B.; writing—review and editing, D.B., R.C. and S.C.; visualization, D.B. and R.C.; supervision, S.C.; project administration, S.C.; funding acquisition, F.V. and S.C. All authors have read and agreed to the published version of the manuscript."

Funding: This work was funded by the German Center for Infection Research (DZIF) (to F.V. and S.C.).

Acknowledgments: We would like to thank Cinatl and Michealis for the comments on the manuscript.

Conflicts of Interest: The authors do not have any commercial or other association that might pose a conflict of interest.

References

1. World Health Organization. *Global Hepatitis Report 2017*; World Health Organization: Geneva, Switzerland, 2017.
2. Ferenci, P.; Fried, M.; Labrecque, D.; Bruix, J.; Sherman, M.; Omata, M.; Heathcote, J.; Piratsivuth, T.; Kew, M.; Otegbayo, J.A.; et al. Hepatocellular Carcinoma (HCC). *J. Clin. Gastroenterol.* **2010**, *44*, 239–245. [CrossRef] [PubMed]
3. Poordad, F.; Hezode, C.; Trinh, R.; Kowdley, K.V.; Zeuzem, S.; Agarwal, K.; Shiffman, M.L.; Wedemeyer, H.; Berg, T.; Yoshida, E.M.; et al. ABT-450/r–Ombitasvir and Dasabuvir with Ribavirin for Hepatitis C with Cirrhosis. *N. Engl. J. Med.* **2014**, *370*, 1973–1982. [CrossRef]
4. Poordad, F.; Schiff, E.R.; Vierling, J.M.; Landis, C.; Fontana, R.J.; Yang, R.; McPhee, F.; Hughes, E.A.; Noviello, S.; Swenson, E.S. Daclatasvir with sofosbuvir and ribavirin for hepatitis C virus infection with advanced cirrhosis or post-liver transplantation recurrence. *Hepatology* **2016**, *63*, 1493–1505. [CrossRef] [PubMed]
5. Charlton, M.; Everson, G.T.; Flamm, S.L.; Kumar, P.; Landis, C.; Brown, R.S.; Fried, M.W.; Terrault, N.A.; O'Leary, J.G.; Vargas, H.E.; et al. Ledipasvir and Sofosbuvir Plus Ribavirin for Treatment of HCV Infection in Patients With Advanced Liver Disease. *Gastroenterology* **2015**, *149*, 649–659. [CrossRef] [PubMed]
6. Conti, F.; Buonfiglioli, F.; Scuteri, A.; Crespi, C.; Bolondi, L.; Caraceni, P.; Foschi, F.G.; Lenzi, M.; Mazzella, G.; Verucchi, G.; et al. Early occurrence and recurrence of hepatocellular carcinoma in HCV-related cirrhosis treated with direct-acting antivirals. *J. Hepatol.* **2016**, *65*, 727–733. [CrossRef] [PubMed]
7. Reig, M.; Mariño, Z.; Perelló, C.; Iñarrairaegui, M.; Ribeiro, A.; Lens, S.; Díaz, A.; Vilana, R.; Darnell, A.; Varela, M.; et al. Unexpected high rate of early tumor recurrence in patients with HCV-related HCC undergoing interferon-free therapy. *J. Hepatol.* **2016**, *65*, 719–726. [CrossRef]
8. Renzulli, M.; Buonfiglioli, F.; Conti, F.; Brocchi, S.; Serio, I.; Foschi, F.G.; Caraceni, P.; Mazzella, G.; Verucchi, G.; Golfieri, R.; et al. Imaging features of microvascular invasion in hepatocellular carcinoma developed after direct-acting antiviral therapy in HCV-related cirrhosis. *Eur. Radiol.* **2017**, *28*, 506–513. [CrossRef]
9. Calleja-Panero, J.L.; Crespo, J.; Rincon, D.; Ruiz-Antorán, B.; Fernández, I.; Perelló, C.; Gea, F.; Lens, S.; García-Samaniego, J.; Sacristán, B.; et al. Effectiveness, safety and clinical outcomes of direct-acting antiviral therapy in HCV genotype 1 infection: Results from a Spanish real-world cohort. *J. Hepatol.* **2017**, *66*, 1138–1148. [CrossRef]
10. Ikeda, K.; Kawamura, Y.; Kobayashi, M.; Kominami, Y.; Fujiyama, S.; Sezaki, H.; Hosaka, T.; Akuta, N.; Saitoh, S.; Suzuki, F.; et al. Direct-Acting Antivirals Decreased Tumor Recurrence After Initial Treatment of Hepatitis C Virus-Related Hepatocellular Carcinoma. *Dig. Dis. Sci.* **2017**, *62*, 2932–2942. [CrossRef]
11. Yang, J.D.; Aqel, B.A.; Pungpapong, S.; Gores, G.J.; Roberts, L.R.; Leise, M.D. Direct acting antiviral therapy and tumor recurrence after liver transplantation for hepatitis C-associated hepatocellular carcinoma. *J. Hepatol.* **2016**, *65*, 859–860. [CrossRef]
12. Ravi, S.; Axley, P.; Jones, D.; Kodali, S.; Simpson, H.; McGuire, B.M.; Singal, A.K. Unusually High Rates of Hepatocellular Carcinoma After Treatment With Direct-Acting Antiviral Therapy for Hepatitis C Related Cirrhosis. *Gastroenterology* **2017**, *152*, 911–912. [CrossRef]
13. Nahon, P.; Layese, R.; Bourcier, V.; Cagnot, C.; Marcellin, P.; Guyader, D.; Pol, S.; Larrey, D.; De Lédinghen, V.; Ouzan, D.; et al. Incidence of Hepatocellular Carcinoma After Direct Antiviral Therapy for HCV in Patients With Cirrhosis Included in Surveillance Programs. *Gastroenterology* **2018**, *155*, 1436–1450.e6. [CrossRef]

14. Serti, E.; Chepa-Lotrea, X.; Kim, Y.J.; Keane, M.; Fryzek, N.; Liang, T.J.; Ghany, M.; Rehermann, B. Successful Interferon-Free Therapy of Chronic Hepatitis C Virus Infection Normalizes Natural Killer Cell Function. *Gastroenterology* **2015**, *149*, 190–200.e2. [CrossRef] [PubMed]
15. Meissner, E.G.; Wu, D.; Osinusi, A.; Bon, D.; Virtaneva, K.; Sturdevant, D.; Porcella, S.; Wang, H.; Herrmann, E.; McHutchison, J.; et al. Endogenous intrahepatic IFNs and association with IFN-free HCV treatment outcome. *J. Clin. Investig.* **2014**, *124*, 3352–3363. [CrossRef]
16. Debes, J.D.; Van Tilborg, M.; Groothuismink, Z.M.; Hansen, B.E.; Wiesch, J.S.Z.; Von Felden, J.; De Knegt, R.J.; Boonstra, A. Levels of Cytokines in Serum Associate With Development of Hepatocellular Carcinoma in Patients With HCV Infection Treated With Direct-Acting Antivirals. *Gastroenterology* **2018**, *154*, 515–517.e3. [CrossRef]
17. Villani, R.; Facciorusso, A.; Bellanti, F.; Tamborra, R.; Piscazzi, A.; Landriscina, M.; Vendemiale, G.; Serviddio, G. DAAs Rapidly Reduce Inflammation but Increase Serum VEGF Level: A Rationale for Tumor Risk during Anti-HCV Treatment. *PLoS ONE* **2016**, *11*. [CrossRef]
18. Faillaci, F.; Marzi, L.; Critelli, R.; Milosa, F.; Schepis, F.; Turola, E.; Andreani, S.; Vandelli, G.; Bernabucci, V.; Lei, B.; et al. Liver Angiopoietin-2 Is a Key Predictor of D e N ovo or Recurrent Hepatocellular Cancer After Hepatitis C Virus Direct-Acting Antivirals. *Hepatology* **2018**, *68*, 1010–1024. [CrossRef]
19. Vondran, F.W.; Katenz, E.; Schwartlander, R.; Morgul, M.H.; Raschzok, N.; Gong, X.; Cheng, X.; Kehr, D.; Sauer, I.M. Isolation of Primary Human Hepatocytes After Partial Hepatectomy: Criteria for Identification of the Most Promising Liver Specimen. *Artif. Organs* **2008**, *32*, 205–213. [CrossRef]
20. Werner, M.; Driftmann, S.; Kleinehr, K.; Kaiser, G.M.; Mathé, Z.; Treckmann, J.W.; Paul, A.; Skibbe, K.; Timm, J.; Canbay, A.; et al. All-In-One: Advanced preparation of Human Parenchymal and Non-Parenchymal Liver Cells. *PLoS ONE* **2015**, *10*, e0138655. [CrossRef]
21. Kirby, B.J.; Symonds, W.T.; Kearney, B.P.; Mathias, A.A. Pharmacokinetic, Pharmacodynamic, and Drug-Interaction Profile of the Hepatitis C Virus NS5B Polymerase Inhibitor Sofosbuvir. *Clin. Pharmacokinet.* **2015**, *54*, 677–690. [CrossRef]
22. Gandhi, Y.; Eley, T.; Fura, A.; Li, W.; Bertz, R.J.; Garimella, T. Daclatasvir: A Review of Preclinical and Clinical Pharmacokinetics. *Clin. Pharmacokinet.* **2018**, *57*, 911–928. [CrossRef]
23. Ouwerkerk-Mahadevan, S.; Beumont-Mauviel, M.; Mortier, S.; Peeters, M.; Verloes, R.; Truyers, C.; Mannens, G.; Wynant, I.; Simion, A. Evaluation of the Pharmacokinetics and Renal Excretion of Simeprevir in Subjects with Renal Impairment. *Drugs R&D* **2015**, *15*, 261–270. [CrossRef]
24. Mumtaz, N.; Jimmerson, L.C.; Bushman, L.R.; Kiser, J.J.; Aron, G.; Reusken, C.B.; Koopmans, M.P.; Van Kampen, J.J. Cell-line dependent antiviral activity of sofosbuvir against Zika virus. *Antivir. Res.* **2017**, *146*, 161–163. [CrossRef]
25. Feng, J.Y. Addressing the selectivity and toxicity of antiviral nucleosides. *Antivir. Chem. Chemother.* **2018**, *26*. [CrossRef]
26. Roos, W.; Thomas, A.; Kaina, B. DNA damage and the balance between survival and death in cancer biology. *Nat. Rev. Cancer* **2015**, *16*, 20–33. [CrossRef]
27. Resnitzky, D.; Gossen, M.; Bujard, H.; Reed, S.I. Acceleration of the G1/S phase transition by expression of cyclins D1 and E with an inducible system. *Mol. Cell. Biol.* **1994**, *14*, 1669–1679. [CrossRef]
28. Musa, J.; Aynaud, M.M.; Mirabeau, O.; Delattre, O.; Grünewald, T.G.P. MYBL2 (B-Myb): A central regulator of cell proliferation, cell survival and differentiation involved in tumorigenesis. *Cell Death Dis.* **2017**, *8*, e2895. [CrossRef]
29. Hanada, N.; Lo, H.W.; Day, C.P.; Pan, Y.; Nakajima, Y.; Hung, M.C. Co-regulation of B-Myb expression by E2F1 and EGF receptor. *Mol. Carcinog.* **2005**, *45*, 10–17. [CrossRef]
30. Lin, S.Y.; Makino, K.; Xia, W.; Matin, A.; Wen, Y.; Kwong, K.Y.; Bourguignon, L.; Hung, M.C. Nuclear localization of EGF receptor and its potential new role as a transcription factor. *Nat. Cell Biol.* **2001**, *3*, 802–808. [CrossRef]
31. Olsen, J.V.; Blagoev, B.; Gnad, F.; Macek, B.; Kumar, C.; Mortensen, P.; Mann, M. Global, In Vivo, and Site-Specific Phosphorylation Dynamics in Signaling Networks. *Cell* **2006**, *127*, 635–648. [CrossRef]
32. Tomas, A.; Jones, S.; Vaughan, S.O.; Hochhauser, D.; Futter, C. Stress-specific p38 MAPK activation is sufficient to drive EGFR endocytosis but not its nuclear translocation. *J. Cell Sci.* **2017**, *130*, 2481–2490. [CrossRef]

33. Zwang, Y.; Yarden, Y. p38 MAP kinase mediates stress-induced internalization of EGFR: Implications for cancer chemotherapy. *EMBO J.* **2006**, *25*, 4195–4206. [CrossRef]
34. Marzi, L.; Combes, E.; Vié, N.; Ayrolles-Torro, A.; Tosi, D.; Desigaud, D.; Perez-Gracia, E.; Larbouret, C.; Montagut, C.; Iglesias, M.; et al. FOXO3a and the MAPK p38 are activated by cetuximab to induce cell death and inhibit cell proliferation and their expression predicts cetuximab efficacy in colorectal cancer. *Br. J. Cancer* **2016**, *115*, 1223–1233. [CrossRef]
35. Wang, Y.N.; Hung, M.C. Nuclear functions and subcellular trafficking mechanisms of the epidermal growth factor receptor family. *Cell Biosci.* **2012**, *2*, 13. [CrossRef] [PubMed]
36. Gong, X.; Ming, X.; Deng, P.; Jiang, Y. Mechanisms regulating the nuclear translocation of p38 MAP kinase. *J. Cell. Biochem.* **2010**, *110*, 1420–1429. [CrossRef] [PubMed]
37. Kozbial, K.; Moser, S.; Schwarzer, R.; Laferl, H.; Al-Zoairy, R.; Stauber, R.; Stättermayer, A.F.; Beinhardt, S.; Graziadei, I.; Freissmuth, C.; et al. Unexpected high incidence of hepatocellular carcinoma in cirrhotic patients with sustained virologic response following interferon-free direct-acting antiviral treatment. *J. Hepatol.* **2016**, *65*, 856–858. [CrossRef] [PubMed]
38. Sampath, D.; Rao, V.A.; Plunkett, W. Mechanisms of apoptosis induction by nucleoside analogs. *Oncogene* **2003**, *22*, 9063–9074. [CrossRef]
39. Frau, M.; Ladu, S.; Calvisi, D.F.; Simile, M.M.; Bonelli, P.; Daino, L.M.E.; Tomasi, M.L.; Seddaiu, M.A.; Feo, F.; Pascale, R.M. Mybl2 expression is under genetic control and contributes to determine a hepatocellular carcinoma susceptible phenotype. *J. Hepatol.* **2011**, *55*, 111–119. [CrossRef]
40. Biliran, H.; Wang, Y.; Banerjee, S.; Xu, H.; Heng, H.; Thakur, A.; Bollig-Fischer, A.; Sarkar, F.H.; Liao, J.D. Overexpression of Cyclin D1 Promotes Tumor Cell Growth and Confers Resistance to Cisplatin-Mediated Apoptosis in an Elastase-myc Transgene-Expressing Pancreatic Tumor Cell Line. *Clin. Cancer Res.* **2005**, *11*, 6075–6086. [CrossRef]
41. Shimura, T.; Noma, N.; Oikawa, T.; Ochiai, Y.; Kakuda, S.; Kuwahara, Y.; Takai, Y.; Takahashi, A.; Fukumoto, M. Activation of the AKT/cyclin D1/Cdk4 survival signaling pathway in radioresistant cancer stem cells. *Oncogenesis* **2012**, *1*, e12. [CrossRef]
42. Calvisi, D.F.; Simile, M.M.; Ladu, S.; Frau, M.; Tomasi, M.L.; Demartis, M.I.; Daino, L.M.E.; Seddaiu, M.A.; Brozzetti, S.; Feo, F.; et al. Activation of v?Myb avian myeloblastosis viral oncogene homolog?like2 (MYBL2)?LIN9 complex contributes to human hepatocarcinogenesis and identifies a subset of hepatocellular carcinoma with mutant p53 †. *Hepatology* **2011**, *53*, 1226–1236. [CrossRef]
43. Feng, J.Y.; Xu, Y.; Barauskas, O.; Perry, J.K.; Ahmadyar, S.; Stepan, G.; Yu, H.; Babusis, D.; Park, Y.; McCutcheon, K.; et al. Role of Mitochondrial RNA Polymerase in the Toxicity of Nucleotide Inhibitors of Hepatitis C Virus. *Antimicrob. Agents Chemother.* **2016**, *60*, 806–817. [CrossRef]
44. Dittmann, K.; Mayer, C.; Kehlbach, R.; Rodemann, H.P. Radiation-induced caveolin-1 associated EGFR internalization is linked with nuclear EGFR transport and activation of DNA-PK. *Mol. Cancer* **2008**, *7*, 69. [CrossRef]
45. Mialon, A.; Sankinen, M.; Söderstroöm, H.; Junttila, T.T.; Holmstroöm, T.; Koivusalo, R.; Papageorgiou, A.C.; Johnson, R.S.; Hietanen, S.; Elenius, K.; et al. DNA Topoisomerase I Is a Cofactor for c-Jun in the Regulation of Epidermal Growth Factor Receptor Expression and Cancer Cell Proliferation. *Mol. Cell. Boil.* **2005**, *25*, 5040–5051. [CrossRef]
46. Johnson, A.; Murphy, B.A.; Matelis, C.M.; Rubinstein, Y.; Piebenga, E.C.; Akers, L.M.; Neta, G.; Vinson, C.; Birrer, M. Activator protein-1 mediates induced but not basal epidermal growth factor receptor gene expression. *Mol. Med.* **2000**, *6*, 17–27. [CrossRef]
47. Brunet, A.; Bonni, A.; Zigmond, M.J.; Lin, M.Z.; Juo, P.; Hu, L.S.; Anderson, M.J.; Arden, K.C.; Blenis, J.; Greenberg, M.E. Akt Promotes Cell Survival by Phosphorylating and Inhibiting a Forkhead Transcription Factor. *Cell* **1999**, *96*, 857–868. [CrossRef]
48. Barlow, C.; Kitiphongspattana, K.; Siddiqui, N.; Roe, M.W.; Mossman, B.T.; Lounsbury, K.M. Protein kinase A-mediated CREB phosphorylation is an oxidant-induced survival pathway in alveolar type II cells. *Apoptosis* **2008**, *13*, 681–692. [CrossRef]
49. Wu, D.; Zhau, H.E.; Huang, W.C.; Iqbal, S.; Habib, F.K.; Sartor, O.; Cvitanovic, L.; Marshall, F.F.; Xu, Z.; Chung, L.W.K. cAMP-responsive element-binding protein regulates vascular endothelial growth factor expression: Implication in human prostate cancer bone metastasis. *Oncogene* **2007**, *26*, 5070–5077. [CrossRef]

50. Wee, P.; Wang, Z. Epidermal Growth Factor Receptor Cell Proliferation Signaling Pathways. *Cancers* **2017**, *9*, 52. [CrossRef]
51. Tanaka, T.; Ozawa, T.; Oga, E.; Muraguchi, A.; Sakurai, H. Cisplatin-induced non-canonical endocytosis of EGFR via p38 phosphorylation of the C-terminal region containing Ser-1015 in non-small cell lung cancer cells. *Oncol. Lett.* **2018**, *15*, 9251–9256. [CrossRef]
52. Brüning, A.; Burger, P.; Gingelmaier, A.; Mylonas, I. The HIV reverse transcriptase inhibitor tenofovir induces cell cycle arrest in human cancer cells. *Investig. New Drugs* **2011**, *30*, 1389–1395. [CrossRef] [PubMed]
53. Fang, J.L.; Beland, F.A. Long-Term Exposure to Zidovudine Delays Cell Cycle Progression, Induces Apoptosis, and Decreases Telomerase Activity in Human Hepatocytes. *Toxicol. Sci.* **2009**, *111*, 120–130. [CrossRef] [PubMed]
54. Olivero, O.A.; Tejera, A.M.; Fernandez, J.J.; Taylor, B.J.; Das, S.; Divi, R.L.; Poirier, M.C. Zidovudine induces S-phase arrest and cell cycle gene expression changes in human cells. *Mutagenesis* **2005**, *20*, 139–146. [CrossRef]
55. Olivero, O.A.; Beland, F.A.; Fullerton, N.F.; Poirier, M.C. Vaginal Epithelial DNA Damageand Expressionof PreneoplasticMarkers. *Cancer Res.* **1994**, *54*, 6235–6242.
56. Hoshida, Y.; Fuchs, B.C.; Bardeesy, N.; Baumert, T.F.; Chung, R.T. Pathogenesis and prevention of hepatitis C virus-induced hepatocellular carcinoma. *J. Hepatol.* **2014**, *61*, S79–S90. [CrossRef]
57. Fuchs, B.C.; Hoshida, Y.; Fujii, T.; Wei, L.; Yamada, S.; Lauwers, G.Y.; McGinn, C.M.; Deperalta, D.K.; Chen, X.; Kuroda, T.; et al. Epidermal growth factor receptor inhibition attenuates liver fibrosis and development of hepatocellular carcinoma. *Hepatology* **2014**, *59*, 1577–1590. [CrossRef]
58. Hoshida, Y.; Villanueva, A.; SanGiovanni, A.; Sole, M.; Hur, C.; Andersson, K.L.; Chung, R.T.; Gould, J.; Kojima, K.; Gupta, S.; et al. Prognostic gene expression signature for patients with hepatitis C-related early-stage cirrhosis. *Gastroenterology* **2013**, *144*, 1024–1030. [CrossRef]
59. Ito, Y.; Takeda, T.; Sakon, M.; Tsujimoto, M.; Higashiyama, S.; Noda, K.; Miyoshi, E.; Monden, M.; Matsuura, N. Expression and clinical significance of erb-B receptor family in hepatocellular carcinoma. *Br. J. Cancer* **2001**, *84*, 1377–1383. [CrossRef]
60. Lupberger, J.; Zeisel, M.B.; Xiao, F.; Thumann, C.; Fofana, I.; Zona, L.; Davis, C.; Mee, C.; Turek, M.; Gorke, S.; et al. EGFR and EphA2 are host factors for hepatitis C virus entry and possible targets for antiviral therapy. *Nat. Med.* **2011**, *17*, 589–595. [CrossRef]
61. Brenndörfer, E.D.; Karthe, J.; Frelin, L.; Cebula, P.; Erhardt, A.; Schulte am Esch, J.; Hengel, H.; Bartenschlager, R.; Sällberg, M.; Häussinger, D.; et al. Nonstructural 3/4A protease of hepatitis C virus activates epithelial growth factor-induced signal transduction by cleavage of the T-cell protein tyrosine phosphatase. *Hepatology* **2009**, *49*, 1810–1820. [CrossRef] [PubMed]
62. Diao, J.; Pantua, H.; Ngu, H.; Komuves, L.; Diehl, L.; Schaefer, G.; Kapadia, S.B. Hepatitis C virus induces epidermal growth factor receptor activation via CD81 binding for viral internalization and entry. *J. Virol.* **2012**, *86*, 10935–10949. [CrossRef] [PubMed]
63. Hamdane, N.; Jühling, F.; Crouchet, E.; El Saghire, H.; Thumann, C.; Oudot, M.A.; Bandiera, S.; Saviano, A.; Ponsolles, C.; Suarez, A.A.R.; et al. HCV-Induced Epigenetic Changes Associated With Liver Cancer Risk Persist After Sustained Virologic Response. *Gastroenterology* **2019**, *156*, 2313–2329.e7. [CrossRef] [PubMed]
64. Perez, S.; Kaspi, A.; Domovitz, T.; Davidovich, A.; Lavi-Itzkovitz, A.; Meirson, T.; Holmes, J.A.; Dai, C.Y.; Huang, C.F.; Chung, R.T.; et al. Hepatitis C virus leaves an epigenetic signature post cure of infection by direct-acting antivirals. *PLoS Genet.* **2019**, *15*, e1008181. [CrossRef] [PubMed]

cells

MDPI

Article

Sofosbuvir Activates EGFR-Dependent Pathways in Hepatoma Cells with Implications for Liver-Related Pathological Processes

Denisa Bojkova [1,2], Sandra Westhaus [1,2], Rui Costa [1], Lejla Timmer [1], Nora Funkenberg [1], Marek Korencak [3], Hendrik Streeck [3], Florian Vondran [4,5], Ruth Broering [6], Stefan Heinrichs [7], Karl S Lang [8] and Sandra Ciesek [1,2,5,*]

1 Institute of Virology, University Hospital Essen, University Duisburg-Essen, 45147 Essen, Germany; denisa.bojkova@kgu.de (D.B.); sandra.westhaus@kgu.de (S.W.); rcosta@sund.ku.dk (R.C.); lejla.timmer@uk-essen.de (L.T.); nora.funkenberg@googlemail.com (N.F.)
2 Institute of Medical Virology, University Hospital, Goethe University Frankfurt am Main, 60590 Frankfurt, Germany
3 Institute for HIV research, University Hospital Essen, University Duisburg-Essen, 45147 Essen, Germany; marek.korencak@uk-essen.de (M.K.); hendrik.streeck@uk-essen.de (H.S.)
4 Clinic for General, Abdominal and Transplant Surgery, Hannover Medical School, 30625 Hannover, Germany; vondran.florian@mh-hannover.de
5 German Center for Infection Research (DZIF), 45147 Essen, Germany
6 Department of Gastroenterology and Hepatology, University Hospital Essen, University Duisburg-Essen, 45147 Essen, Germany; ruth.broering@uni-due.de
7 Institute for Transfusion Medicine, University Hospital Essen, University Duisburg-Essen, 45147 Essen, Germany; stefan.heinrichs@uk-essen.de
8 Institute of Immunology, University Hospital Essen, University Duisburg-Essen, 45147 Essen, Germany; KarlSebastian.Lang@uk-essen.de
* Correspondence: sandra.ciesek@kgu.de; Tel.: +49-69-63015219

Received: 9 March 2020; Accepted: 13 April 2020; Published: 17 April 2020

1. Materials and Methods

1.1 Measurement of mitochondrial respiration and the glycolytic function

Cells were cultured with SOF for four consecutive days. At day five, the cells were seeded in a concentration of $4x10^4$ cells/well in XFe 96-well plates (Agilent, Waldbronn, Germany) and let to attach overnight. Mitochondrial respiration was monitored by the oxygen consumption rate (OCR) and glycolysis was controlled by the extracellular acidification rate (ECAR) using a Seahorse XFe Cell Mito Stress Test Kit (Agilent, Waldbronn, Germany) according to the manufacturer´s protocol. The OCR and ECAR values were normalized to the atotal protein amount determined by a Pierce™ BCA Protein Assay Kit (Thermo Fisher Scientific, Schwerte, Germany).

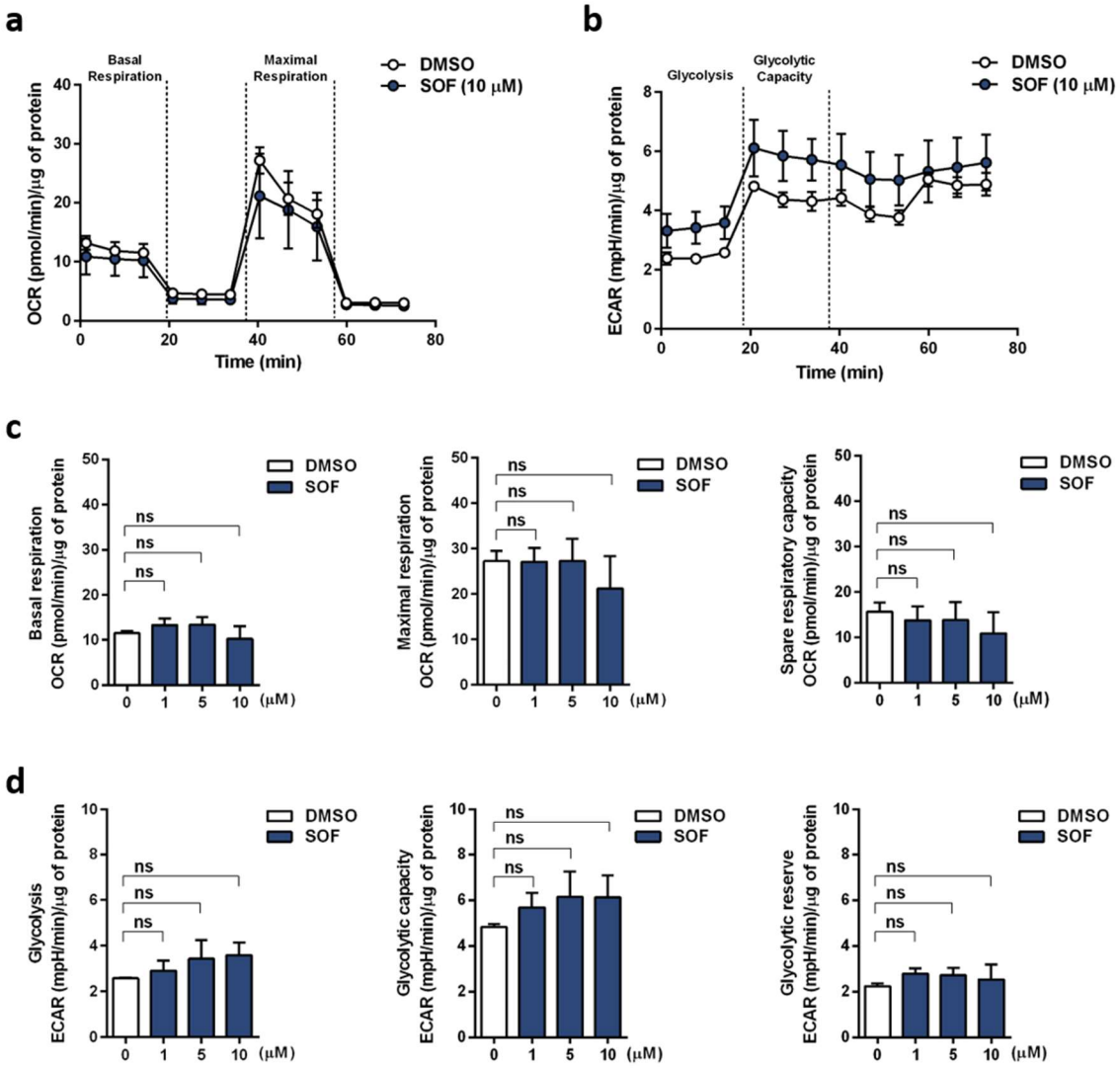

Figure S1. Sofosbuvir treatment does not impair mitochondrial respiration. Cells were cultured with different concentrations of SOF for four consecutive days. At day five, $4x10^4$ cells/well were seeded in XF 96-well plates and mitochondrial respiration and glycolytic function were quantified using a Seahorse extracellular flux analyzer (XFe-96, Agilent). (a, c) Basal respiration, maximal respiration, and spare respiratory capacity were calculated based on the oxygen consumption rate (OCR). (b, d) Glycolysis, glycolytic capacity, and glycolytic reserve were assessed based on the extracellular acidification rate (ECAR). Data are normalized to μg of the total protein amount. Mean + s.d. from three independent experiments are displayed. Statistical significance was determined through one-way ANOVA. ns: not significant.

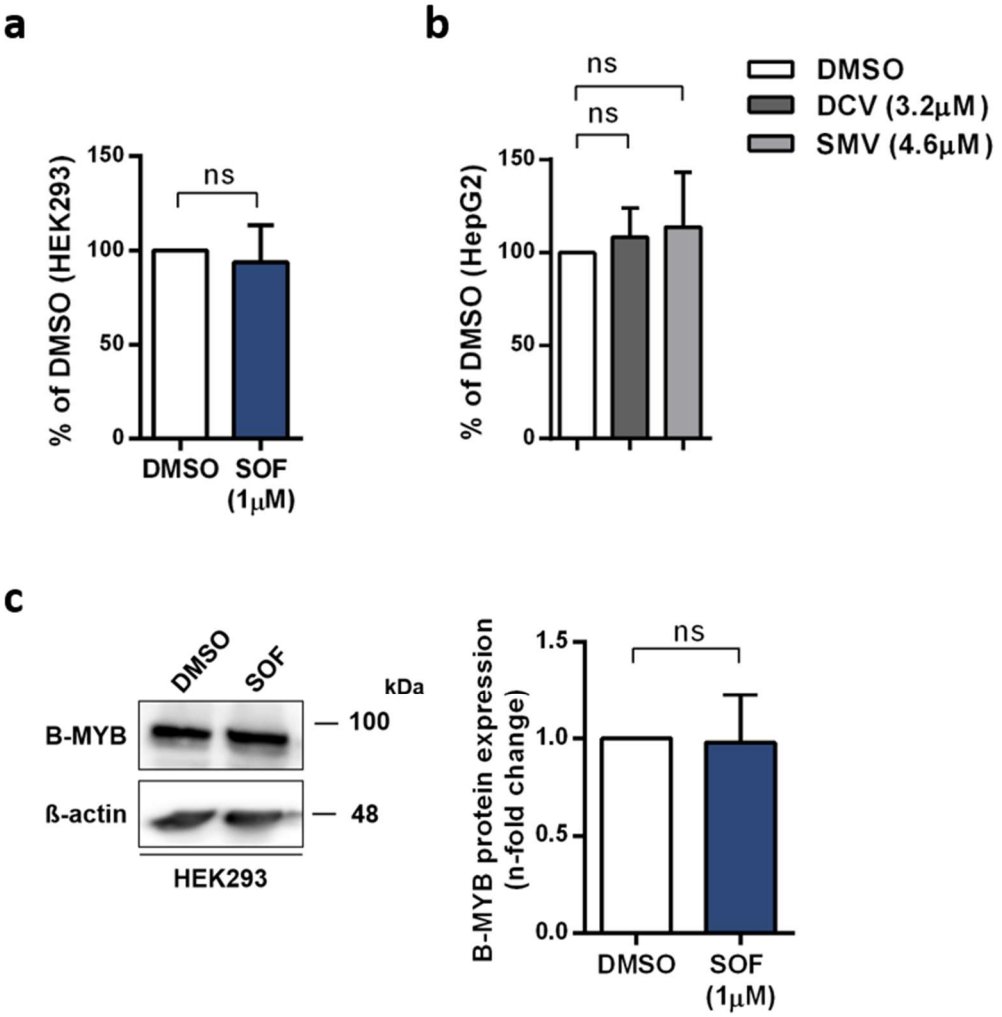

Figure S2. Non-hepatic cells HEK-293 and other DAA do not support an SOF-induced phenotype. (a, b) Proliferation rates of HEK293 cells after SOF treatment (a) and HepG2 cells after DCV or SMV treatment (b) were determined by utilizing trypan blue exclusion. Bar graphs displays results in relation to DMSO. (c) B-MYB protein levels in HEK293 cultured in the presence of SOF were determined by immunoblot analysis. One representative immunoblot is displayed. Relative protein expression is presented as a fold change in relation to the vehicle control DMSO. Displayed data represent mean + s.d. from three independent experiments (a, b) and two independent experiments (c). Statistical significance was determined through an unpaired t-test (a, c) and one-way ANOVA (b). ns: not significant.

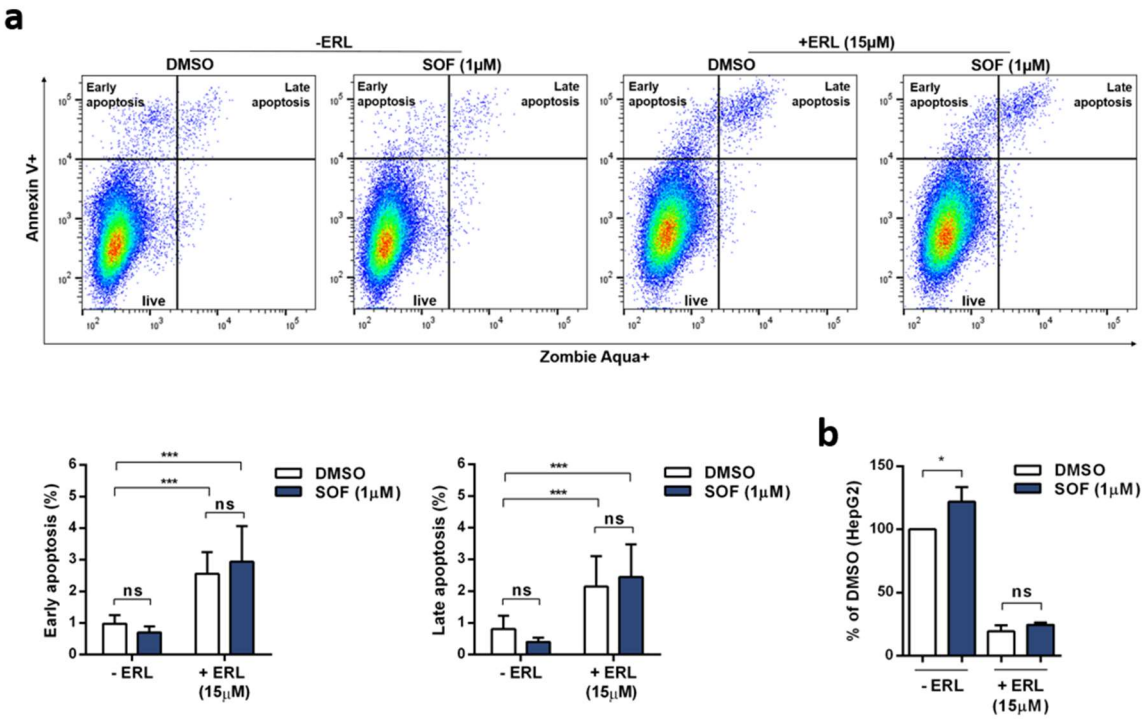

Figure S3. Application of erlotinib during SOF treatment induces apoptosis and inhibits proliferation. HepG2 cells were incubated with ERL and SOF for four consecutive days. At day five, all following analyses were performed. (a) Proportion of apoptotic cells was determined with Annexin V and live/dead cells staining by flow cytometry. Bar graph displays the percentage of cells in early apoptosis and late apoptosis. (b) The proliferation rates were evaluated by trypan blue exclusion and shown as a percentage in relation to the vehicle control DMSO. All experiments are shown as mean + s.d. from three independent experiments. Statistical significance was determined through two-way ANOVA (a, b). ns: not significant; * $p \leq 0.05$; ** $p \leq 0.01$; *** $p \leq 0.005$.

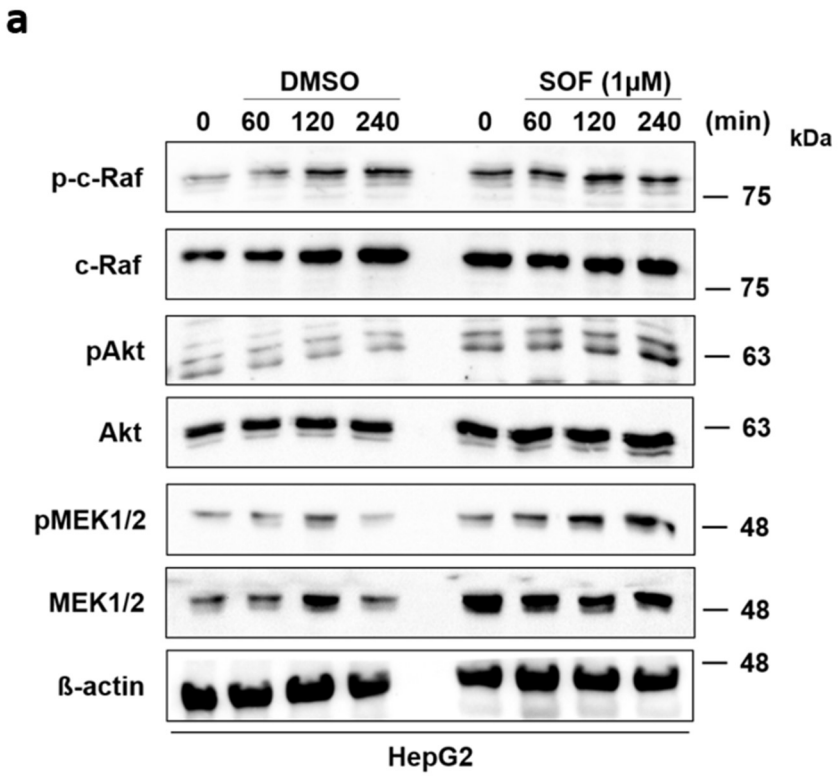

Figure S4. Activation of EGFR downstream signaling targets after SOF treatment. (a) Total protein expression and phosphorylation of target proteins was evaluated by immunoblot analysis. One representative immunoblot is shown.

Table S1. Predicted activated STK kinases after SOF treatment. Based on the comparison of phosphorylated peptides on the array with the databases of documented interactions, such as HPRD, PhosphoSitePlus, as well as the in-silico predictions database PhosphoNET, a specificity and significance score was calculated. The resulting list of kinases is based on the final score, the sum of the median final score, and the median kinase statistics (MKS).

Kinase Name	HepG2	HuH-6	HEK-293
AurB/Aur1	4.374217	3.03169	1.164061
PKD1	4.055393	1.906143	0.359733
RSKL2	3.490924	1.435201	0.035775
IKK[beta]	3.483465	1.730221	0.322747
DAPK2	3.421873	0.252112	0.216946
CaMK2[alpha]	3.346736	1.584383	0.273212
PRKX	3.182962	1.948886	0.088726
CDKL2	3.018253	0.97972	0.814038
PKC[epsilon]	2.875098	2.101545	0.07466
PKA[alpha]	2.856334	2.026203	0.114149
PKC[eta]	2.834951	2.396981	0.056223
IKK[epsilon]	2.788357	1.199546	0.703098
SGK2	2.787967	1.070037	0.187933
PKC[alpha]	2.783897	2.553313	0.129696
PKC[gamma]	2.730528	2.07841	0.052023
PAK1	2.645182	1.851696	0.391424
RSKL1	2.64077	2.990542	0.665425
DAPK3	2.625414	2.804247	0.893947
Akt1/PKB[alpha]	2.619971	1.567764	0.355081
Pim1	2.599516	2.549547	0.788302
CHK2	2.598952	2.640358	1.24863
CaMK4	2.551329	0.967793	0.351173
ERK7	2.519317	2.358516	1.06546
Pim2	2.518634	2.372009	0.890485
PKC[theta]	2.514123	2.181327	0.021492
Pim3	2.486877	2.417713	0.728759
p70S6K[beta]	2.47629	1.824834	0.156769
PKC[delta]	2.468173	1.892108	0.127955
CHK1	2.444178	0.894619	1.44397
PCTAIRE2	2.434013	1.002181	0.227832
MAPKAPK2	2.428079	1.540451	1.421561
TBK1	2.406283	1.295958	0.248604
p38[beta]	2.401599	1.037017	0.126575
ANP[alpha]	2.376676	1.645016	0.306188
SGK1	2.375803	1.982021	0.382716
AurA/Aur2	2.372234	2.23801	1.020769
AMPK[alpha]1	2.3582	1.937989	0.22292
RSK1/p90RSK	2.354727	1.916767	0.262217
JNK2	2.349282	1.046434	0.859831
MSK1	2.318733	2.390597	0.893688
ADCK3	2.308174	1.139974	0.354651

RSK2	2.300832	1.743994	0.587068
CDKL5	2.287687	1.495935	1.22353
PKG1	2.285522	2.2881	0.273141
PKN1/PRK1	2.268168	0.911223	0.004627
Akt2/PKB[beta]	2.253581	1.415509	0.020258
ROCK2	2.220144	1.856898	0.025676
NuaK1	2.215376	2.222923	0.4455
RAF1	2.208523	2.030399	0.371386
BRAF	2.20384	1.39262	0.325423
ATR	2.201845	0.984706	0.704188
PKG2	2.178193	2.71447	0.425434
JNK1	2.146313	1.198105	1.250477
JNK3	2.146313	1.196041	1.235999
MAPKAPK3	2.138058	1.531832	0.396041
RSK3	2.106249	1.518089	0.656172
p70S6K	2.075926	1.819077	0.048804
TNIK/ZC2	2.072682	2.060233	0.923134
PKC[iota]	2.054825	1.065091	0.107054
MAPK14	2.044332	0.875708	0.30967
CK1[alpha]	2.037583	2.375999	0.339512
GSK3[alpha]	2.03709	1.620186	0.370045
ICK	2.027002	1.930407	0.691457
AlphaK1	2.008525	1.915913	1.155768
p38[delta]	1.995322	0.657916	0.072428
DCAMKL1	1.983109	2.736141	0.610241
CDK10	1.88127	3.704281	0.158586
PRKY	1.857864	1.523384	0.155114
CDK9	1.842812	1.682931	1.389388
GSK3[beta]	1.799007	1.960006	0.210386
PKC[beta]	1.760804	2.056166	0.134231
HGK/ZC1	1.750192	1.87224	0.128969
PKC[zeta]	1.702525	1.555805	0.238692
mTOR/FRAP	1.62584	2.778769	0.795234
CDK6	1.578003	0.921009	0.687531
CDK7	1.529946	1.867462	1.072142
ERK5	1.502921	2.7675	1.721496
CDC2/CDK1	1.496093	0.648602	0.882162
CDK4	1.473681	0.99875	0.716556
CDK5	1.462478	1.144918	1.004356
CDK11	1.456666	0.8954	0.834509
PFTAIRE2	1.443057	0.280623	2.180737
p38[gamma]	1.441417	1.957767	0.903558
ERK1	1.430379	3.222845	0.942129
SgK307	1.372155	0.199722	1.269961
CDK2	1.324337	1.958866	1.413946
CDKL1	1.264317	2.85879	0.51856

ROCK1	1.24158	0.988067	0.069619
ERK2	1.170484	2.952321	1.841095
CK1[epsilon]	1.155203	1.23929	0.030355
CDK3	1.130101	1.3681	1.104966
COT	0.368523	2.281348	0.436554

2.2 Study 2: Proteomics of SARS-CoV-2-infected host cells reveals therapy targets

Article

Proteomics of SARS-CoV-2-infected host cells reveals therapy targets

https://doi.org/10.1038/s41586-020-2332-7

Received: 27 February 2020

Accepted: 6 May 2020

Published online: 14 May 2020

Check for updates

Denisa Bojkova[1,7], Kevin Klann[2,7], Benjamin Koch[3,7], Marek Widera[1], David Krause[2], Sandra Ciesek[1,4], Jindrich Cinatl[1]✉ & Christian Münch[2,5,6]✉

A new coronavirus was recently discovered and named severe acute respiratory syndrome coronavirus 2 (SARS-CoV-2). Infection with SARS-CoV-2 in humans causes coronavirus disease 2019 (COVID-19) and has been rapidly spreading around the globe[1,2]. SARS-CoV-2 shows some similarities to other coronaviruses; however, treatment options and an understanding of how SARS-CoV-2 infects cells are lacking. Here we identify the host cell pathways that are modulated by SARS-CoV-2 and show that inhibition of these pathways prevents viral replication in human cells. We established a human cell-culture model for infection with a clinical isolate of SARS-CoV-2. Using this cell-culture system, we determined the infection profile of SARS-CoV-2 by translatome[3] and proteome proteomics at different times after infection. These analyses revealed that SARS-CoV-2 reshapes central cellular pathways such as translation, splicing, carbon metabolism, protein homeostasis (proteostasis) and nucleic acid metabolism. Small-molecule inhibitors that target these pathways prevented viral replication in cells. Our results reveal the cellular infection profile of SARS-CoV-2 and have enabled the identification of drugs that inhibit viral replication. We anticipate that our results will guide efforts to understand the molecular mechanisms that underlie the modulation of host cells after infection with SARS-CoV-2. Furthermore, our findings provide insights for the development of therapies for the treatment of COVID-19.

At the end of 2019, a cluster of cases of severe pneumonia of unknown cause was described in Wuhan (eastern China), and a SARS-like acute respiratory distress syndrome was noted in many patients. Early in January 2020, next-generation sequencing revealed that a novel coronavirus (named SARS-CoV-2) was the causal factor for the disease[1], which was later designated COVID-19. SARS-CoV-2 shows high infectivity, which has resulted in rapid global spreading[2].

Currently, there is no established therapy for the treatment of COVID-19. Treatment is based mainly on supportive and symptomatic care[4,5]. Therefore, the development of therapies that inhibit infection with or replication of SARS-CoV-2 are urgently needed. Molecular examination of infected cells by unbiased proteomics approaches offers a potent strategy for revealing pathways that are relevant for viral pathogenicity to identify potential drug targets. However, this strategy depends on the availability of cell-culture models that are amenable to virus infection and sensitive proteomics approaches that can be used for temporal infection profiling in cells. SARS-CoV-2 was recently successfully isolated using the human colon epithelial carcinoma cell line[6] Caco-2. SARS-CoV-2 replicates in gastrointestinal cells in vivo[7] and is frequently detected in stool—regardless of the occurrence of diarrhoea[8]. Caco-2 cells were extensively used to study infection with SARS-CoV and can be used for SARS-CoV-2 infection[6,9]. For proteome analysis, a method—multiplexed enhanced protein dynamics (mePROD) proteomics—was recently described that enables the determination of translatome and proteome changes at high temporal resolution[3]. Owing to the quantification of translational changes by naturally occurring heavy isotope labelling using stable isotope labelling by amino acids in cell culture (SILAC), this method does not affect cellular behaviour and therefore enables the perturbation-free and unbiased analysis of the response of cells to viral infection.

In this study, we used quantitative translatome and proteome proteomics to obtain an unbiased profile of the cellular response to SARS-CoV-2 infection in human cells. We monitored different time points after infection and identified key determinants of the host cell response to infection. These findings revealed pathways that are relevant for SARS-CoV-2 infection. We tested several drugs that target these pathways, including translation, proteostasis, glycolysis, splicing and nucleotide synthesis pathways. These drugs inhibited SARS-CoV-2 replication at concentrations that were not toxic to the human cells, potentially providing therapeutic strategies for the treatment of COVID-19.

SARS-CoV-2 rapidly replicates in cells

To investigate potential antiviral compounds that inhibit SARS-CoV-2, we established a highly permissive SARS-CoV-2 cell-culture model in Caco-2 cells. Addition of SARS-CoV-2 at a multiplicity of infection (MOI) of one (to enable the infection of most of the cells while preventing multiple infections) led to a fast progression of viral infection and visible cytopathogenic effects were apparent after 24 h (Fig. 1a). To

[1]Institute of Medical Virology, University Hospital Frankfurt, Goethe University, Frankfurt am Main, Germany. [2]Institute of Biochemistry II, Faculty of Medicine, Goethe University, Frankfurt am Main, Germany. [3]Medical Clinic III, Nephrology, University Hospital Frankfurt, Frankfurt am Main, Germany. [4]German Centre for Infection Research (DZIF), External Partner Site Frankfurt, Frankfurt am Main, Germany. [5]Frankfurt Cancer Institute, Frankfurt am Main, Germany. [6]Cardio-Pulmonary Institute, Frankfurt am Main, Germany. [7]These authors contributed equally: Denisa Bojkova, Kevin Klann, Benjamin Koch. ✉e-mail: cinatl@em.uni-frankfurt.de; ch.muench@em.uni-frankfurt.de

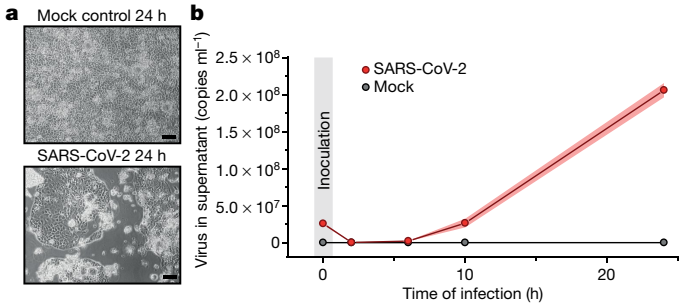

Fig. 1 | SARS-CoV-2-replication model in human cells. a, Caco-2 cells were either mock-infected or infected with SARS-CoV-2 and cultured for 24 h. Microscopy images show the cytopathogenic effects of SARS-CoV-2 infection. Scale bars, 100 µm. Representative images from three independent biological replicates are shown. **b**, Quantitative PCR analysis of viral genome copies per ml of cell culture after the indicated infection time ($n = 3$ independent biological samples). Points indicate the mean of replicate measurements and shades represent the s.d.

determine whether productive viral infection takes place in this model, we measured the number of viral RNA copies in the supernatant during a 24-h time period. SARS-CoV-2 RNA molecules increased continuously after infection (Fig. 1b), indicating that the virus underwent full replication cycles. Staining for viral nucleoprotein additionally revealed the production of viral proteins in most cells (Extended Data Fig. 1). Taken together, we established a functional SARS-CoV-2 cell-culture model that enables the investigation of the different steps of the life cycle of SARS-CoV-2 in cells.

Translation inhibitors block replication

To determine the temporal profile of SARS-CoV-2 infection, we infected Caco-2 cells with SARS-CoV-2, cultured them for a range of 2–24 h and quantified translatome and proteome changes by mePROD proteomics compared with time-matched mock-infected samples (Fig. 2a). Across all replicates, we quantified translation for 2,715 proteins and total protein levels for 6,382 proteins (Supplementary Table 1). Principal component analysis showed that replicates clustered closely and that infected samples showed the first separation from control clusters after 6 h (Extended Data Fig. 2a). Many RNA viruses decrease protein synthesis in cells, as has been suggested for SARS-CoV[10]. When monitoring global translation rates, only minor changes in translation were observed (Fig. 2b and Extended Data Fig. 2b). We detected translation rates for five viral proteins, all of which exhibited increasing translation rates over time (Fig. 2c). To identify pathways that are potentially important for virus amplification, we determined host proteins that exhibited translation kinetics, which correlated with viral proteins. Averaged profiles of all quantified viral proteins were used as reference profiles; the distance to this profile was calculated for all quantified host proteins and a network analysis was carried out for the top 10% quantile of nearest profiles (244 proteins) (Extended Data Fig. 2c–f). Pathway analyses of the network revealed an extensive increase in the translation machinery of the host (Fig. 2d and Extended Data Fig. 2g). In addition, we detected significant enrichment of components of several other pathways, such as splicing and nucleobase synthesis (Fig. 2d).

Host translation has previously been targeted to pharmacologically inhibit the replication of diverse coronaviruses, such as SARS-CoV or MERS-CoV[11,12] (Extended Data Fig. 2h). As components of the translation machinery were translated at higher rates (Fig. 2d), we hypothesized that SARS-CoV-2 replication might be sensitive to inhibition of translation. We tested two translation inhibitors—cycloheximide (an inhibitor of translation elongation) and emetine (an inhibitor of the 40S ribosomal protein S14)—for their ability to reduce SARS-CoV-2 replication. Both compounds significantly inhibited SARS-CoV-2 replication at

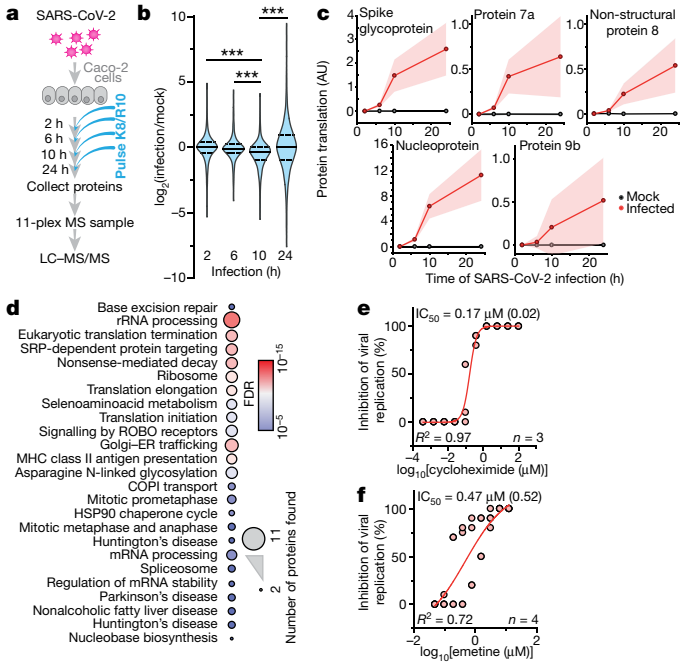

Fig. 2 | Host cell translation changes after infection with SARS-CoV-2. **a**, Experimental scheme for translatome and proteome measurements. Caco-2 cells were infected with SARS-CoV-2 isolated from patients, incubated as indicated and analysed by quantitative translation and whole-cell proteomics. K8, lysine with 8 heavy isotopes; R10, arginine with 10 heavy isotopes; LC–MS/MS, Liquid chromatography–tandem mass spectrometry. **b**, Global translation rates, showed by distribution plots of mean $\log_2$-transformed fold changes of infected replicates to mock control for each time point and protein. The black line indicates the median and the dashed lines indicate 25% and 75% quantiles. Significance was tested by one-way ANOVA and two-sided post hoc Bonferroni test. ***$P < 0.001$ (10 h compared with 2 h, 4×10^{-26}; 10 h compared with 6 h, 2.4×10^{-23}; 10 h compared with 24 h, 2.3×10^{-28}; $n = 2{,}716$ measured proteins averaged from 3 independent biological samples). **c**, Translation of viral proteins over time. Mean translation in arbitrary units (AU; normalized and corrected summed peptide spectrum matches were averaged) is plotted for control and infected samples. Shading indicates the s.d. ($n = 3$). **d**, Reactome pathway analysis of top 10% proteins following viral gene expression. Pathway results are shown with the number of proteins found in the dataset and computed FDRs for pathway enrichment. ER, endoplasmic reticulum. **e**, **f**, The antiviral assays show that the inhibition of viral replication is dependent on the concentrations of cycloheximide (**e**, $n = 3$) and emetine (**f**, $n = 4$). Each data point indicates biological replicates and the red line shows the dose–response curve fit. R^2 and half-maximum inhibitory concentration (IC_{50}) values were computed from the curve fit and the s.d. of the IC_{50} is indicated in parentheses. All n numbers represent independent biological samples if not stated otherwise.

concentrations that are not toxic to human Caco-2 cells (Fig. 2e, f and Extended Data Fig. 2i, j). Taken together, translatome analyses of cells infected with SARS-CoV-2 revealed the temporal profile of viral and host protein responses with prominent increases in the translation machinery. Translation inhibitors prevented SARS-CoV-2 replication in cells.

Pathways changed by SARS-CoV-2 infection

To obtain a general understanding of changes in the host proteome after infection, we analysed system-wide differences in protein levels over time (Fig. 3a and Supplementary Table 2). Whereas early time points showed only minor changes in the host proteome, the proteome underwent extensive modulation 24 h after infection (Fig. 3a and Extended Data Fig. 3). Hierarchical clustering identified two main clusters of proteins that were differentially regulated. The first cluster consisted of proteins that were reduced during infection and was enriched in proteins that belonged to cholesterol metabolism (Extended Data Fig. 4a,

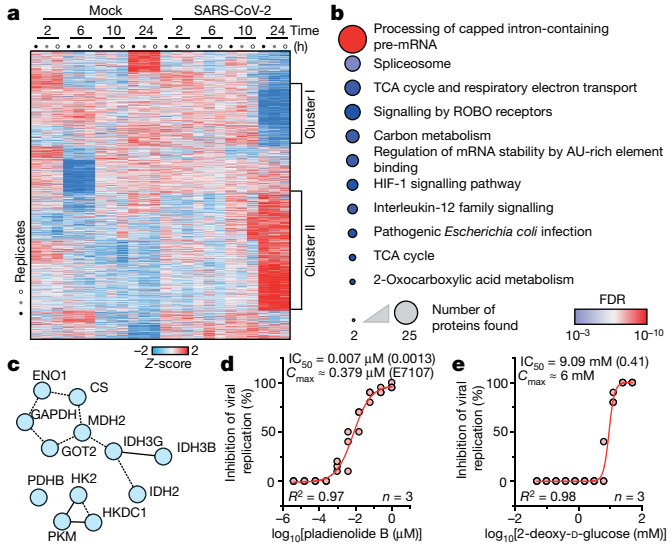

Fig. 3 | SARS-CoV-2 infection profiling reveals cellular pathways that are essential for replication. a, Patterns of protein levels across all samples. The proteins that were significantly up- or downregulated (two-sided, unpaired Student's *t*-test with equal variance assumed, $P < 0.05$, $n = 3$) in at least one infected sample compared with the corresponding control are shown. Data were standardized using *Z*-scoring before row-wise clustering and plotting. TCA, tricarboxylic acid. **b**, Reactome pathway analysis of the protein network created from cluster II, which includes host cell proteins that are increased after SARS-CoV-2 infection (**a**; Supplementary Table 4). Pathway results are shown with the number of proteins found in the dataset and computed FDR for pathway enrichment. **c**, Functional interaction network of proteins found annotated to carbon metabolism in the Reactome pathway analysis. Lines indicate functional interactions. **d**, **e**, The antiviral assays show that the inhibition of viral replication is dependent on the concentrations of pladienolide B (**d**, $n = 3$) and 2-deoxy-D-glucose (**e**, $n = 3$). Each data point indicates a biological replicate and the red line shows the dose–response curve fit. R^2 and IC_{50} values were computed from the curve fit and the s.d. of IC_{50} is indicated in parentheses. C_{max}, maximum plasma concentration; E7107, the indicated C_{max} was obtained for the E7107, a derivative of pladienolide B. All *n* numbers represent independent biological samples.

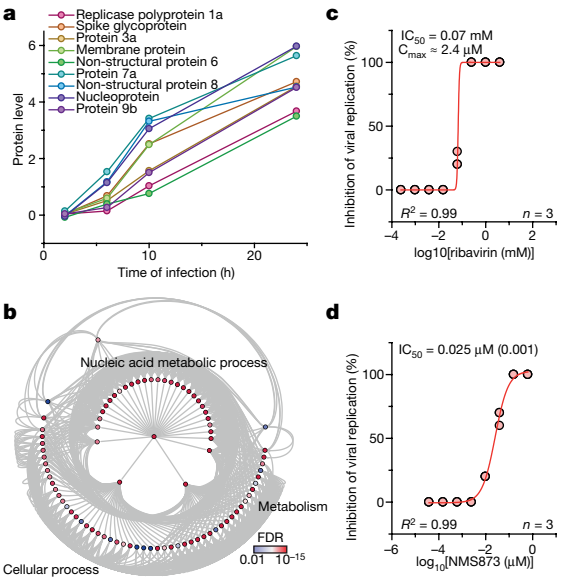

Fig. 4 | Inhibition of host cell pathways induced by infection prevent SARS-CoV-2 replication. a, Protein levels of all detected viral proteins are plotted with their $\log_2$-transformed changes compared with the corresponding control for different infection times. Mean fold changes are plotted ($n = 3$). **b**, Gene ontology network analysis of host proteins that correlated with viral protein expression (FDR-adjusted $P < 0.01$). Proteins were clustered according to the gene ontology term of the biological process and plotted as a network with FDR colour coding. Annotated pathways represent parent pathways in the network. **c**, **d**, The antiviral assays show that the inhibition of viral replication is dependent on the concentrations of ribavirin (**c**, $n = 3$) and NMS873 (**d**, $n = 3$). Each data point indicates a biological replicate and the red line indicates the dose–response curve fit. R^2 and IC_{50} values were computed from the curve fit and the s.d. of IC_{50} is indicated in parentheses. All *n* numbers represent independent biological samples.

b and Supplementary Table 3). The second cluster was composed of proteins that were increased by infection and revealed strong increases in RNA-modifying proteins, such as spliceosome components (consistent with translatome measurements in Fig. 2d), and carbon metabolism (Fig. 3b, c, Extended Data Fig. 5a and Supplementary Table 4). Notably, for 14 out of 25 spliceosome components that were increased after infection with SARS-CoV-2, direct binding to viral proteins of SARS-CoV or other coronaviruses had been shown[13–16] (Extended Data Fig. 5b). We therefore tested whether the inhibition of splicing or glycolysis may be able to prevent SARS-CoV-2 replication. Addition of pladienolide B, a spliceosome inhibitor that targets the splicing factor SF3B1[17], prevented viral replication at concentrations that were not toxic to the human Caco-2 cells (Fig. 3d and Extended Data Fig. 5c), revealing that splicing is an essential pathway for SARS-CoV-2 replication and a potential therapeutic target.

Next, we assessed the effects of the inhibition of carbon metabolism (that is, glycolysis) on SARS-CoV-2 replication. 2-deoxy-D-Glucose, an inhibitor of hexokinase (the rate-limiting enzyme in glycolysis), has previously been shown to be effective against other viruses in cell culture and suppressed infection with rhinovirus in mice[18]. Blocking glycolysis with non-toxic concentrations of 2-deoxy-D-glucose prevented SARS-CoV-2 replication in Caco-2 cells (Fig. 3e and Extended Data Fig. 5d). Notably, we also observed changes in proteins that reside in the endoplasmic reticulum and that are involved in lipid metabolism (Extended Data Fig. 6), consistent with previous reports on other coronaviruses[19]. Together, our quantitative analyses of proteome changes after infection with SARS-CoV-2 revealed host pathways that change after infection and revealed that spliceosome and glycolysis inhibitors are potential therapeutic agents for the treatment of COVID-19.

Kinetic profiling of the infection proteome

To identify additional potential inhibitors of SARS-CoV-2 replication, we determined proteins with abundance trajectories that were similar to the nine detected viral proteins (Fig. 4a and Extended Data Fig. 7a–d; measurement depth does not allow us to distinguish polyprotein from processed protein). We compared the distance and false-discovery rate (FDR) for each protein to an averaged viral protein profile and performed gene ontology analysis (459 proteins with a FDR-adjusted $P < 0.01$). We identified a major cluster of metabolic pathways, which consisted of diverse nucleic acid metabolism sub-pathways (Fig. 4b and Supplementary Table 5). Coronavirus replication depends on the availability of cellular nucleotide pools[20]. Compounds that interfere with nucleic acid metabolism, such as ribavirin, have been used in the past to inhibit viral replication[21]. We tested the effect of the inhibition of nucleotide synthesis on SARS-CoV-2 replication in cells. Ribavirin, which inhibits inosine monophosphate dehydrogenase (IMPDH), the rate-limiting enzyme in de novo synthesis of guanosine nucleotides, inhibited SARS-CoV-2 replication at low micromolar and clinically achievable concentrations[22] (Fig. 4c and Extended Data Fig. 7e), consistent with data in monkey cells[23]. Inhibition of IMPDH had been shown to prevent replication of coronaviruses HCoV-43, CoV-NL63 and MERS-CoV but not of SARS-CoV[24]. Considering the clinical use of ribavirin to treat viruses such as hepatitis C and respiratory syncytial virus[25,26], it may be regarded as a treatment option for patients with COVID-19.

Components of the proteostasis machinery also acted in a comparable manner to the viral proteins (Extended Data Fig. 3e), consistent with the perturbation of host cell proteostasis due to the higher folding load, which is the results of the high translation rates of viral proteins. We therefore tested the effects of proteostasis perturbation on SARS-CoV-2 replication using NMS-873, a small-molecule inhibitor of the AAA ATPase p97. p97 is a key component of proteostasis, which affects protein degradation, membrane fusion, vesicular trafficking and disassembly of stress granules[27]. NMS-873 has previously been shown to inhibit the replication of influenza A and B[28]. We show that NMS-873 inhibits SARS-CoV-2 replication at low nanomolar concentrations (Fig. 4d and Extended Data Fig. 7f). In summary, analyses of the effects of SARS-CoV-2 infection on the host cell proteome revealed major readjustments in cellular function, particularly of splicing, proteostasis and nucleotide biosynthesis. Compounds that modulate these pathways prevented SARS-CoV-2 replication in human cells.

Discussion

Identifying and testing potential drug candidates for the treatment of COVID-19 is of high priority. So far, only limited data have been obtained that describes the response of the host cell to infection with SARS-CoV-2, preventing a databased assessment of treatment options. We describe a SARS-CoV-2 cell-infection system that can be used to determine the changes in host cell pathways after infection, which result from host cell (antiviral) responses or viral effector proteins, and assess inhibitors. At the MOI used, most of the cells were infected, enabling us to determine global changes across the whole cell population with minimal ratio compression from uninfected cells. We found that the expression of the previously described SARS-CoV-2 entry receptor ACE2 was mildly reduced after infection (Extended Data Fig. 8), consistent with a drop in ACE2 levels due to shedding by ADAM10 that has been described for SARS-CoV[29]. Temporal proteome and translatome proteomics showed limited translation attenuation and revealed core cellular pathways that were modulated after infection (Fig. 2). For SARS-CoV and other RNA viruses, severe effects on translation have been described[30]. Our observations suggest that SARS-CoV-2 reshapes host cell translation, probably by increasing the production of translation machinery components to compensate for the inhibition of host cell translation. We tested two translation inhibitors with different modes of action and found that these to efficiently prevented viral replication in cells. These findings encourage further testing of translation inhibitors for the prevention of SARS-CoV-2 replication.

Overall, our proteomics analyses highlight cellular pathways for therapeutic interventions, including a marked increase in components of the spliceosome, proteostasis and nucleotide biosynthesis pathways. This enabled us to assess new drug targets, which were based on the behaviour of SARS-CoV-2 in human cells and which had not previously been tested with other coronaviruses. Some of the inhibitors, for which we observed inhibition of SARS-CoV-2, are approved drugs, such as ribavirin, or are undergoing clinical trials (that is, 2-deoxy-D-glucose). A clinical trial for ribavirin was recently initiated (ClinicalTrials.gov; NCT04356677).

Analysis of pathways that are important for viral infection in cells by combinatorial profiling using proteomics and translatomics represents a useful tool to propose likely pathways that inhibit viral replication. Determining possible compounds based on the specific cellular infection profile of the virus enables an unbiased determination of potential drug targets. Here, using such an experimental-data-driven approach, we identified several drugs that prevent SARS-CoV-2 replication in cells for further testing in clinical settings for the treatment of COVID-19.

Online content

Any methods, additional references, Nature Research reporting summaries, source data, extended data, supplementary information, acknowledgements, peer review information; details of author contributions and competing interests; and statements of data and code availability are available at https://doi.org/10.1038/s41586-020-2332-7.

1. Zhu, N. et al. A novel coronavirus from patients with pneumonia in China, 2019. *N. Engl. J. Med.* **382**, 727–733 (2020).
2. Zhao, S. et al. Preliminary estimation of the basic reproduction number of novel coronavirus (2019-nCoV) in China, from 2019 to 2020: a data-driven analysis in the early phase of the outbreak. *Int. J. Infect. Dis.* **92**, 214–217 (2020).
3. Klann, K., Tascher, G. & Münch, C. Functional translatome proteomics reveal converging and dose-dependent regulation by mTORC1 and eIF2α. *Mol. Cell* **77**, 913–925 (2020).
4. Jin, Y.-H. et al. A rapid advice guideline for the diagnosis and treatment of 2019 novel coronavirus (2019-nCoV) infected pneumonia (standard version). *Mil. Med. Res.* **7**, 4 (2020).
5. She, J. et al. 2019 novel coronavirus of pneumonia in Wuhan, China: emerging attack and management strategies. *Clin. Transl. Med.* **9**, 19 (2020).
6. Hoehl, S. et al. Evidence of SARS-CoV-2 infection in returning travelers from Wuhan, China. *N. Engl. J. Med.* **382**, 1278–1280 (2020).
7. Xiao, F. et al. Evidence for gastrointestinal infection of SARS-CoV-2. *Gastroenterology* **158**, 1831–1833 (2020).
8. Young, B. E. et al. Epidemiologic features and clinical course of patients infected with SARS-CoV-2 in Singapore. *J. Am. Med. Assoc.* **323**, 1488–1494 (2020).
9. Cinatl, J. et al. Treatment of SARS with human interferons. *Lancet* **362**, 293–294 (2003).
10. Kamitani, W., Huang, C., Narayanan, K., Lokugamage, K. G. & Makino, S. A two-pronged strategy to suppress host protein synthesis by SARS coronavirus Nsp1 protein. *Nat. Struct. Mol. Biol.* **16**, 1134–1140 (2009).
11. Shen, L. et al. High-throughput screening and identification of potent broad-spectrum inhibitors of coronaviruses. *J. Virol.* **93**, e00023-19 (2019).
12. Pillaiyar, T., Meenakshisundaram, S. & Manickam, M. Recent discovery and development of inhibitors targeting coronaviruses. *Drug Discov. Today* **25**, 668–688 (2020).
13. Neuman, B. W. et al. Proteomics analysis unravels the functional repertoire of coronavirus nonstructural protein 3. *J. Virol.* **82**, 5279–5294 (2008).
14. Jourdan, S. S., Osorio, F. & Hiscox, J. A. An interactome map of the nucleocapsid protein from a highly pathogenic North American porcine reproductive and respiratory syndrome virus strain generated using SILAC-based quantitative proteomics. *Proteomics* **12**, 1015–1023 (2012).
15. Song, T. et al. Quantitative interactome reveals that porcine reproductive and respiratory syndrome virus nonstructural protein 2 forms a complex with viral nucleocapsid protein and cellular vimentin. *J. Proteomics* **142**, 70–81 (2016).
16. Emmott, E. et al. The cellular interactome of the coronavirus infectious bronchitis virus nucleocapsid protein and functional implications for virus biology. *J. Virol.* **87**, 9486–9500 (2013).
17. Cretu, C. et al. Structural basis of splicing modulation by antitumor macrolide compounds. *Mol. Cell* **70**, 265–273 (2018).
18. Gualdoni, G. A. et al. Rhinovirus induces an anabolic reprogramming in host cell metabolism essential for viral replication. *Proc. Natl. Acad. Sci. USA* **115**, E7158–E7165 (2018).
19. Yan, B. et al. Characterization of the lipidomic profile of human coronavirus-infected cells: implications for lipid metabolism remodeling upon coronavirus replication. *Viruses* **11**, 73 (2019).
20. Pruijssers, A. J. & Denison, M. R. Nucleoside analogues for the treatment of coronavirus infections. *Curr. Opin. Virol.* **35**, 57–62 (2019).
21. Saijo, M. et al. Inhibitory effect of mizoribine and ribavirin on the replication of severe acute respiratory syndrome (SARS)-associated coronavirus. *Antiviral Res.* **66**, 159–163 (2005).
22. Wu, L. S. et al. Population pharmacokinetic modeling of plasma and intracellular ribavirin concentrations in patients with chronic hepatitis c virus infection. *Antimicrob. Agents Chemother.* **59**, 2179–2188 (2015).
23. Wang, M. et al. Remdesivir and chloroquine effectively inhibit the recently emerged novel coronavirus (2019-nCoV) in vitro. *Cell Res.* **30**, 269–271 (2020).
24. Cinatl, J. et al. Glycyrrhizin, an active component of liquorice roots, and replication of SARS-associated coronavirus. *Lancet* **361**, 2045–2046 (2003).
25. Martin, P. & Jensen, D. M. Ribavirin in the treatment of chronic hepatitis C. *J. Gastroenterol. Hepatol.* **23**, 844–855 (2008).
26. Marcelin, J. R., Wilson, J. W. & Razonable, R. R. Oral ribavirin therapy for respiratory syncytial virus infections in moderately to severely immunocompromised patients. *Transpl. Infect. Dis.* **16**, 242–250 (2014).
27. Ye, Y., Tang, W. K., Zhang, T. & Xia, D. A mighty "protein extractor" of the cell: structure and function of the p97/CDC48 ATPase. *Front. Mol. Biosci.* **4**, 39 (2017).
28. Zhang, J. et al. Identification of NMS-873, an allosteric and specific p97 inhibitor, as a broad antiviral against both influenza A and B viruses. Eur. *J. Pharm. Sci.* **133**, 86–94 (2019).
29. Jia, H. P. et al. Ectodomain shedding of angiotensin converting enzyme 2 in human airway epithelia. *Am. J. Physiol. Lung Cell. Mol. Physiol.* **297**, L84–L96 (2009).
30. Narayanan, K. et al. Severe acute respiratory syndrome coronavirus nsp1 suppresses host gene expression, including that of type I interferon, in infected cells. *J. Virol.* **82**, 4471–4479 (2008).

Methods

Cell culture

Human Caco-2 cells, derived from colon carcinoma, were obtained from the Deutsche Sammlung von Mikroorganismen und Zellkulturen (DSMZ; AC169). The cell-authentification certificate from DSMZ is available and cells have been tested negative for mycoplasma infection.

Cells were grown at 37 °C in minimal essential medium (MEM) supplemented with 10% fetal bovine serum (FBS) and containing 100 IU/ml penicillin and 100 µg/ml streptomycin. All culture reagents were purchased from Sigma.

Virus preparation

SARS-CoV-2 was isolated from samples of travellers returning from Wuhan (China) to Frankfurt (Germany) using the human colon carcinoma cell line Caco-2 as described previously[6]. SARS-CoV-2 stocks used in the experiments had undergone one passage on Caco-2 cells and were stored at −80 °C. Virus titres were determined as $TCID_{50}$/ml in confluent cells in 96-well microtitre plates.

Quantification of viral RNA

SARS-CoV-2 RNA from cell-culture supernatant samples was isolated using AVL buffer and the QIAamp Viral RNA Kit (Qiagen) according to the manufacturer's instructions. Absorbance-based quantification of the RNA yield was performed using the Genesys 10S UV-Vis Spectrophotometer (Thermo Scientific). RNA was subjected to OneStep qRT–PCR analysis using the Luna Universal One-Step RT-qPCR Kit (New England Biolabs) and a CFX96 Real-Time System, C1000 Touch Thermal Cycler. Primers were adapted from the WHO protocol[31] targeting the open-reading frame for RNA-dependent RNA polymerase (RdRp): RdRP_SARSr-F2 (GTGARATGGTCATGTGTGGCGG) and RdRP_SARSr-R1 (CARATGTTAAASACACTATTAGCATA) using 0.4 µM per reaction. Standard curves were created using plasmid DNA (pEX-A128-RdRP) that contained the corresponding amplicon regions of the *RdRP* target sequence according to GenBank accession number NC_045512. For each condition three biological replicates were used. Mean ± s.d. were calculated for each group.

Antiviral and cell viability assays

Confluent layers of Caco-2 cells in 96-well plates were infected with SARS-CoV-2 at a MOI of 0.01. Virus was added together with drugs and incubated in MEM supplemented with 2% FBS with different drug dilutions. Cytopathogenic effects were assessed visually 48 h after infection. To assess the effects of drugs on Caco-2 cell viability, confluent cell layers were treated with different drug concentration in 96-well plates. The viability was measured using the Rotitest Vital (Roth) according to the manufacturer's instructions. Data for each condition were collected for at least three biological replicates. For dose–response curves, data were fitted with all replicates using OriginPro 2020 with the following equation:

$$y = A1 + \frac{A2 - A1}{1 + 10^{(\log x_0 - x)p}}$$

IC_{50} values were generated by Origin together with metrics for curve fits.

Detection of the nucleoprotein of SARS-CoV-2

Viral infection was assessed by staining of SARS-CoV-2 nucleoprotein. In brief, cells were fixed with acetone:methanol (40:60) solution and immunostaining was performed using a monoclonal antibody directed against the nucleoprotein of SARS-CoV-2 (1:500, Sinobiological, 40143-R019-100ul), which was detected with a peroxidase-conjugated anti-rabbit secondary antibody (1:1,000, Dianova), followed by addition of AEC substrate.

Isotope labelling and cell lysis

In brief, 2 h before collection, cells were washed twice with warm PBS to remove interfering medium and cultured for an additional 2 h with DMEM medium containing 84 mg/l L-arginine ($^{13}C6^{15}N4$ (R10); Cambridge Isotope Laboratories, CNLM-539-H) and 146 mg/l L-lysine ($^{13}C6^{15}N2$ (K8), Cambridge Isotope Laboratories, CNLM-291-H) to label nascent proteins. After labelling culture, the cells were washed three times with warm PBS and lysed with 95 °C hot lysis buffer (100 mM EPPS pH 8.2, 2% sodium deoxycholate, 1 mM TCEP, 4 mM 2-chloracetamide, protease inhibitor tablet mini EDTA-free (Roche)). Samples were then incubated for an additional 5min at 95 °C, followed by sonication for 30 s and a further 10-min incubation at 95 °C.

Sample preparation for LC–MS/MS

Samples were prepared as previously described[3]. In brief, proteins were precipitated using methanol:chloroform precipitation and resuspended in 8 M urea and 10 mM EPPS pH 8.2. Isolated proteins were digested with 1:50 w/w LysC (Wako Chemicals) and 1:100 w/w trypsin (Promega, Sequencing-grade) overnight at 37 °C after dilution to a final urea concentration of 1 M. Digests were then acidified (pH 2–3) using TFA. Peptides were purified using C18 (50 mg) SepPak columns (Waters) as previously described. Desalted peptides were dried and 25 µg of peptides were resuspended in TMT-labelling buffer (200 mM EPPS pH 8.2, 10% acetonitrile). Peptides were subjected to TMT labelling with 1:2 peptide TMT ratio (w/w) for1 h at room temperature. The labelling reaction was quenched by addition of hydroxylamine to a final concentration of 0.5% and incubation at room temperature for an additional 15 min. Labelled peptides were pooled and subjected to high pH reverse Phase fractionation with the HpH RP Fractionation kit (ThermoFisher Scientific) following the manufacturer's instructions. All multiplex reactions were mixed with a bridge channel, which consists of a control sample labelled in one reaction and split to all multiplexed reactions in equimolar amounts.

LC–MS/MS

Peptides were resuspended in 0.1% formic acid and separated on an Easy nLC 1200 (ThermoFisher Scientific) and a 22-cm-long, 75-µm-inner-diameter fused-silica column, which had been packed in house with 1.9-µm C18 particles (ReproSil-Pur, Dr. Maisch), and kept at 45 °C using an integrated column oven (Sonation). Peptides were eluted by a nonlinear gradient from 5–38% acetonitrile over 120 min and directly sprayed into a QExactive HF mass spectrometer equipped with a nanoFlex ion source (ThermoFisher Scientific) at a spray voltage of 2.3 kV. Full-scan MS spectra (350–1,400 m/z) were acquired at a resolution of 120,000 at m/z 200, a maximum injection time of 100 ms and an AGC target value of 3×10^6. Up to 20 most intense peptides per full scan were isolated using a 1 Th window and fragmented using higher-energy collisional dissociation (normalized collision energy of 35). MS/MS spectra were acquired with a resolution of 45,000 at m/z 200, a maximum injection time of 80 ms and an AGC target value of 1×10^5. Ions with charge states of 1 and >6 as well as ions with unassigned charge states were not considered for fragmentation. Dynamic exclusion was set to 20 s to minimize repeated sequencing of already acquired precursors.

LC–MS/MS data analysis

Raw files were analysed using Proteome Discoverer 2.4 software (ThermoFisher Scientific). Spectra were selected using default settings and database searches performed using SequestHT node in Proteome Discoverer. Database searches were performed against a trypsin-digested *Homo sapiens* SwissProt database, the SARS-CoV-2 database (Uniprot pre-release) and FASTA files of common contaminants ('contaminants.fasta' provided with MaxQuant) for quality control. Fixed modifications were set as TMT6 at the N terminus and carbamidomethyl at cysteine residues. One search node was

set up to search with TMT6 (K) and methionine oxidation as static modifications to search for light peptides and one search node was set up with TMT6+K8 (K, +237.177), Arg10 (R, +10.008) and methionine oxidation as static modifications to identify heavy peptides. Searches were performed using Sequest HT. After each search, posterior error probabilities were calculated and peptide spectrum matches (PSMs) filtered using Percolator using default settings. Consensus Workflow for reporter ion quantification was performed with default settings, except the minimal signal-to-noise ratio was set to 5. Results were then exported to Excel files for further processing. For proteome quantification all PSMs were summed intensity normalized, followed by IRS[32] and TMM[33] normalization and peptides corresponding to a given UniProt accession were summed, including all modification states.

For translatome measurements, Excel files were processed in Python, as previously described[3]. Python 3.6 was used together with the following packages: pandas 0.23.4[34], numpy 1.15.4[35] and scipy 1.3.0. Excel files with normalized PSM data were read in and each channel was normalized to the lowest channel based on total intensity. For each peptide sequence, all possible modification states containing a heavy label were extracted and the intensities for each channel were averaged between all modified peptides. Baseline subtraction was performed by subtracting the measured intensities for the non-SILAC-labelled sample from all other values. Negative intensities were treated as zero. The heavy label incorporation at the protein level was calculated by summing the intensities of all peptide sequences belonging to one unique protein accession. These values were combined with the standard protein output of Proteome Discoverer 2.4 to add annotation data to the master protein accessions.

Hierarchical clustering and profile comparison

Hierarchical cluster analysis and comparison with viral protein profiles for all samples was performed using Perseus[36] software package (version 1.6.5.0) after centring and scaling of data (*Z*-scores). *K*-means pre-processing was performed with a cluster number of 12 and a maximum of 10 iterations. For the comparison of profiles, the viral profiles were *Z*-scored and averaged to generate reference profile. Profiles of all proteins were compared to the reference (Pearson), distances and FDRs were computed.

Network analysis

For network analysis, Cytoscape 3.7.1[37] software was used with the BiNGO 3.0.3[38] plugin for gene ontology analysis, EnrichmentMap 3.1.0[39] and ReactomeFI 6.1.0[40]. For gene ontology analyses, gene sets were extracted from data as indicated using fold change and significance cut-offs.

Statistical analysis

No statistical methods were used to predetermine sample size. Significance was, unless stated otherwise, tested using unpaired two-sided Student's *t*-tests with equal variance assumed. Statistical analysis was performed using OriginPro 2020 analysis software. For network and gene ontology analysis all statistical computations were performed by the corresponding packages.

Reporting summary

Further information on research design is available in the Nature Research Reporting Summary linked to this paper.

Data availability

The LC–MS/MS proteomics data have been deposited in the ProteomeXchange Consortium via the PRIDE[41] partner repository with the dataset identifier PXD017710. We furthermore created a webpage (http://corona.papers.biochem2.com/), in which the presented data is visualized for easy access of the published data.

31. Corman, V. M. et al. Detection of 2019 novel coronavirus (2019-nCoV) by real-time RT-PCR. *Euro Surveill.* **25**, 2000045 (2020).
32. Plubell, D. L. et al. Extended multiplexing of tandem mass tags (TMT) labeling reveals age and high fat diet specific proteome changes in mouse epididymal adipose tissue. *Mol. Cell. Proteomics* **16**, 873–890 (2017).
33. Robinson, M. D. & Oshlack, A. A scaling normalization method for differential expression analysis of RNA-seq data. *Genome Biol.* **11**, R25 (2010).
34. McKinney, W. Data structures for statistical computing in Python. In *Proc. 9th Python in Science Conference* 56–61 (SCIPY, 2010).
35. van der Walt, S., Colbert, S. C. & Varoquaux, G. The NumPy Array: a structure for efficient numerical computation. *Comput. Sci. Eng.* **13**, 22–30 (2011).
36. Tyanova, S. et al. The Perseus computational platform for comprehensive analysis of (prote)omics data. *Nat. Methods* **13**, 731–740 (2016).
37. Shannon, P. et al. Cytoscape: a software environment for integrated models of biomolecular interaction networks. *Genome Res.* **13**, 2498–2504 (2003).
38. Maere, S., Heymans, K. & Kuiper, M. BiNGO: a Cytoscape plugin to assess overrepresentation of gene ontology categories in biological networks. *Bioinformatics* **21**, 3448–3449 (2005).
39. Merico, D., Isserlin, R., Stueker, O., Emili, A. & Bader, G. D. Enrichment map: a network-based method for gene-set enrichment visualization and interpretation. *PLoS ONE* **5**, e13984 (2010).
40. Wu, G. & Haw, R. Functional interaction network construction and analysis for disease discovery. *Methods Mol. Biol.* **1558**, 235–253 (2017).
41. Perez-Riverol, Y. et al. The PRIDE database and related tools and resources in 2019: improving support for quantification data. *Nucleic Acids Res.* **47**, D442–D450 (2019).
42. Chen, J.-Y. et al. Interaction between SARS-CoV helicase and a multifunctional cellular protein (Ddx5) revealed by yeast and mammalian cell two-hybrid systems. *Arch. Virol.* **154**, 507–512 (2009).
43. Wong, H.-H. et al. Genome-wide screen reveals valosin-containing protein requirement for coronavirus exit from endosomes. *J. Virol.* **89**, 11116–11128 (2015).

Acknowledgements We thank C. Pallas and L. Stegmann for experimental support and G. Tascher and M. Adrian-Allgood for proteomics support. J.C. acknowledges funding by the Hilfe für krebskranke Kinder Frankfurt and the Frankfurter Stiftung für krebskranke Kinder. C.M. was supported by the European Research Council under the European Union's Seventh Framework Programme (ERC StG 803565), CRC 1177 and the Emmy Noether Programme of the Deutsche Forschungsgemeinschaft (DFG, MU 4216/1-1), the Johanna Quandt Young Academy at Goethe and an Aventis Foundation Bridge Award.

Author contributions B.K., J.C. and C.M. conceived the study. D.B. carried out tissue-culture work, virus experiments and cytotoxicity assays. K.K. performed proteomic analyses of viral infection kinetics and bioinformatics analyses. M.W. carried out quantitative PCRs. B.K. analysed literature for established inhibitors in viral therapy. D.K. developed the online tool for data visualization. S.C., J.C. and C.M. supervised the work. K.K., J.C. and C.M. wrote the initial manuscript, with contributions from all authors. All authors read and approved the final manuscript.

Competing interests The authors declare no competing interests.

Additional information

Supplementary information is available for this paper at https://doi.org/10.1038/s41586-020-2332-7.

Correspondence and requests for materials should be addressed to J.C. or C.M.

Peer review information *Nature* thanks Ileana M. Cristea, Michael P. Weekes and the other, anonymous, reviewer(s) for their contribution to the peer review of this work.

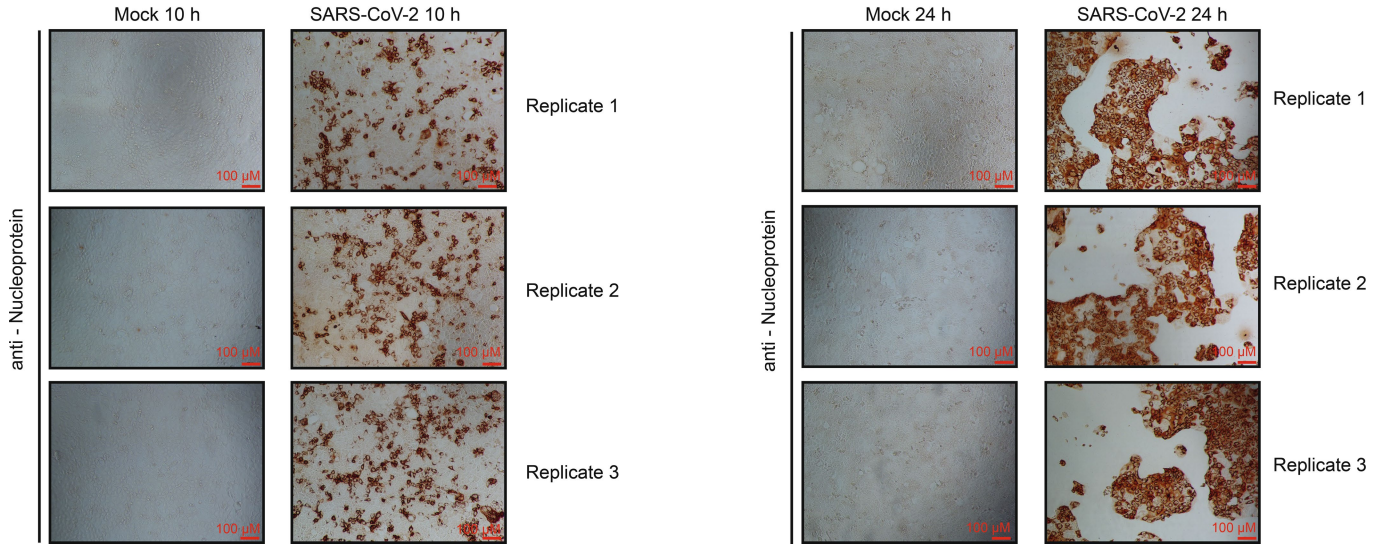

Extended Data Fig. 1 | Viral protein accumulation in Caco-2 cells after SARS-CoV-2 infection. Cells were infected with SARS-CoV-2 at a MOI of 1 and incubated for 10 or 24 h. Cells were fixed and stained with an antibody against the nucleoprotein of SARS-CoV-2, followed by staining with a peroxidase-conjugated secondary antibody and the addition of substrate. Three independent biological samples are shown. $n = 3$ independent biological samples.

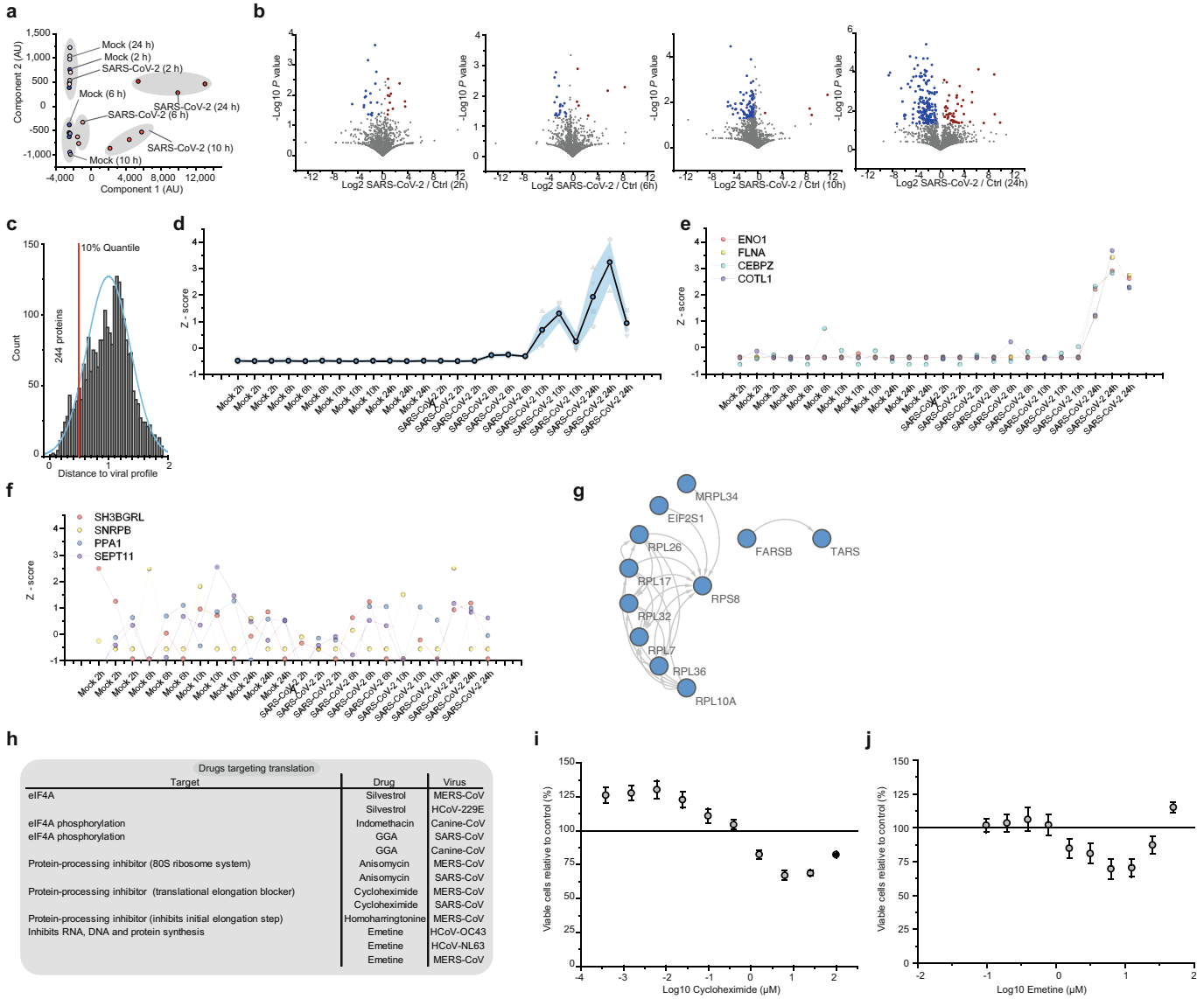

Target	Drug	Virus
eIF4A	Silvestrol	MERS-CoV
	Silvestrol	HCoV-229E
eIF4A phosphorylation	Indomethacin	Canine-CoV
eIF4A phosphorylation	GGA	SARS-CoV
	GGA	Canine-CoV
Protein-processing inhibitor (80S ribosome system)	Anisomycin	MERS-CoV
	Anisomycin	SARS-CoV
Protein-processing inhibitor (translational elongation blocker)	Cycloheximide	MERS-CoV
	Cycloheximide	SARS-CoV
Protein-processing inhibitor (inhibits initial elongation step)	Homoharringtonine	MERS-CoV
Inhibits RNA, DNA and protein synthesis	Emetine	HCoV-OC43
	Emetine	HCoV-NL63
	Emetine	MERS-CoV

Extended Data Fig. 2 | Translatome analysis of cells infected with SARS-CoV-2. a, Principal component analysis of all replicate translatome measurements. Blue dots and red dots (both shaded according to time after infection) represent different mock controls and SARS-CoV-2 infected samples, respectively. **b**, Volcano plots showing differentially translated genes between infected cells and the mock control group for each time point. $\log_2$-transformed fold changes (FC) are plotted against *P* values (two-sided unpaired Student's *t*-test with equal variance assumed; $n = 3$ independent biological samples). Blue dots indicate significant decrease in translation ($FC < -0.5$, $P < 0.05$), red dots indicate significant increase in translation ($FC > 0.5$, $P < 0.05$). **c**, Histogram of distances from host protein expression profile to viral proteins. Viral protein translation profiles were *Z*-scored, averaged (5 viral proteins) and used as a reference profile to compare to each host protein in dataset. The blue curve shows a distribution curve fitted to data, the red line indicates the top 10% quantile of distances used for pathway analysis (in Fig. 2). **d**, Averaged viral protein-translation *Z*-score profile over all replicate samples (5 viral proteins). Grey shade indicates s.d. of averaged profiles, coloured profiles in the background represent individual viral proteins. **e**, Translation *Z*-score profiles for four example proteins (ENO1, FLNA, CEBPZ and COTL1) following the viral profile from **c**. **f**, Translation *Z*-score profiles for four example proteins (SH3BGRL, SNRPB, PPA1 and SEPT11) that do not follow the viral reference profile. **g**, Network of functional interactions between proteins annotated with function in host translation. Arrows indicate functional interactions. **h**, Drugs targeting host translation that have been used in vitro for treatment of other (that is, non-SARS-CoV-2) coronavirus infections. **i**, **j**, Cytotoxicity assays for different concentrations of cycloheximide (**i**) and emetine (**j**) relative to control. Mean values ± s.d. are plotted ($n = 3$ independent biological samples). Line represents 100% viable cells.

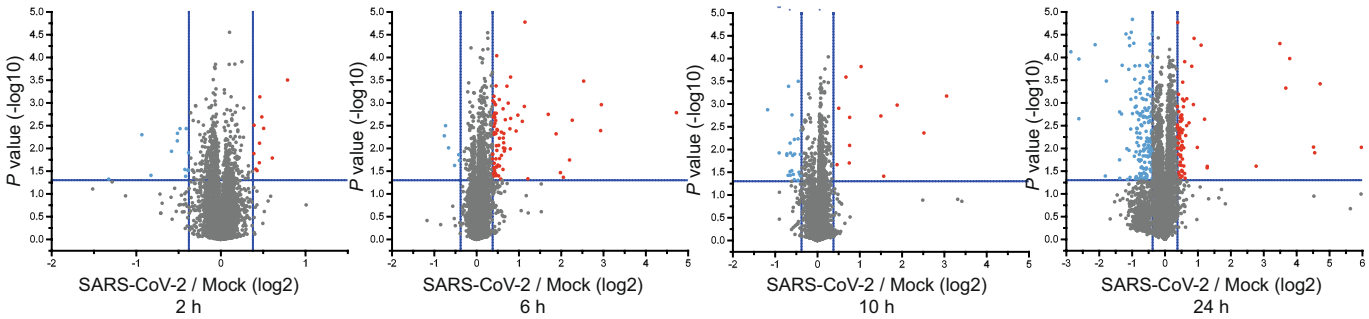

Extended Data Fig. 3 | Volcano plots of the change in total protein levels over time. *P* values have been calculated using a two-sided, unpaired Student's *t*-test with equal variance assumed and were plotted against the $\log_2$-transformed ratio between SARS-CoV-2-infected and mock cells for each time point ($n = 3$ independent biological samples).

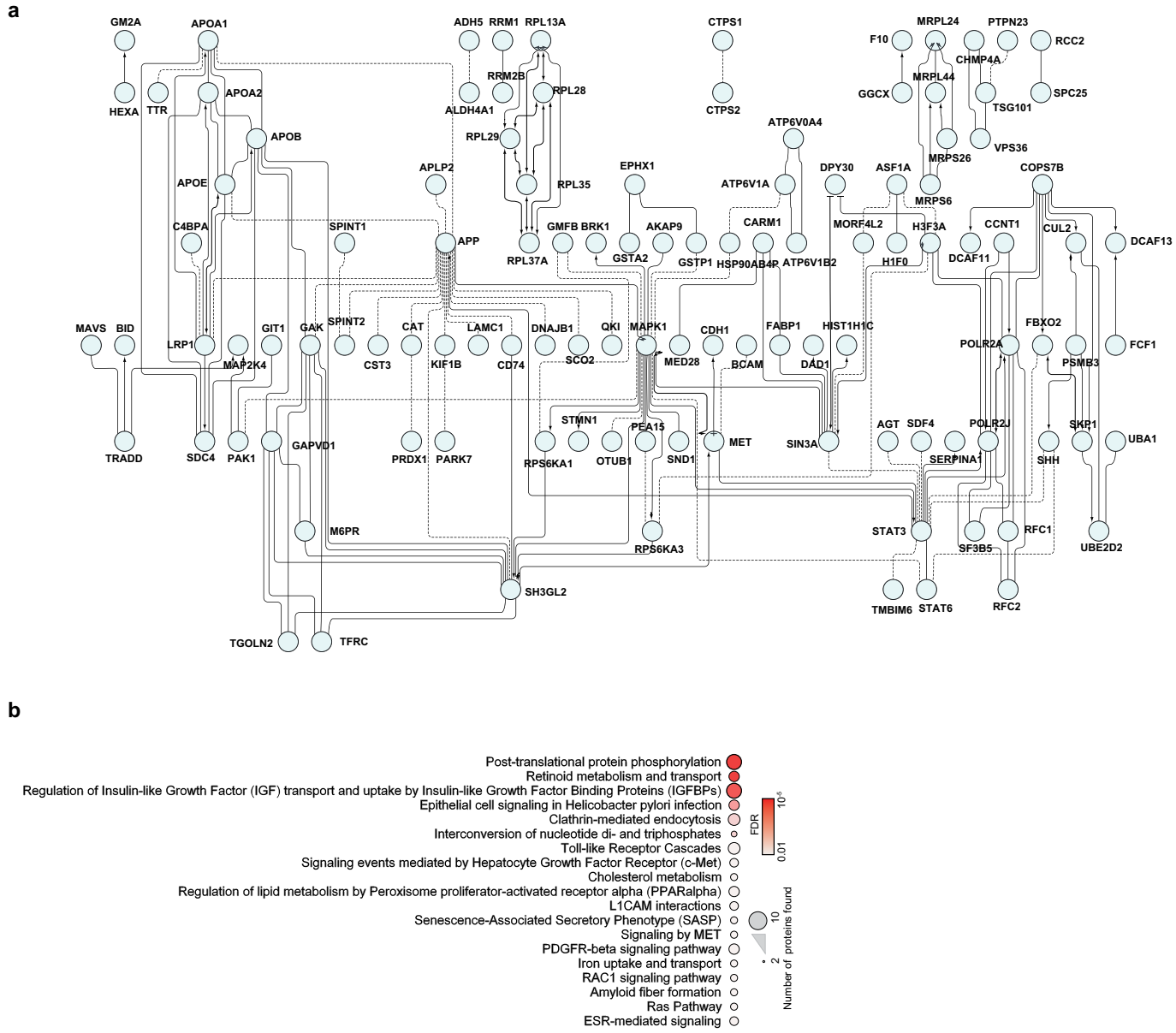

Extended Data Fig. 4 | Network of proteins that are decreased during SARS-CoV-2 infection. a, Proteins belonging to cluster I in Fig. 3a were used for the creation of a functional interaction network. Lines indicate functional interactions. The network was created using the ReactomeFI plugin in Cytoscape, protein names were added in the plugin and the network adjusted by the yFiles Layout algorithm. **b**, ReactomeFI network analysis of proteins downregulated in total protein levels. Circle size represents number of proteins found in the pathway, colour shows the FDR for enrichment.

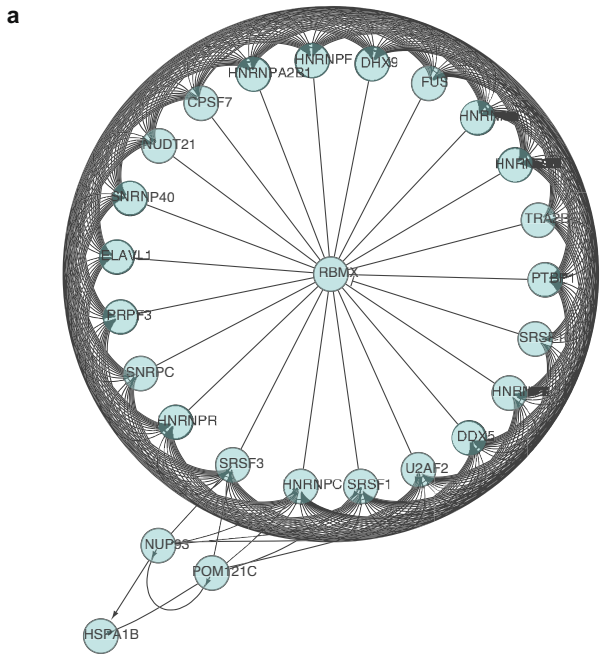

b

Gene	Virus interacting protein	Study
PRPF3 SRSF3 SNRPC	PRRSV (N), IBV (N)	Jourdan et al., Emmott et al.
DDX5	SARS-CoV-1 (nsp3), SARS-CoV-1 (nsp13), PRRSV (N), IBV (N)	Neuman et al., Chen et al., Jourdan et al., Emmott et al.
HNRNPK HNRNPC	SARS-CoV-1 (nsp3), PRRSV (N), IBV (N) SARS-CoV-1 (nsp3), PRRSV (N), IBV (N)	Neuman et al., Jourdan et al., Emmott et al. Neuman et al., Jourdan et al., Emmott et al.
SRSF1 U2AF2 TRA2B SRSF10	PRRSV (N), IBV (N) IBV (N)	Jourdan et al., Emmott et al. Wong et al.
HNRNPA3 SNRNP40	SARS-CoV-1 (nsp3), PRRSV (N), IBV (N)	Neuman et al., Jourdan et al., Emmott et al.
RBMX HSPA1B	PRRSV (N) PRRSV (nsp2)	Jourdan et al. Song et al.

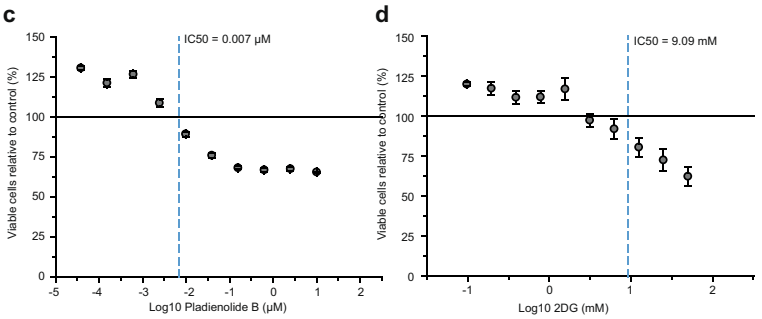

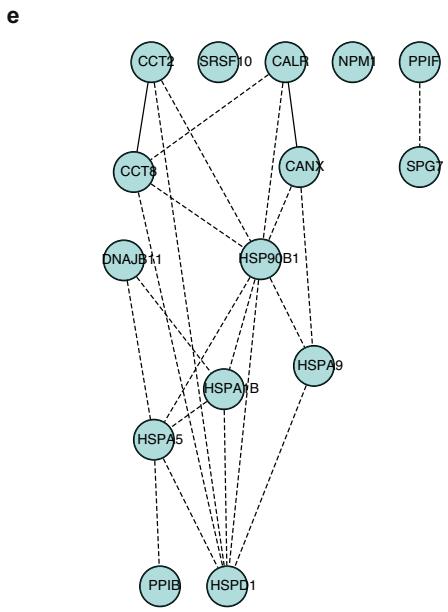

Extended Data Fig. 5 | Networks of proteins that are increased during SARS-CoV-2 infection. a, Network of proteins increased during SARS-CoV-2 infection with spliceosome annotation in reactome pathway analysis. Lines indicate functional interactions. **b**, Table summarizing viral proteins (from different coronaviruses) interacting with various spliceosome components[13–16,42,43]. **c**, **d**, Cytotoxicity assays for different concentrations of pladienolide B (**c**) and 2-deoxy-D-glucose (**d**) relative to control. Mean values ± s.d. ($n = 3$ independent biological samples). Line represents 100% viable cells. **e**, Protein network showing increased proteins during infection with annotation to the molecular function of 'unfolded protein binding'. Lines indicate functional interactions.

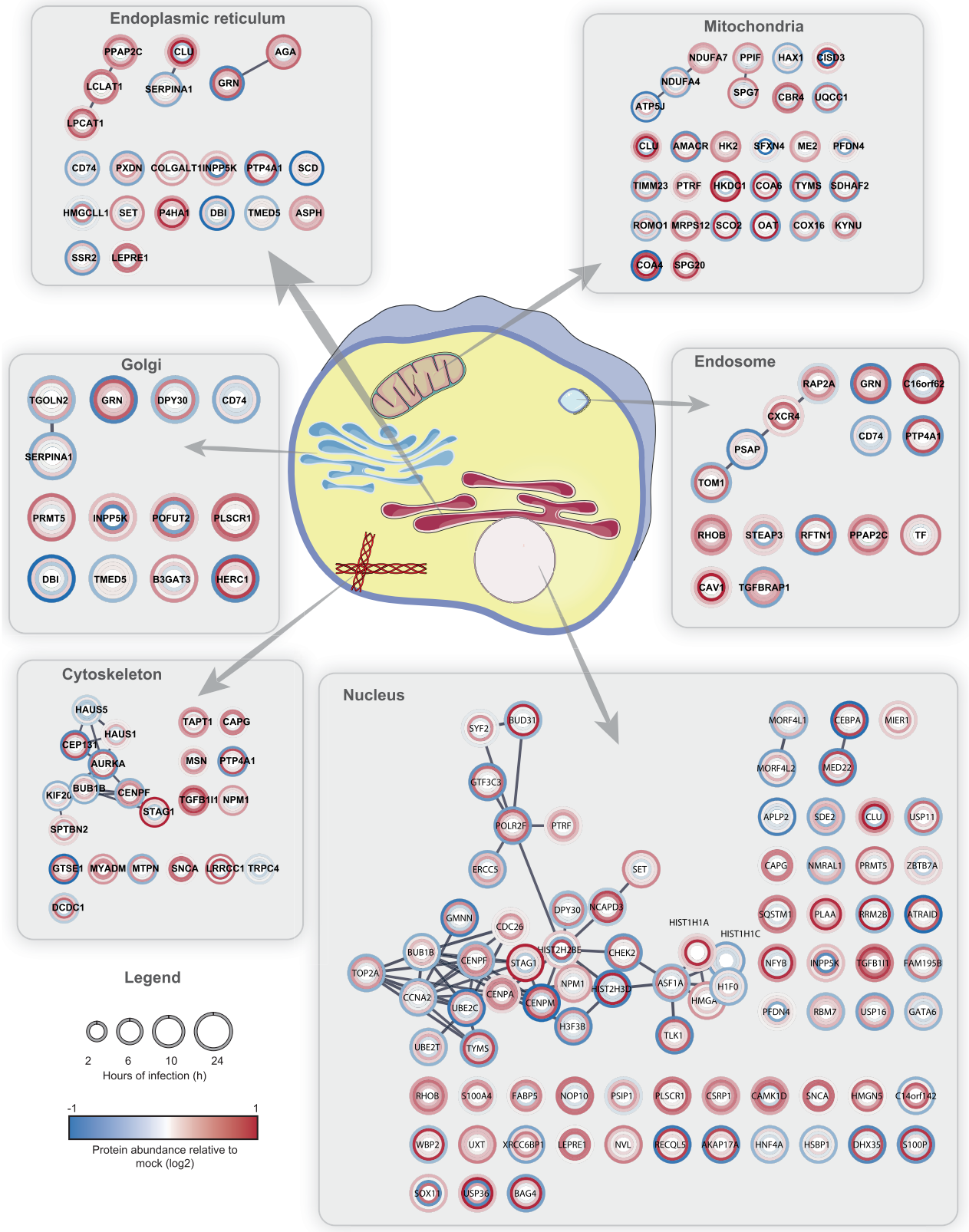

Extended Data Fig. 6 | Compartment analysis of proteins that were significantly regulated. The STRING network was created with proteins filtered for significant changes in protein levels (log_2-transformed fold change; FC > |0.35|, $P < 0.05$) and filtered for each compartment (cut-off maximum of [5]). Circle heat maps represent the log_2-transformed ratios between infected and mock cells at different time points of infection starting from the innermost circle (2 h) to the outer circle (24 h).

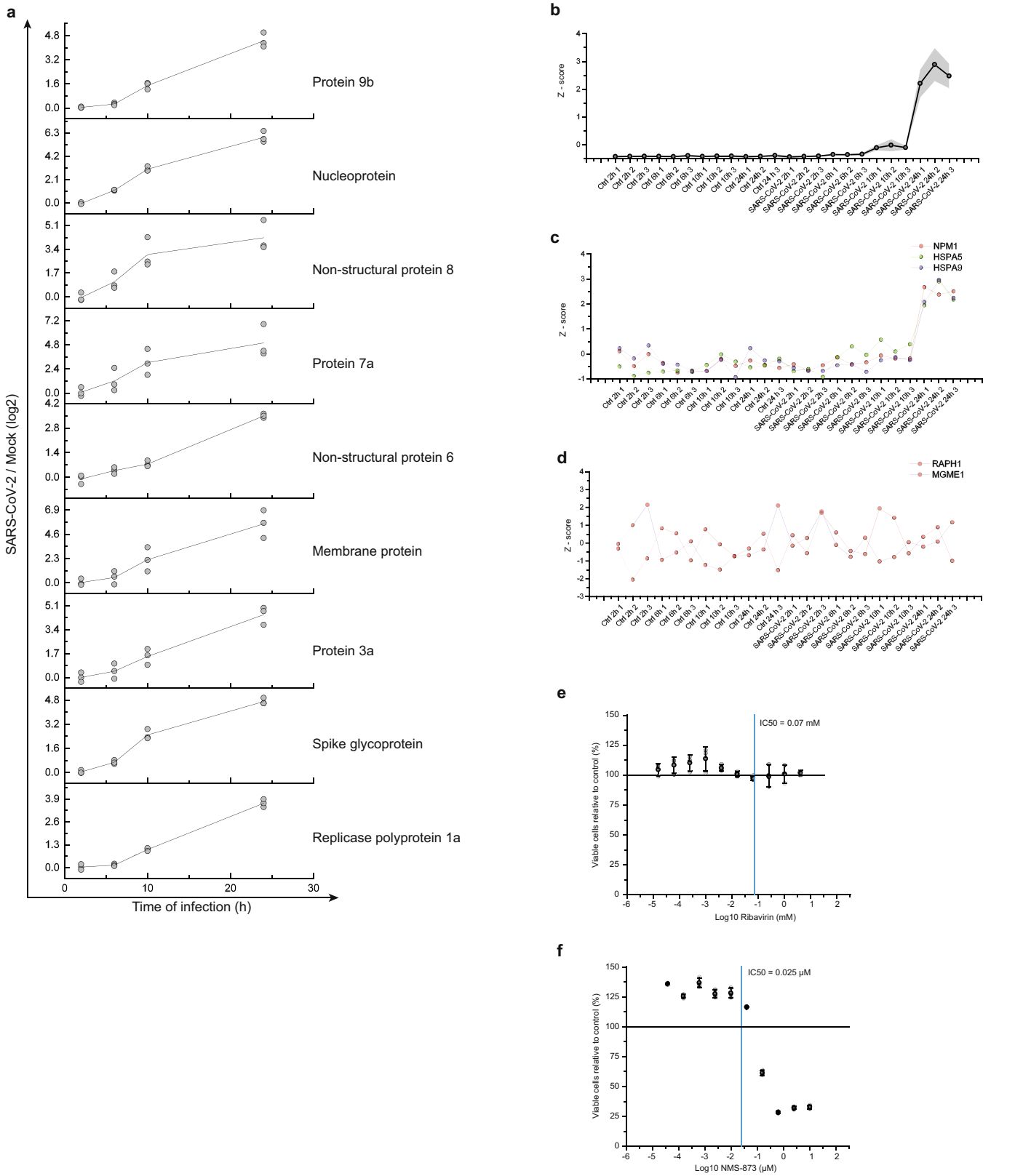

Extended Data Fig. 7 | Viral protein profiles and cytotoxicity assay for nucleic acid and p97 inhibitors. a, Total protein profiles for each viral protein with individual replicate measurements to indicate variation. log_2-transformed ratios of infected versus mock cells are plotted against time of infection. Line indicates averaged curve ($n = 3$ independent biological samples) and dots represent individual measurements. **b**, Averaged reference profile of total protein levels for all viral proteins from **a** (9 viral proteins). Shade indicates s.d. **c**, Example profiles of three proteins (NPM1, HSPA5 and HSPA9) that significantly follow the viral reference profile (Fig. 4). **d**, Example profiles of proteins (RAPH1 and MGME1) that do not follow the viral reference profile. **e**, **f**, Cytotoxicity assays for different concentrations of ribavirin (**e**) and NSM-873 (**f**) relative to control. Mean values ± s.d. are plotted ($n = 3$ independent biological samples). Line represents 100% viable cells.

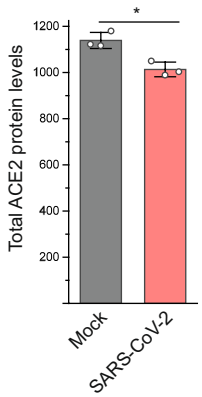

Extended Data Fig. 8 | ACE2 total protein levels after 24 h of infection. Total ACE2 protein levels 24 h after infection compared to mock samples ($n = 3$ independent biological samples). Significance was assessed by an unpaired, two-sided Student's t-test. $^*P < 0.05$.

nature research

Corresponding author(s): Jindrich Cinatl, Christian Münch

Last updated by author(s): Apr 30, 2020

Reporting Summary

Nature Research wishes to improve the reproducibility of the work that we publish. This form provides structure for consistency and transparency in reporting. For further information on Nature Research policies, see Authors & Referees and the Editorial Policy Checklist.

Statistics

For all statistical analyses, confirm that the following items are present in the figure legend, table legend, main text, or Methods section.

n/a	Confirmed
☐	☒ The exact sample size (*n*) for each experimental group/condition, given as a discrete number and unit of measurement
☐	☒ A statement on whether measurements were taken from distinct samples or whether the same sample was measured repeatedly
☐	☒ The statistical test(s) used AND whether they are one- or two-sided *Only common tests should be described solely by name; describe more complex techniques in the Methods section.*
☒	☐ A description of all covariates tested
☐	☒ A description of any assumptions or corrections, such as tests of normality and adjustment for multiple comparisons
☐	☒ A full description of the statistical parameters including central tendency (e.g. means) or other basic estimates (e.g. regression coefficient) AND variation (e.g. standard deviation) or associated estimates of uncertainty (e.g. confidence intervals)
☒	☐ For null hypothesis testing, the test statistic (e.g. *F*, *t*, *r*) with confidence intervals, effect sizes, degrees of freedom and *P* value noted *Give P values as exact values whenever suitable.*
☒	☐ For Bayesian analysis, information on the choice of priors and Markov chain Monte Carlo settings
☒	☐ For hierarchical and complex designs, identification of the appropriate level for tests and full reporting of outcomes
☒	☐ Estimates of effect sizes (e.g. Cohen's *d*, Pearson's *r*), indicating how they were calculated

Our web collection on statistics for biologists contains articles on many of the points above.

Software and code

Policy information about availability of computer code

Data collection	Tune 2.9-290033/2.9.0.2926, Xcalibur 4.0
Data analysis	Microsoft Excel 2016, OriginPro 2020, Proteome Discoverer 2.4, Perseus 1.6.5.0., Python 3.6, numpy 1.15.4, scipy 1.3.0,pandas 0.23.4, Cytoscape 3.7.1, BiNGO 3.0.3, EnrichmentMap 3.1.0, ReactomeFI 6.1.0

For manuscripts utilizing custom algorithms or software that are central to the research but not yet described in published literature, software must be made available to editors/reviewers. We strongly encourage code deposition in a community repository (e.g. GitHub). See the Nature Research guidelines for submitting code & software for further information.

Data

Policy information about availability of data

All manuscripts must include a data availability statement. This statement should provide the following information, where applicable:

- Accession codes, unique identifiers, or web links for publicly available datasets
- A list of figures that have associated raw data
- A description of any restrictions on data availability

All mass spectrometry data is available via the PRIDE repository under the accession PXD017710 and processed data under http://corona.papers.biochem2.com/.

Field-specific reporting

Please select the one below that is the best fit for your research. If you are not sure, read the appropriate sections before making your selection.

☒ Life sciences ☐ Behavioural & social sciences ☐ Ecological, evolutionary & environmental sciences

Life sciences study design

All studies must disclose on these points even when the disclosure is negative.

Sample size	Sample size was chosen balancing technical capacities during large scale proteomic experiments and statistical power. For each analysis at least 3 independent biological replicates have been used.
Data exclusions	No data has been excluded from analysis.
Replication	Reproducibility of results has been assessed by at least three independent biological replicates and was tested by statistical tests as stated in methods and figure legends.
Randomization	Experiments have been carried out using cell culture systems, making randomization not necessary. To control technical covariates, technical sample preparations have been carried out in parallel and samples have been multiplexed, where applicable.
Blinding	Investigators have not been blinded for the experiments, since data analysis and acquistion methods are unbiased by investigator. Data from different groups was analyzed together to ensure same handling and eliminate analysis bias.

Reporting for specific materials, systems and methods

We require information from authors about some types of materials, experimental systems and methods used in many studies. Here, indicate whether each material, system or method listed is relevant to your study. If you are not sure if a list item applies to your research, read the appropriate section before selecting a response.

Materials & experimental systems

n/a	Involved in the study
☐	☒ Antibodies
☐	☒ Eukaryotic cell lines
☒	☐ Palaeontology
☒	☐ Animals and other organisms
☒	☐ Human research participants
☒	☐ Clinical data

Methods

n/a	Involved in the study
☒	☐ ChIP-seq
☒	☐ Flow cytometry
☒	☐ MRI-based neuroimaging

Antibodies

Antibodies used	SARS-CoV-2 Nucleoprotein, Sino Biological, CAT #40143-R019-100ul
Validation	Antibody has been validated by manufacturer for WB,ELISA,IHC-P,FCM,ICC/IF and IP with recombinant SARS-CoV-2 protein.

Eukaryotic cell lines

Policy information about cell lines

Cell line source(s)	Caco-2: DSMZ (ACC. 169)
Authentication	Cell lines have been used without further validation, Authentication certificate was delivered by DSMZ
Mycoplasma contamination	Cell line used in this study was tested negative for mycoplasma infection
Commonly misidentified lines (See ICLAC register)	None

3 Discussion

3.1 Mechanisms of HCC recurrence after DAA treatment

In addition to the suppression of virus replication, antiviral agents may influence properties of non-infected cells. For example, previous studies with HIV protease inhibitors and ribavirin showed that the drugs may display antitumor activity [55,159–161]. However, up to date there is no evidence that any of the currently applied DAAs used for treatment of HCV possess antitumor activity. Conversely, we could show that SOF, a nucleoside analogue and backbone of DAA therapy, induced the activation of EGFR signalling pathway resulting in cell cycle progression and proliferation of hepatoma cells [157].

SOF-mediated activation of the EGFR signalling pathway and its downstream targets in hepatoma cells may not reflect the situation in livers of SOF-treated patients. Therefore, the examination of paired liver biopsies before and after treatment could shed light on the *in vivo* effect of exposure to SOF. However, the limited availability of liver biopsies due to its invasiveness did not allow us to directly access liver tissue samples. To overcome this limitation, we searched for publicly available transcriptional data of IFN-free pre- and post-treatment liver biopsies from cirrhotic patients treated with SOF. Only one data set met these criteria (GSE70799). In this study, Meissner and colleagues focused mainly on differences in the expression of interferon stimulated genes [162]. However, their analysis also showed mitogen activated kinase 1 (MAPK1, also known as ERK-2) and TRIpartite Motif-containing protein 24 (TRIM24) to be upregulated in liver tissues of cirrhotic patients treated with SOF-containing regimen. Importantly, both MAPK1 and TRIM24 are direct part of downstream EGFR signalling pathway promoting EGFR-driven tumorigenesis [163,164]. Notably, the pathways enriched in this network as growth hormone signalling pathway and prolactin signalling pathway share distinct signal transducers with EGFR signalling pathway and are related to EGFR phosphorylation in a ligand-independent manner [165]. Taken together, the analysis of the available transcriptional data from liver tissue of cirrhotic patients treated with SOF displayed the activation of molecules which are part of EGFR signalling pathway and pathways which crosstalk results to EGFR phosphorylation. On that account, SOF-induced activation of EGFR signalling network could be an

additional factor how DAA treatment can contribute to a proliferative signalling in a local pro-oncogenic environment.

The onset of HCC development is mediated through the progression of neoplastic clones whose growth is favoured by an outbalance of stimulatory factors and loss of inhibitory mechanisms. In this regard, the sudden reduction of immunostimulatory signals due to a rapid decrease of HCV viremia can represent such a loss of immune control. Indeed, the abrupt virus elimination appears to cause a temporal immunosuppressive phase due to immune reconstitution. This is also in line with an increase in HBV and herpes virus reactivations in DAA-treated patients [166–168]. As supported by several studies, DAA treatment reduces endogenous IFN signalling resulting in a decreased expression of ISGs [162,169]. Additionally, DAA therapy causes a decrease in natural killer (NK) cell activation followed by a restoration of normal phenotype and function [170]. This is particularly interesting, since NK cells exert antitumor activity by their ability to recognize and lyse transformed cells. Importantly, the rapid decrease in NKG2D activator receptor expression in NK cells after DAA, but not IFN-based therapy was correlated with an increased risk of HCC recurrence [171]. Interestingly, stress-induced EGFR activation can induce the expression of NKG2D ligands on the cell surface. As a results, effected cells are more visible to NK-cell mediated lysis [172]. However, tumour cells are able to escape such recognition by increased shedding of NKG2D ligands. In consequence, soluble NKG2D ligands can downregulate NKG2D from the cell surface of NK cells [173]. This mechanism of immune escape has been already documented in advanced HCC [174]. Moreover, EGFR signalling may upregulate PD-L1 which is mostly associated with HCC progression due to disruption of immune checkpoint [175]. However, if these could be concomitant effects of SOF-induced EGFR signalling has to be further addressed.

After HCV elimination by DAA treatment, not all the cellular signalling pathways previously disturbed by HCV infection are restored. As reported by a recent study, IFN-α-based treatment restored the p53 level while ribavirin, SOF, and ledipasvir showed no effect. Since the loss of p53 function is mediated through several HCV proteins, these results suggest that despite the clearance of viral proteins the HCV-induced phenotype persists [176]. Moreover, this unresolved downregulation of p53 expression after HCV clearance by DAAs could contribute to the risk of HCC development. This is in line with the observation that the recurrence rate of HCC after a viral cure with IFN-α-based therapy is lower in comparison to DAA treatment [55,159,177]. However, the

mechanism of IFN-provided benefits in reduced risk of HCC development is not well understood.

Altogether, our data further reinforces the concerns regarding the administration of SOF-based DAA therapy in a specific population of patients who are at high risk of HCC relapse. These patients probably possess a favourable microenvironment for HCC progression, which persists despite the clearance of HCV. In those patients, even a temporal increase in the activation of EGFR signalling can disturb the fragile balance between stimulatory and inhibitory signals. This could lead to a selection of neoplastic clones and enable them to progress in the context of transitory immunosuppression. Even though several studies tried to identify biomarkers signalling pre-existing risks of HCC relapse, there are no diagnostic markers available to distinguish patients who are at high risk of early HCC recurrence before starting SOF-based antiviral treatment.

3.2 Host-target therapy as supplement to DAA treatment

Even though DAAs efficiently resolve viral infection, they do not revert pro-oncogenic processes and do not restore a normal microenvironment [115]. In this context, combined direct target and host target therapy could be beneficial for the population of patients with ongoing pro-oncogenic signalling and thus with high risk of HCC recurrence. Importantly, host targeted therapy, which supports both the clearance of the virus and prevents hepatocarcinogenesis, is of a high interest.

One of such host targets constitute host cell kinases whose druggable potential has been extensively studied. Host cell kinases play a crucial role in facilitating each step of the HCV replication cycle. Moreover, they are often deregulated and continuously activated in HCV-induced HCC. One of the most promising host cell kinase candidates for drug targeting is EGFR. As one of HCV entry factors, activated EGFR facilitates the assembly of the co-receptor complex, its internalization and fusion with the host membrane [178–181]. The crucial role of ongoing EGFR activation for HCV infection is demonstrated by modulation of EGFR activation by HCV NS5A protein. It has been documented that NS5A disturbs EGFR degradation which results in prolonged EGFR signalling [182,183]. Based on multiple evidence, there is no doubt that the ongoing activation of EGFR signalling is one of the key drivers of carcinogenesis. On that account, several small molecules or antibodies targeting EGFR have been developed and introduced in clinical use. Particularly, erlotinib has been shown to regress fibrosis and inhibit HCC development in rodent models of cirrhosis-driven HCC [184]. This is

in line with our results where the employment of erlotinib during SOF treatment prevented the activation of EGFR signalling as well as the expression of its downstream targets cyclin D1 and B-MYB. As a consequence, cell cycle progression and proliferation were supressed and apoptosis was induced [157]. Interestingly, recent studies documented HCV-induced epigenetic changes which persisted even after DAA-mediated viral clearance [56,185]. One of these studies suggested EGFR as a driver of these epigenetic signatures. Indeed, the inhibition of EGFR by erlotinib reverted epigenetic changes and decreased the level of epigenetic marker H3K9Ac [185]. Importantly, erlotinib can inhibit HCV infection as it has been first shown by the successful reduction of HCV infection in human liver chimeric mice [178]. Notably, one case report showed that erlotinib administrated as monotherapy led to a rapid virological response in a patient with diagnosed HCC [186]. On that account, a clinical trial (NCT01835938) for the treatment of chronic HCV infection with erlotinib was initiated. However, due to the enormous success of DAA therapy it has been discontinued. Even though erlotinib showed rather modest benefits in the treatment of advanced HCC, it could be a suitable option for supplementing DAA therapy in patients with high risk of HCC development [187]. Moreover, a new generation of EGFR inhibitors with a favourable safety profile has been introduced into clinical use. Therefore, further research should evaluate the possibility of repurposing this class of drugs for HCV therapy and for HCC prevention in high-risk patients.

3.3 SARS-CoV-2 infection model

The lack of an effective therapy for COVID-19 has driven many attempts to discover a potent antiviral treatment. Many suggestions were primary based on similarities of SARS-CoV-2 with other coronaviruses or computational modelling without experimental confirmation in infection models [154,188].

In February 2020, we have successfully isolated SARS-CoV-2 isolates from two asymptomatic patients returning from China to Germany. We established and described human colon epithelial carcinoma cell line, Caco-2 cells, as an infection model for SARS-CoV-2 [158,189]. The choice of cell line was based on previous results describing pronounced infection of SARS-CoV in Caco-2 cells [190]. We have confirmed that Caco-2 cells also support lytic infection of SARS-CoV-2 with visible cytopathogenic effect (CPE) [158,189]. Human colon-derived cell line, Caco-2 cells,

may represent a relevant model for studying SARS-CoV-2 infection profile. Even though SARS-CoV-2 causes mainly respiratory infection, a significant number of patients with COVID-19 exhibited signs of enteric infection. Indeed, biopsies from different parts of the gastrointestinal tract of COVID-19 patients showed presence of SARS-CoV-2 antigen [191] and virus replication was demonstrated in primary cultures of intestinal cells [192,193]. Notably, the detection of SARS-CoV-2 RNA in stool despite negative results for respiratory infection implies prolonged gastro-intestinal infection [194].

A cell culture system allowing efficient viral infection with straightforward read-out is highly desirable for high-throughput screening of antiviral substances. The ability of CaCo-2 cells to support rapid viral infection with pronounced CPE enable them for rapid testing of antiviral substances based only on visual assessment of CPE even without any additional tools [158,195]. This allowed us to quickly confirm the antiviral effect of remdesivir as well as show that there is no antiviral activity of darunavir, HIV protease inhibitor, which was suggested for treatment of COVID-19 patients based on *in silico* studies [196]. Moreover, SARS-CoV-2 infected Caco-2 cells provide an optimal platform for high-throughput screening of antiviral drug libraries. As a proof of concept, we performed a screening of library containing 5632 compounds. Out of 5632 compounds, 271 showed inhibition of CPE higher than 70%. The majority of these drugs are in clinical use and could be immediately repurposed for antiviral treatment [197].

3.4 Host-targeted therapy for COVID-19

To yield host targets likely inhibiting SARS-CoV-2 infections, we applied multiplexed enhanced protein dynamics (mePROD) proteomics recently established by Klann and colleagues, to generate a blueprint of host translatome and proteome during the course of infection [158,198].

Proteomics of host and viral translatome revealed that the global cellular protein synthesis underwent only minor attenuation in SARS-CoV-2 infected cells. Furthermore, host proteins with the same elevated amplification profile of translation as viral proteins depicted high enrichment of host translation machinery. Therefore, we tested if translation could represent a target for pharmacological intervention against SARS-CoV-2. On that account we utilized cycloheximide, an inhibitor of translation elongation and emetine, inhibitor of 40S ribosomal subunit, during SARS-CoV-2

infection. Both inhibitors exhibited a strong impact on viral replication with profound inhibitory effect even in low nanomolar concentrations [158]. Additionally, a recent study on protein-protein interaction of SARS-CoV-2 with host cells reported translation as one the most pronounced therapeutic targets. It is worthy to mention that this study included our proteomic data set to confirm the relevance of their interaction map in the context of viral infection [199]. Notably, translation inhibitors have been already shown to be highly potent across several coronaviruses, SARS-CoV and MERS-CoV included [200,201], and are also promising candidates for antitumor therapy [202,203]. Therefore, blocking host translation machinery represents an interesting target for broadly active compounds against coronaviruses.

Another essential pathway for SARS-CoV-2 infection that was identified in our analysis was splicing. Strikingly, the majority of detected components of spliceosome showed increased levels in both translatome and proteome proteomics [158]. The interactions between the coronavirus proteins and splicing factors have been already documented for several members of coronaviruses [204–207]. It has been speculated that components of splicing machinery facilitate replication and transcription of viral RNA and can even functionally substitute each other [208]. Pladienolide B, an inhibitor of SF3B1, effectively blocked SARS-CoV-2 replication in Caco-2 cells. It should be also noted that deregulated RNA splicing may play a role in pathogenesis of acute lung injury and ARDS [209]. Therefore, components of splicing may serve as novel targets for antiviral treatment in respiratory infection with coronaviruses [158].

Since all viruses ultimately depend on the host cell supply of the macromolecules required for their life cycle, they have evolved numerous strategies to reshape cellular metabolism in their favour. Indeed, the major cluster of cellular proteins deregulated during SARS-CoV-2 infection was involved in diverse metabolic pathways. While proteins involved in cholesterol metabolism were rather downregulated, carbon metabolism and nucleic acid metabolic processes were strongly upregulated. On that account, we further determined if the elevated expression of these pathways signals increased sensitivity of SARS-CoV-2 infection to their inhibition [158].

Many viruses increase glucose demand and enhance glycolysis in infected cells. Therefore, an increase in components of glycolysis during SARS-CoV-2 infection could represent a druggable target for antiviral therapy. Blocking viral infection by limiting glycolysis has been previously shown to be effective against herpesviruses, rhinovirus, influenza virus and norovirus [210–213]. On that account, we evaluated the therapeutic effect of 2-deoxy-D-glucose (2-DG), a glucose analogue able to suppress glycolysis

by competitively inhibiting hexokinase 2, against SARS-CoV-2 infection. We confirmed that 2-DG is a potent inhibitor of SARS-CoV-2 infection. Since 2-DG exhibits an inhibitory effect in non-toxic concentration it could represent a novel antiviral strategy for clinical trials. Here we have also highlighted the relevance of the virus-host proteomics for discovering potential therapeutic targets, since the effect of 2-DG has not been previously described for other coronaviruses [195].

Based on the similar abundance of cellular components to viral proteins we also identified pathways involved in nucleic acid metabolism to be increasingly enriched during the course of infection. This could be expected since coronaviruses as well as other RNA viruses rely on cellular biosynthesis of nucleotides. Ribavirin interferes with a synthesis of guanosine nucleotides by an inhibition of an inosine-5′-*monophosphate dehydrogenase* (IMPDH), which negatively affects both RNA and DNA synthesis. Application of ribavirin during SARS-CoV-2 infection resulted in inhibition of CPE at physiological concentrations [158]. Ribavirin is active against a broad spectrum of RNA viruses (HCV, RSV, and influenza virus) [7]. Interestingly, ribavirin displays rather weak activity against SARS-CoV replication [214]. Recently, triple combination of ribavirin with lopinavir-ritonavir and interferon beta-1b was superior to lopinavir-ritonavir alone in treatment of COVID-19 patients [151]. However, if ribavirin can efficiently supress viral replication in COVID-19 patients has yet to be determined in ongoing clinical trials.

Remarkably, we have observed that the host response to viral infection was significantly delayed. In accordance to translatome profile, the antiviral responses causing host-translation shut-off were largely absent [158]. This suggests that SARS-CoV–2 evokes mechanisms to delay or prevent the host cell response. Indeed, *in vitro* as well as *in vivo* analysis of host transcriptional landscape depicted lower antiviral response marked by low IFN-I and IFN-III levels [215]. In part, this can be mediated by PLpro of SARS-CoV-2, which has shown to be responsible for cleavage of ISG15 from interferon responsive factor 3 resulting in reduction of IFN-I responses [216]. Conversely, SARS-CoV-2 seems to be highly sensitive to antiviral activity of exogenous IFNs [217].

Although translatome and proteome proteomics offer a robust assessment of changes in cellular pathways during viral infection, numerous crucial changes involved in infection outcome take place on the level of cell signalling. Building up on our well-established infection model and proteome analysis, we determined changes in the host phospho-protein networks during SARS-CoV-2 infection [195]. Notably, we observed extensive signalling enhancement of the spliceosome components. Together

with a previously observed increase in translation and overall abundance of splicing machinery, our findings further emphasize this pathway as crucial part of SARS-CoV-2 replication and thereby a potential therapeutic target. We made the same observation for glycolysis, where we identified differential post-translational modification of most members of the pentose phosphate and TCA cycle. This further encourages research on utilizing 2-DG as an antiviral strategy against SARS-CoV-2 infection [158,195].

Importantly, we identified an extensive overall increase in phosphorylation of growth factor receptor (GFR) signalling and its downstream pathways [195]. The GFR signalling has been already implicated in SARS-CoV induced fibrosis [218]. However, the role of GFR signalling in SARS-CoV-2 pathogenesis needs to be still elucidated. Host kinases represent druggable targets for therapeutic intervention. On that account, we applied pictilisib and omipalisib, PI3K and dual PI3K/mTOR inhibitors, respectively, which resulted in an effective inhibition of SARS-CoV-2 replication. Additionally, several inhibitors of Raf/Ras/Mek axis showed promising antiviral effects [195]. Notably, in addition to their antiviral effects these inhibitors of cellular pathways may positively influence lung fibrosis.

Taken together, our proteomic analysis provided key insights into host response during SARS-CoV-2 infection. As a proof of concept, we confirmed that targeting of identified host pathways can sufficiently supress viral infection. Furthermore, together with the previous study, our data support host-targeted therapy as part of antiviral strategy to not only supress viral infections but also prevent pathological processes. On that account, our findings can accelerate research on the discovery and development of host-targeted therapy against two viral pathogens which currently greatly challenge global health care and therefore urgently require highly efficient antiviral treatment.

List of abbreviations

(+)ssRNA	Positive-sense single stranded RNA
2019-nCoV	2019 novel coronavirus
2-DG	2-deoxy-D-glucose
3CLpro	3C-like protease
ACE2	Angiotensin-converting enzyme 2
ARDS	Acute respiratory distress syndrome
bat-SL-CoV-ZC45	bat SARS-like coronavirus ZC45
CCR5	C-C chemokine receptor type 5
CD4	Cluster of differentiation 4
CFR	Case fatality rate
COVID-19	Coronavirus disease 2019
CPE	Cytopathogenic effect
CT	Computed tomography
CXCR4	C-X-C chemokine receptor type 4
DAAs	Direct acting antivirals
DNA	Deoxyribonucleic acid
E protein	Envelope protein
ECM	Extracellular matrix
EGFR	Epidermal growth factor receptor
ERK-2	Extracellular signal-regulated kinase 2
FDA	U.S. Food and Drug Administration
GFR	Growth factor receptor
gp41	Glycoprotein 41
h	Hour
HCC	Hepatocellular carcinoma
HBV	Hepatitis B virus
HCV	Hepatitis C virus
HDV	Hepatitis D virus
HIV	Human immunodeficiency virus
HPV	Human papillomavirus

HSCs	Hepatic stellate cells
HTA	Host-targeting antivirals
IFN	Interferon
IMPDH	Inosine-5′-*monophosphate dehydrogenase*
ISG	Interferon-stimulated gene
kb	Kilobase
M protein	Membrane protein
MAPK1	Mitogen-activated protein kinase 1
mePROD	Multiplexed enhanced protein dynamics
MERS-CoV	Middle East respiratory syndrome coronavirus
mil	Million
mRNA	Messenger RNA
mTOR	Mechanistic target of rapamycin
N protein	Nucleocapsid protein
NAs	Nucleoside/nucleotide analogues
NK cells	Natural killer cells
NKG2D	Natural killer group 2 member D
NPIs	Nucleoside/nucleotide polymerase inhibitors
NNPIs	Non-nucleoside/nucleotide polymerase inhibitors
NNRTIs	Non-nucleoside reverse transcriptase inhibitors
NS	Nonstructural protein
nsp	Non-structural protein
NTCP	Sodium taurocholate co-transporting polypeptide
ORFs	Open reading frames
PD-L1	Programmed death-ligand 1
pegIFN-α2	Pegylated interferon alpha 2
PI3K	Phosphoinositide 3-kinase
PLpro	Papain-like protease
pp	Polyprotein
pRb	Retinoblastoma protein
RdRp	RNA-dependent RNA polymerase

RNA	Ribonucleic acid
ROS	Reactive oxygen species
RSV	Respiratory syncytial virus
S protein	Spike protein
SARS-CoV	Severe acute respiratory syndrome coronavirus
SARS-CoV-2	Severe acute respiratory syndrome coronavirus 2
SF3B1	Splicing factor 3B subunit 1
sgRNAs	Subgenomic RNAs
SOF	Sofosbuvir
SVR	Sustained virological response
TCA	Trichloroacetic acid
TGF-β	Transforming growth factor beta
TMPRSS2	Transmembrane serine protease 2
TRIM24	TRIpartite Motif-containing protein 24
TLR	Toll-like-receptor
VariZIG	Varicella zoster immune globulin (human)
VZV	Varicella-zoster virus
WHO	World Health Organization

List of figures

List of tables

List of references

[1] Greenwood B. The contribution of vaccination to global health: Past, present and future. Philos Trans R Soc B Biol Sci 2014;369. doi:10.1098/rstb.2013.0433.

[2] Manns MP, Buti M, Gane E, Pawlotsky JM, Razavi H, Terrault N, et al. Hepatitis C virus infection. Nat Rev Dis Prim 2017;3. doi:10.1038/nrdp.2017.6.

[3] Burton DR. Advancing an HIV vaccine; advancing vaccinology. Nat Rev Immunol 2019;19:77–8. doi:10.1038/s41577-018-0103-6.

[4] Karesh WB, Dobson A, Lloyd-Smith JO, Lubroth J, Dixon MA, Bennett M, et al. Ecology of zoonoses: Natural and unnatural histories. Lancet 2012;380:1936–45. doi:10.1016/S0140-6736(12)61678-X.

[5] Rauch S, Jasny E, Schmidt KE, Petsch B. New vaccine technologies to combat outbreak situations. Front Immunol 2018;9. doi:10.3389/fimmu.2018.01963.

[6] Gillim-Ross L, Subbarao K. Emerging respiratory viruses: Challenges and vaccine strategies. Clin Microbiol Rev 2006;19:614–36. doi:10.1128/CMR.00005-06.

[7] Clercq E de, E. DC. Approved antiviral drugs over the past 50 years. . Clin Microbiol Rev 2016;29:695–747. doi:10.1128/CMR.00102-15.Address.

[8] Scheel TKH, Rice CM. Understanding the hepatitis C virus life cycle paves the way for highly effective therapies. Nat Med 2013;19:837–49. doi:10.1038/nm.3248.

[9] Dimitrov DS. Virus entry: Molecular mechanisms and biomedical applications. Nat Rev Microbiol 2004;2:109–22. doi:10.1038/nrmicro817.

[10] Yamauchi Y, Greber UF. Principles of Virus Uncoating: Cues and the Snooker Ball. Traffic 2016;17:569–92. doi:10.1111/tra.12387.

[11] Novoa RR, Calderita G, Arranz R, Fontana J, Granzow H, Risco C. Virus factories: associations of cell organelles for viral replication and morphogenesis. Biol Cell 2005;97:147–72. doi:10.1042/bc20040058.

[12] Schmid M, Speiseder T, Dobner T, Gonzalez RA. DNA Virus Replication Compartments. J Virol 2014;88:1404–20. doi:10.1128/jvi.02046-13.

[13] Perlmutter JD, Hagan MF. Mechanisms of Virus Assembly. Annu Rev Phys Chem 2015;66:217–39. doi:10.1146/annurev-physchem-040214-121637.

[14] Afdhal N, Zeuzem S, Kwo P, Chojkier M, Gitlin N, Puoti M, et al. Ledipasvir and sofosbuvir for untreated HCV genotype 1 infection. N Engl J Med

2014;370:1889–98. doi:10.1056/NEJMoa1402454.

[15] Kaufmann SHE, Dorhoi A, Hotchkiss RS, Bartenschlager R. Host-directed therapies for bacterial and viral infections. Nat Rev Drug Discov 2018;17:35–56. doi:10.1038/nrd.2017.162.

[16] Lou Z, Sun Y, Rao Z. Current progress in antiviral strategies. Trends Pharmacol Sci 2014;35:86–102. doi:10.1016/j.tips.2013.11.006.

[17] Calleja JL, Crespo J, Rincón D, Ruiz-Antorán B, Fernandez I, Perelló C, et al. Effectiveness, safety and clinical outcomes of direct-acting antiviral therapy in HCV genotype 1 infection: Results from a Spanish real-world cohort. J Hepatol 2017;66:1138–48. doi:10.1016/j.jhep.2017.01.028.

[18] De Clercq E. Antivirals and antiviral strategies. Nat Rev Microbiol 2004;2:704–20. doi:10.1038/nrmicro975.

[19] De Clercq E. Anti-HIV drugs: 25 compounds approved within 25 years after the discovery of HIV. Int J Antimicrob Agents 2009;33:307–20. doi:10.1016/j.ijantimicag.2008.10.010.

[20] Wyles DL, Luetkemeyer AF. Understanding Hepatitis C Virus Drug Resistance: Clinical Implications for Current and Future Regimens. Top Antivir Med 2017;25:103–9.

[21] Piret J, Boivin G. Resistance of herpes simplex viruses to nucleoside analogues: Mechanisms, prevalence, and management. Antimicrob Agents Chemother 2011;55:459–72. doi:10.1128/AAC.00615-10.

[22] Bartlett JG. HIV drug resistance. Infect Dis Clin Pract 2004;12:254–5. doi:10.1097/01.idc.0000130889.35482.ee.

[23] Marsh M, Helenius A. Virus entry: Open sesame. Cell 2006;124:729–40. doi:10.1016/j.cell.2006.02.007.

[24] Kilby JM, Eron JJ. Novel therapies based on mechanisms of HIV-1 cell entry. N Engl J Med 2003;348:2228–38. doi:10.1056/NEJMra022812.

[25] Lalezari JP, Henry K, O'Hearn M, Montaner JSG, Piliero PJ, Trottier B, et al. Enfuvirtide, an HIV-1 Fusion Inhibitor, for Drug-Resistant HIV Infection in North and South America. N Engl J Med 2003;348:2175–85. doi:10.1056/NEJMoa035026.

[26] Wild CT, Shugars DC, Greenwell TK, McDanal CB, Matthews TJ. Peptides corresponding to a predictive α-helical domain of human immunodeficiency virus type 1 gp41 are potent inhibitors of virus infection. Proc Natl Acad Sci U S A 1994;91:9770–4. doi:10.1073/pnas.91.21.9770.

[27] Pelegrin M, Naranjo-Gomez M, Piechaczyk M. Antiviral Monoclonal Antibodies: Can They Be More Than Simple Neutralizing Agents? Trends Microbiol 2015;23:653–65. doi:10.1016/j.tim.2015.07.005.

[28] Wang D, Bayliss S, Meads C. Palivizumab for immunoprophylaxis of respiratory syncytial virus (RSV) bronchiolitis in high-risk infants and young children: A systematic review and additional economic modelling of subgroup analyses. Health Technol Assess (Rockv) 2011;15. doi:10.3310/hta15050.

[29] Marin M. Updated recommendations for use of VariZIG - United States, 2013. Am J Transplant 2013;13:2765–7. doi:10.1111/ajt.12477.

[30] Krammer F, Smith GJD, Fouchier RAM, Peiris M, Kedzierska K, Doherty PC, et al. Influenza. Nat Rev Dis Prim 2018;4:1–21. doi:10.1038/s41572-018-0002-y.

[31] Mar C Del, Doshi P, Hama R, Jones M, Jefferson T, Heneghan C, et al. Neuraminidase inhibitors for influenza complications. Lancet 2014;384:1260–1. doi:10.1016/S0140-6736(14)61706-2.

[32] Sharma A, Gupta SP. Fundamentals of viruses and their proteases. vol. 1. Elsevier Inc.; 2017. doi:10.1016/B978-0-12-809712-0.00001-0.

[33] Raney KD, Sharma SD, Moustafa IM, Cameron CE. Hepatitis C virus non-structural protein 3 (HCV NS3): A multifunctional antiviral target. J Biol Chem 2010;285:22725–31. doi:10.1074/jbc.R110.125294.

[34] Pettit SC, Clemente JC, Jeung JA, Dunn BM, Kaplan AH. Ordered Processing of the Human Immunodeficiency Virus Type 1 GagPol Precursor Is Influenced by the Context of the Embedded Viral Protease. J Virol 2005;79:10601–7. doi:10.1128/jvi.79.16.10601-10607.2005.

[35] Malcolm BA, Liu R, Lahser F, Agrawal S, Belanger B, Butkiewicz N, et al. SCH 503034, a mechanism-based inhibitor of hepatitis C virus NS3 protease, suppresses polyprotein maturation and enhances the antiviral activity of alpha interferon in replicon cells. Antimicrob Agents Chemother 2006;50:1013–20. doi:10.1128/AAC.50.3.1013-1020.2006.

[36] Perni RB, Almquist SJ, Byrn RA, Chandorkar G, Chaturvedi PR, Courtney LF, et al. Preclinical profile of VX-950, a potent, selective, and orally bioavailable inhibitor of hepatitis C virus NS3-4A serine protease. Antimicrob Agents Chemother 2006;50:899–909. doi:10.1128/AAC.50.3.899-909.2006.

[37] Gordon SC, Muir AJ, Lim JK, Pearlman B, Argo CK, Ramani A, et al. Real world experience from HCV-TARGET 2016;62:286–93. doi:10.1016/j.jhep.2014.08.052.Safety.

[38] Pawlotsky JM, Negro F, Aghemo A, Berenguer M, Dalgard O, Dusheiko G, et al. EASL Recommendations on Treatment of Hepatitis C 2018. J Hepatol 2018;69:461–511. doi:10.1016/j.jhep.2018.03.026.

[39] Ghosh AK, Osswald HL, Prato G. Recent Progress in the Development of HIV-1 Protease Inhibitors for the Treatment of HIV/AIDS. J Med Chem 2016;59:5172–208. doi:10.1021/acs.jmedchem.5b01697.

[40] Lv Z, Chu Y, Wang Y. HIV protease inhibitors: A review of molecular selectivity and toxicity. HIV/AIDS - Res Palliat Care 2015;7:95–104. doi:10.2147/HIV.S79956.

[41] Engelman A, Mizuuchi K, Craigie R. HIV-1 DNA integration: Mechanism of viral DNA cleavage and DNA strand transfer. Cell 1991;67:1211–21. doi:10.1016/0092-8674(91)90297-C.

[42] Steigbigel RT, Cooper DA, Kumar PN, Eron JE, Schechter M, Markowitz M, et al. Raltegravir with Optimized Background Therapy for Resistant HIV-1 Infection. N Engl J Med 2008;359:339–54. doi:10.1056/NEJMoa0708975.

[43] Raffi F, Jaeger H, Quiros-Roldan E, Albrecht H, Belonosova E, Gatell JM, et al. Once-daily dolutegravir versus twice-daily raltegravir in antiretroviral-naive adults with HIV-1 infection (SPRING-2 study): 96 week results from a randomised, double-blind, non-inferiority trial. Lancet Infect Dis 2013;13:927–35. doi:10.1016/S1473-3099(13)70257-3.

[44] Wohl DA, Yazdanpanah Y, Baumgarten A, Clarke A, Thompson MA, Brinson C, et al. Bictegravir combined with emtricitabine and tenofovir alafenamide versus dolutegravir, abacavir, and lamivudine for initial treatment of HIV-1 infection: week 96 results from a randomised, double-blind, multicentre, phase 3, non-inferiority trial. Lancet HIV 2019;6:e355–63. doi:10.1016/S2352-3018(19)30077-3.

[45] De Clercq E, Holý A. Case history: Acyclic nucleoside phosphonates: A key class of antiviral drugs. Nat Rev Drug Discov 2005;4:928–40. doi:10.1038/nrd1877.

[46] Jordheim LP, Durantel D, Zoulim F, Dumontet C. Advances in the development of nucleoside and nucleotide analogues for cancer and viral diseases. Nat Rev Drug Discov 2013;12:447–64. doi:10.1038/nrd4010.

[47] De Clercq E. A 40-Year Journey in Search of Selective Antiviral Chemotherapy*. Annu Rev Pharmacol Toxicol 2011;51:1–24. doi:10.1146/annurev-pharmtox-010510-100228.

[48] Feld J. Interferon-Free Strategies with a Nucleoside/Nucleotide Analogue. Semin Liver Dis 2014;34:037–46. doi:10.1055/s-0034-1371009.

[49] Wang M, Ng KKS, Cherney MM, Chan L, Yannopoulos CG, Bedard J, et al. Non-nucleoside analogue inhibitors bind to an allosteric site on HCV NS5B polymerase: Crystal structures and mechanism of inhibition. J Biol Chem 2003;278:9489–95. doi:10.1074/jbc.M209397200.

[50] Poordad F, Hezode C, Trinh R, Kowdley K V., Zeuzem S, Agarwal K, et al. ABT-450/r–Ombitasvir and Dasabuvir with Ribavirin for Hepatitis C with Cirrhosis. N Engl J Med 2014;370:1973–82. doi:10.1056/NEJMoa1402869.

[51] Namasivayam V, Vanangamudi M, Kramer VG, Kurup S, Zhan P, Liu X, et al. The Journey of HIV-1 Non-Nucleoside Reverse Transcriptase Inhibitors (NNRTIs) from Lab to Clinic. J Med Chem 2019;62:4851–83. doi:10.1021/acs.jmedchem.8b00843.

[52] Ahlquist P, Noueiry AO, Lee W-M, Kushner DB, Dye BT. Host Factors in Positive-Strand RNA Virus Genome Replication. J Virol 2011;77:1–8. doi:10.1128/JVI.77.15.8181–8186.2003.

[53] Hsu TH, Spindler KR. Identifying host factors that regulate viral infection. PLoS Pathog 2012;8:3. doi:10.1371/journal.ppat.1002772.

[54] Tan SL, Ganji G, Paeper B, Proll S, Katze MG. Systems biology and the host response to viral infection. Nat Biotechnol 2007;25:1383–9. doi:10.1038/nbt1207-1383.

[55] Reig M, Mariño Z, Perelló C, Iñarrairaegui M, Ribeiro A, Lens S, et al. Unexpected high rate of early tumor recurrence in patients with HCV-related HCC undergoing interferon-free therapy. J Hepatol 2016;65:719–26. doi:10.1016/j.jhep.2016.04.008.

[56] Hamdane N, Jühling F, Crouchet E, El Saghire H, Thumann C, Oudot MA, et al. HCV-Induced Epigenetic Changes Associated With Liver Cancer Risk Persist After Sustained Virologic Response. Gastroenterology 2019;156:2313-2329.e7. doi:10.1053/j.gastro.2019.02.038.

[57] Principi N, Camilloni B, Alunno A, Polinori I, Argentiero A, Esposito S. Drugs for Influenza Treatment: Is There Significant News? Front Med 2019;6:1–7. doi:10.3389/fmed.2019.00109.

[58] Fätkenheuer G, Pozniak AL, Johnson MA, Plettenberg A, Staszewski S, Hoepelman AIM, et al. Efficacy of short-term monotherapy with maraviroc, a new CCR5 antagonist, in patients infected with HIV-1. Nat Med 2005;11:1170–

2. doi:10.1038/nm1319.

[59] Vicenzi E, Liò P, Poli G. The puzzling role of CXCR4 in human immunodeficiency virus infection. Theranostics 2013;3:18–25. doi:10.7150/thno.5392.

[60] Vandekerckhove LPR, Wensing AMJ, Kaiser R, Brun-Vézinet F, Clotet B, De Luca A, et al. European guidelines on the clinical management of HIV-1 tropism testing. Lancet Infect Dis 2011;11:394–407. doi:10.1016/S1473-3099(10)70319-4.

[61] Wedemeyer H, Bogomolov P, Blank A, Allweiss L, Dandri-Petersen M, Bremer B, et al. Final results of a multicenter, open-label phase 2b clinical trial to assess safety and efficacy of Myrcludex B in combination with Tenofovir in patients with chronic HBV/HDV co-infection. J Hepatol 2018;68:S3. doi:10.1016/s0168-8278(18)30224-1.

[62] Bogomolov P, Alexandrov A, Voronkova N, Macievich M, Kokina K, Petrachenkova M, et al. Treatment of chronic hepatitis D with the entry inhibitor myrcludex B: First results of a phase Ib/IIa study. J Hepatol 2016;65:490–8. doi:10.1016/j.jhep.2016.04.016.

[63] Isaacs A, Lindenmann J. Virus interference. I. The interferon. Proc R Soc London Ser B - Biol Sci 1957;147:258–67. doi:10.1098/rspb.1957.0048.

[64] Fensterl V, Chattopadhyay S, Sen GC. No Love Lost Between Viruses and Interferons. Annu Rev Virol 2015;2:549–72. doi:10.1146/annurev-virology-100114-055249.

[65] Mesev E V., LeDesma RA, Ploss A. Decoding type I and III interferon signalling during viral infection. Nat Microbiol 2019;4:914–24. doi:10.1038/s41564-019-0421-x.

[66] Petersen J, Thompson AJ, Levrero M. Aiming for cure in HBV and HDV infection. J Hepatol 2016;65:835–48. doi:10.1016/j.jhep.2016.05.043.

[67] Perrillo R. Benefits and risks of interferon therapy for hepatitis B. Hepatology 2009;49. doi:10.1002/hep.22956.

[68] Suslov A, Wieland S, Menne S. Modulators of innate immunity as novel therapeutics for treatment of chronic hepatitis B. Curr Opin Virol 2018;30:9–17. doi:10.1016/j.coviro.2018.01.008.

[69] Alexopoulou L, Holt AC, Medzhitov R FR. Recognition of double-stranded RNA and activation of NF-kappaB by Toll. Nature 2001;413:732–8.

[70] Schön MP, Schön M. Imiquimod: Mode of action. Br J Dermatol 2007;157:8–

13. doi:10.1111/j.1365-2133.2007.08265.x.
[71] Baltimore D. Expression of animal virus genomes. Bacteriol Rev 1971;35:235–41. doi:10.1128/mmbr.35.3.235-241.1971.
[72] Ahlquist P. Parallels among positive-strand RNA viruses, reverse-transcribing viruses and double-stranded RNA viruses. Nat Rev Microbiol 2006;4:371–82. doi:10.1038/nrmicro1389.
[73] Romero-Brey I, Bartenschlager R. Membranous replication factories induced by plus-strand RNA viruses. vol. 6. 2014. doi:10.3390/v6072826.
[74] Paul D. Architecture and biogenesis of plus-strand RNA virus replication factories. World J Virol 2013;2:32. doi:10.5501/wjv.v2.i2.32.
[75] Comas-Garcia M. Packaging of genomic RNA in positive-sense single-stranded RNA viruses: A complex story. Viruses 2019;11:1–23. doi:10.3390/v11030253.
[76] Choo QL, Kuo G, Weiner AJ, Overby LR, Bradley DW, Houghton M. Isolation of a cDNA clone derived from a blood-borne non-A, non-B viral hepatitis genome. Science (80-) 1989;244:359–62. doi:10.1126/science.2523562.
[77] Oestringer BP, Bolivar JH, Claridge JK, Almanea L, Chipot C, Dehez F, et al. Hepatitis C virus sequence divergence preserves p7 viroporin structural and dynamic features. Sci Rep 2019;9:1–10. doi:10.1038/s41598-019-44413-x.
[78] Dubuisson J, Cosset FL. Virology and cell biology of the hepatitis C virus life cycle - An update. J Hepatol 2014;61:S3–13. doi:10.1016/j.jhep.2014.06.031.
[79] Smith DB, Bukh J, Kuiken C, Muerhoff AS, Rice CM, Stapleton JT, et al. Expanded classification of hepatitis C virus into 7 genotypes and 67 subtypes: Updated criteria and genotype assignment web resource. Hepatology 2014;59:318–27. doi:10.1002/hep.26744.
[80] Global hepatitis report, 2017. Geneva: World Health Organization: 2017.
[81] Di Bisceglie AM. Natural history of hepatitis C: Its impact on clinical management. Hepatology 2000;31:1014–8. doi:10.1053/he.2000.5762.
[82] Spearman CW, Dusheiko GM, Hellard M, Sonderup M. Hepatitis C. Lancet 2019;394:1451–66. doi:10.1016/S0140-6736(19)32320-7.
[83] Paradis V, Mathurin P, Kollinger M, Imbert-Bismut F, Charlotte F, Piton A, et al. In situ detection of lipid peroxidation in chronic hepatitis C: Correlation with pathological features. J Clin Pathol 1997;50:401–6. doi:10.1136/jcp.50.5.401.
[84] Fujita N, Horiike S, Sugimoto R, Tanaka H, Iwasa M, Kobayashi Y, et al. Hepatic oxidative DNA damage correlates with iron overload in chronic

hepatitis C patients. Free Radic Biol Med 2007;42:353–62. doi:10.1016/j.freeradbiomed.2006.11.001.

[85] Lee UE, Friedman SL. Mechanisms of hepatic fibrogenesis. Best Pract Res Clin Gastroenterol 2011;25:195–206. doi:10.1016/j.bpg.2011.02.005.

[86] Arzumanyan A, Reis HMGPV, Feitelson MA. Pathogenic mechanisms in HBV- and HCV-associated hepatocellular carcinoma. Nat Rev Cancer 2013;13:123–35. doi:10.1038/nrc3449.

[87] Lupberger J, Croonenborghs T, Roca Suarez AA, Van Renne N, Jühling F, Oudot MA, et al. Combined Analysis of Metabolomes, Proteomes, and Transcriptomes of Hepatitis C Virus–Infected Cells and Liver to Identify Pathways Associated With Disease Development. Gastroenterology 2019;157:537-551.e9. doi:10.1053/j.gastro.2019.04.003.

[88] Arima N, Kao CY, Licht T, Padmanabhan R, Sasaguri Y, Padmanabhan R. Modulation of Cell Growth by the Hepatitis C Virus Nonstructural Protein NS5A. J Biol Chem 2001;276:12675–84. doi:10.1074/jbc.M008329200.

[89] Fukutomi T, Zhou Y, Kawai S, Eguchi H, Wands JR, Li J. Hepatitis C virus core protein stimulates hepatocyte growth: Correlation with upregulation of wnt-1 expression. Hepatology 2005;41:1096–105. doi:10.1002/hep.20668.

[90] Street A, Macdonald A, Crowder K, Harris M. The Hepatitis C Virus NS5A Protein Activates a Phosphoinositide 3-Kinase-dependent Survival Signaling Cascade. J Biol Chem 2004;279:12232–41. doi:10.1074/jbc.M312245200.

[91] Zemel R, Gerechet S, Greif H, Bachmatove L, Birk Y, Golan-Goldhirsh A, et al. Cell transformation induced by hepatitis C virus NS3 serine protease. J Viral Hepat 2001;8:96–102. doi:10.1046/j.1365-2893.2001.00283.x.

[92] Munakata T, Nakamura M, Liang Y, Li K, Lemon SM. Down-regulation of the retinoblastoma tumor suppressor by the hepatitis C virus NS5B RNA-dependent RNA polymerase. Proc Natl Acad Sci U S A 2005;102:18159–64. doi:10.1073/pnas.0505605102.

[93] Deng L, Nagano-Fujii M, Tanaka M, Nomura-Takigawa Y, Ikeda M, Kato N, et al. NS3 protein of hepatitis C virus associates with the tumour suppressor p53 and inhibits its function in an NS3 sequence-dependent manner. J Gen Virol 2006;87:1703–13. doi:10.1099/vir.0.81735-0.

[94] Kao CF, Chen SY, Chen JY, Lee YHW. Modulation of p53 transcription regulatory activity and post-translational modification by hepatitis C virus core protein. Oncogene 2004;23:2472–83. doi:10.1038/sj.onc.1207368.

[95] Battaglia S, Benzoubir N, Nobilet S, Charneau P, Samuel D, Zignego AL, et al. Liver cancer-derived hepatitis C virus core proteins shift TGF-beta responses from tumor suppression to epithelial-mesenchymal transition. PLoS One 2009;4. doi:10.1371/journal.pone.0004355.

[96] Chen C-H, Yu M-L. Evolution of Interferon-Based Therapy for Chronic Hepatitis C. Hepat Res Treat 2010;2010:1–12. doi:10.1155/2010/140953.

[97] Zeuzem S, Welsch C, Herrmann E. Pharmacokinetics of peginterferons. Semin Liver Dis 2003;23:23–8. doi:10.1055/s-2003-41631.

[98] Fried MW, Shiffman ML, Reddy KR, Smith C, Marinos G, Gonçales FL, et al. Peginterferon Alfa-2a plus Ribavirin for Chronic Hepatitis C Virus Infection. N Engl J Med 2002;347:975–82. doi:10.1056/NEJMoa020047.

[99] Lindsay KL, Trepo C, Heintges T, Shiffman ML, Gordon SC, Hoefs JC, et al. A randomized, double-blind trial comparing pegylated interferon alfa-2b to interferon alfa-2b as initial treatment for chronic hepatitis C. Hepatology 2001;34:395–403. doi:10.1053/jhep.2001.26371.

[100] Bukh J. The history of hepatitis C virus (HCV): Basic research reveals unique features in phylogeny, evolution and the viral life cycle with new perspectives for epidemic control. J Hepatol 2016;65:S2–21. doi:10.1016/j.jhep.2016.07.035.

[101] Lohmann V, Körner F, Koch JO, Herian U, Theilmann L, Bartenschlager R. Replication of subgenomic hepatitis C virus RNAs in a hepatoma cell line. Science (80-) 1999;285:110–3. doi:10.1126/science.285.5424.110.

[102] Wakita T, Pietschmann T, Kato T, Date T, Miyamoto M, Zhao Z, et al. Production of infectious hepatitis C virus in tissue culture from a cloned viral genome. Nat Med 2005;11:791–6. doi:10.1038/nm1268.

[103] Poordad F, Schiff ER, Vierling JM, Landis C, Fontana RJ, Yang R, et al. Daclatasvir with sofosbuvir and ribavirin for hepatitis C virus infection with advanced cirrhosis or post-liver transplantation recurrence. Hepatology 2016;63:1493–505. doi:10.1002/hep.28446.

[104] Bourlière M, Gordon SC, Flamm SL, Cooper CL, Ramji A, Tong M, et al. Sofosbuvir, velpatasvir, and voxilaprevir for previously treated HCV infection. N Engl J Med 2017;376:2134–46. doi:10.1056/NEJMoa1613512.

[105] Zeuzem S, Foster GR, Wang S, Asatryan A, Gane E, Feld JJ, et al. Glecaprevir-pibrentasvir for 8 or 12 weeks in HCV genotype 1 or 3 infection. N Engl J Med 2018;378:354–69. doi:10.1056/NEJMoa1702417.

[106] McGivern DR, Masaki T, Lovell W, Hamlett C, Saalau-Bethell S, Graham B. Protease Inhibitors Block Multiple Functions of the NS3/4A Protease-Helicase during the Hepatitis C Virus Life Cycle. J Virol 2015;89:5362–70. doi:10.1128/jvi.03188-14.

[107] Fridell RA, Qiu D, Valera L, Wang C, Rose RE, Gao M. Distinct Functions of NS5A in Hepatitis C Virus RNA Replication Uncovered by Studies with the NS5A Inhibitor BMS-790052. J Virol 2011;85:7312–20. doi:10.1128/jvi.00253-11.

[108] Tellinghuisen TL, Foss KL, Treadaway J. Regulation of hepatitis C virion production via phosphorylation of the NS5A protein. PLoS Pathog 2008;4. doi:10.1371/journal.ppat.1000032.

[109] Ouzan D, Larrey D, Guyader D, Remy AJ, Riachi G, Heluwaert F, et al. Evolution of Hepatitis C Virus Treatment During the Era of Sofosbuvir-Based Therapies: A Real-World Experience in France. Dig Dis Sci 2020. doi:10.1007/s10620-020-06234-1.

[110] Law M. Hepatitis C Virus Protocols. vol. 1911. New York, NY: Springer New York; 2019. doi:10.1007/978-1-4939-8976-8.

[111] Abozeid M, Alsebaey A, Abdelsameea E, Othman W, Elhelbawy M, Rgab A, et al. High efficacy of generic and brand direct acting antivirals in treatment of chronic hepatitis C. Int J Infect Dis 2018;75:109–14. doi:10.1016/j.ijid.2018.07.025.

[112] Bruggmann P, Berg T, Øvrehus ALH, Moreno C, Brandão Mello CE, Roudot-Thoraval F, et al. Historical epidemiology of hepatitis C virus (HCV) in selected countries. J Viral Hepat 2014;21:5–33. doi:10.1111/jvh.12247.

[113] Forner A, Reig M, Bruix J. Hepatocellular carcinoma. Lancet 2018;391:1301–14. doi:10.1109/FCS.2017.8088863.

[114] Bartenschlager R, Baumert TF, Bukh J, Houghton M, Lemon SM, Lindenbach BD, et al. Critical challenges and emerging opportunities in hepatitis C virus research in an era of potent antiviral therapy: Considerations for scientists and funding agencies. Virus Res 2018;248:53–62. doi:10.1016/j.virusres.2018.02.016.

[115] Baumert TF, Jühling F, Ono A, Hoshida Y. Hepatitis C-related hepatocellular carcinoma in the era of new generation antivirals. BMC Med 2017;15:1–10. doi:10.1186/s12916-017-0815-7.

[116] Zhu N, Zhang D, Wang W, Li X, Yang B, Song J, et al. A Novel Coronavirus

from Patients with Pneumonia in China, 2019. N Engl J Med 2020:1–7. doi:10.1056/NEJMoa2001017.

[117] Gorbalenya AE, Baker SC, Baric RS, de Groot RJ, Drosten C, Gulyaeva AA, et al. The species Severe acute respiratory syndrome-related coronavirus: classifying 2019-nCoV and naming it SARS-CoV-2. Nat Microbiol 2020;5:536–44. doi:10.1038/s41564-020-0695-z.

[118] Dong E, Du H, Gardner L. An interactive web-based dashboard to track COVID-19 in real time. Lancet Infect Dis 2020;20:533–4. doi:10.1016/S1473-3099(20)30120-1.

[119] Kim JM, Chung YS, Jo HJ, Lee NJ, Kim MS, Woo SH, et al. Identification of coronavirus isolated from a patient in Korea with covid-19. Osong Public Heal Res Perspect 2020;11:3–7. doi:10.24171/j.phrp.2020.11.1.02.

[120] Chan JFW, Yuan S, Kok KH, To KKW, Chu H, Yang J, et al. A familial cluster of pneumonia associated with the 2019 novel coronavirus indicating person-to-person transmission: a study of a family cluster. Lancet 2020;395:514–23. doi:10.1016/S0140-6736(20)30154-9.

[121] Zhang T, Wu Q, Zhang Z. Probable Pangolin Origin of SARS-CoV-2 Associated with the COVID-19 Outbreak. Curr Biol 2020;30:1346-1351.e2. doi:10.1016/j.cub.2020.03.022.

[122] Andersen KG, Rambaut A, Lipkin WI, Holmes EC, Garry RF. The proximal origin of SARS-CoV-2. Nat Med 2020;26:450–2. doi:10.1038/s41591-020-0820-9.

[123] Zhang YZ, Holmes EC. A Genomic Perspective on the Origin and Emergence of SARS-CoV-2. Cell 2020;181:223–7. doi:10.1016/j.cell.2020.03.035.

[124] Snijder EJ, Decroly E, Ziebuhr J. The Nonstructural Proteins Directing Coronavirus RNA Synthesis and Processing. Adv. Virus Res., vol. 96. 1st ed., Elsevier Inc.; 2016, p. 59–126. doi:10.1016/bs.aivir.2016.08.008.

[125] De Wit E, Van Doremalen N, Falzarano D, Munster VJ. SARS and MERS: Recent insights into emerging coronaviruses. Nat Rev Microbiol 2016;14:523–34. doi:10.1038/nrmicro.2016.81.

[126] Gao Y, Yan L, Huang Y, Liu F, Zhao Y, Cao L, et al. Structure of the RNA-dependent RNA polymerase from COVID-19 virus. Science (80-) 2020;782:eabb7498. doi:10.1126/science.abb7498.

[127] Kim D, Lee JY, Yang JS, Kim JW, Kim VN, Chang H. The Architecture of SARS-CoV-2 Transcriptome. Cell 2020;181:914-921.e10.

doi:10.1016/j.cell.2020.04.011.

[128] Wrapp D, Wang N, Corbett KS, Goldsmith JA, Hsieh CL, Abiona O, et al. Cryo-EM structure of the 2019-nCoV spike in the prefusion conformation. Science (80-) 2020;367:1260–3. doi:10.1126/science.aax0902.

[129] Letko M, Marzi A, Munster V. Functional assessment of cell entry and receptor usage for SARS-CoV-2 and other lineage B betacoronaviruses. Nat Microbiol 2020;5:562–9. doi:10.1038/s41564-020-0688-y.

[130] Hoffmann M, Kleine-Weber H, Schroeder S, Krüger N, Herrler T, Erichsen S, et al. SARS-CoV-2 Cell Entry Depends on ACE2 and TMPRSS2 and Is Blocked by a Clinically Proven Protease Inhibitor. Cell 2020;181:271-280.e8. doi:10.1016/j.cell.2020.02.052.

[131] Li Q, Guan X, Wu P, Wang X, Zhou L, Tong Y, et al. Early transmission dynamics in Wuhan, China, of novel coronavirus-infected pneumonia. N Engl J Med 2020;382:1199–207. doi:10.1056/NEJMoa2001316.

[132] Wu P, Hao X, Lau EHY, Wong JY, Leung KSM, Wu JT, et al. Real-time tentative assessment of the epidemiological characteristics of novel coronavirus infections in Wuhan, China, as at 22 January 2020. Eurosurveillance 2020;25:1–6. doi:10.2807/1560-7917.ES.2020.25.3.2000044.

[133] Huang C, Wang Y, Li X, Ren L, Zhao J, Hu Y, et al. Clinical features of patients infected with 2019 novel coronavirus in Wuhan, China. Lancet 2020;395:497–506. doi:10.1016/S0140-6736(20)30183-5.

[134] Xu Z, Shi L, Wang Y, Zhang J, Huang L, Zhang C, et al. Pathological findings of COVID-19 associated with acute respiratory distress syndrome. Lancet Respir Med 2020;8:420–2. doi:10.1016/S2213-2600(20)30076-X.

[135] Tian S, Hu W, Niu L, Liu H, Xu H, Xiao SY. Pulmonary Pathology of Early-Phase 2019 Novel Coronavirus (COVID-19) Pneumonia in Two Patients With Lung Cancer. J Thorac Oncol 2020;15:700–4. doi:10.1016/j.jtho.2020.02.010.

[136] Chen N, Zhou M, Dong X, Qu J, Gong F, Han Y, et al. Epidemiological and clinical characteristics of 99 cases of 2019 novel coronavirus pneumonia in Wuhan, China: a descriptive study. Lancet 2020;395:507–13. doi:10.1016/S0140-6736(20)30211-7.

[137] Peiris JSM, Chu CM, Cheng VCC, Chan KS, Hung IFN, Poon LLM, et al. Clinical progression and viral load in a community outbreak of coronavirus-associated SARS pneumonia: A prospective study. Lancet 2003;361:1767–72. doi:10.1016/S0140-6736(03)13412-5.

[138] Poutanen SM, Low DE, Henry B, Finkelstein S, Rose D, Green K, et al. Identification of severe acute respiratory syndrome in Canada. N Engl J Med 2003;348:1995–2005. doi:10.1056/NEJMoa030634.

[139] Assiri A, Al-Tawfiq JA, Al-Rabeeah AA, Al-Rabiah FA, Al-Hajjar S, Al-Barrak A, et al. Epidemiological, demographic, and clinical characteristics of 47 cases of Middle East respiratory syndrome coronavirus disease from Saudi Arabia: A descriptive study. Lancet Infect Dis 2013;13:752–61. doi:10.1016/S1473-3099(13)70204-4.

[140] Al-Abdallat MM, Payne DC, Alqasrawi S, Rha B, Tohme RA, Abedi GR, et al. Hospital-associated outbreak of middle east respiratory syndrome coronavirus: A serologic, epidemiologic, and clinical description. Clin Infect Dis 2014;59:1225–33. doi:10.1093/cid/ciu359.

[141] Aylward, Bruce (WHO); Liang W (PRC). Report of the WHO-China Joint Mission on Coronavirus Disease 2019 (COVID-19). WHO 2020;2019:16–24.

[142] WHO. Consensus document on the epidemiology of severe acute respiratory syndrome (SARS). WHO 2003.

[143] Sai JK, Suyama M, Kubokawa Y, Matsumura Y, Inami K, Watanabe S. Efficacy of camostat mesilate against dyspepsia associated with non-alcoholic mild pancreatic disease. J Gastroenterol 2010;45:335–41. doi:10.1007/s00535-009-0148-1.

[144] Hirota M, Shimosegawa T, Kitamura K, Takeda K, Takeyama Y, Mayumi T, et al. Continuous regional arterial infusion versus intravenous administration of the protease inhibitor nafamostat mesilate for predicted severe acute pancreatitis: a multicenter, randomized, open-label, phase 2 trial. J Gastroenterol 2020;55:342–52. doi:10.1007/s00535-019-01644-z.

[145] Wang M, Cao R, Zhang L, Yang X, Liu J, Xu M, et al. Remdesivir and chloroquine effectively inhibit the recently emerged novel coronavirus (2019-nCoV) in vitro. Cell Res 2020;30:269–71. doi:10.1038/s41422-020-0282-0.

[146] Liu J, Cao R, Xu M, Wang X, Zhang H, Hu H, et al. Hydroxychloroquine, a less toxic derivative of chloroquine, is effective in inhibiting SARS-CoV-2 infection in vitro. Cell Discov 2020;6:6–9. doi:10.1038/s41421-020-0156-0.

[147] Devaux CA, Rolain JM, Colson P, Raoult D. New insights on the antiviral effects of chloroquine against coronavirus: what to expect for COVID-19? Int J Antimicrob Agents 2020;55. doi:10.1016/j.ijantimicag.2020.105938.

[148] Geleris J, Sun Y, Platt J, Zucker J, Baldwin M, Hripcsak G, et al. Observational

Study of Hydroxychloroquine in Hospitalized Patients with Covid-19. N Engl J Med 2020:1–8. doi:10.1056/NEJMoa2012410.

[149] De Wilde AH, Jochmans D, Posthuma CC, Zevenhoven-Dobbe JC, Van Nieuwkoop S, Bestebroer TM, et al. Screening of an FDA-approved compound library identifies four small-molecule inhibitors of Middle East respiratory syndrome coronavirus replication in cell culture. Antimicrob Agents Chemother 2014;58:4875–84. doi:10.1128/AAC.03011-14.

[150] Yao TT, Qian JD, Zhu WY, Wang Y, Wang GQ. A systematic review of lopinavir therapy for SARS coronavirus and MERS coronavirus—A possible reference for coronavirus disease-19 treatment option. J Med Virol 2020;92:556–63. doi:10.1002/jmv.25729.

[151] Cao B, Wang Y, Wen D, Liu W, Wang J, Fan G, et al. A Trial of Lopinavir-Ritonavir in Adults Hospitalized with Severe Covid-19. N Engl J Med 2020:1787–99. doi:10.1056/NEJMoa2001282.

[152] Siegel D, Hui HC, Doerffler E, Clarke MO, Chun K, Zhang L, et al. Discovery and Synthesis of a Phosphoramidate Prodrug of a Pyrrolo[2,1-f][triazin-4-amino] Adenine C-Nucleoside (GS-5734) for the Treatment of Ebola and Emerging Viruses. J Med Chem 2017;60:1648–61. doi:10.1021/acs.jmedchem.6b01594.

[153] Holshue ML, DeBolt C, Lindquist S, Lofy KH, Wiesman J, Bruce H, et al. First case of 2019 novel coronavirus in the United States. N Engl J Med 2020;382:929–36. doi:10.1056/NEJMoa2001191.

[154] Li G, De Clercq E. Therapeutic options for the 2019 novel coronavirus (2019-nCoV). Nat Rev Drug Discov 2020;19:149–50. doi:10.1038/d41573-020-00016-0.

[155] Shiraki K, Daikoku T. Favipiravir, an anti-influenza drug against life-threatening RNA virus infections. Pharmacol Ther 2020;209:107512. doi:10.1016/j.pharmthera.2020.107512.

[156] Rossignol JF. Nitazoxanide, a new drug candidate for the treatment of Middle East respiratory syndrome coronavirus. J Infect Public Health 2016;9:227–30. doi:10.1016/j.jiph.2016.04.001.

[157] Bojkova D, Westhaus S, Costa R, Timmer L, Funkenberg N, Korencak M, et al. Sofosbuvir Activates EGFR-Dependent Pathways in Hepatoma Cells with Implications for Liver-Related Pathological Processes. Cells 2020;9:1–18. doi:10.3390/cells9041003.

[158] Bojkova D, Klann K, Koch B, Widera M, Krause D, Ciesek S, et al. Proteomics of SARS-CoV-2-infected host cells reveals therapy targets. Nature 2020. doi:10.1038/s41586-020-2332-7.

[159] Conti F, Buonfiglioli F, Scuteri A, Crespi C, Bolondi L, Caraceni P, et al. Early occurrence and recurrence of hepatocellular carcinoma in HCV-related cirrhosis treated with direct-acting antivirals. J Hepatol 2016;65:727–33. doi:10.1016/j.jhep.2016.06.015.

[160] Bernstein WB, Dennis PA. Repositioning HIV protease inhibitors as cancer therapeutics. Curr Opin HIV AIDS 2008;3:666–75. doi:10.1097/COH.0b013e328313915d.

[161] De La Cruz-Hernandez E, Medina-Franco JL, Trujillo J, Chavez-Blanco A, Dominguez-Gomez G, Perez-Cardenas E, et al. Ribavirin as a tri-targeted antitumor repositioned drug. Oncol Rep 2015;33:2384–92. doi:10.3892/or.2015.3816.

[162] Meissner EG, Kohli A, Virtaneva K, Sturdevant D, Martens C, Porcella SF, et al. Achieving sustained virologic response after interferon-free hepatitis C virus treatment correlates with hepatic interferon gene expression changes independent of cirrhosis. J Viral Hepat 2016;23:496–505. doi:10.1111/jvh.12510.

[163] Wee P, Wang Z. Epidermal growth factor receptor cell proliferation signaling pathways. Cancers (Basel) 2017;9:1–45. doi:10.3390/cancers9050052.

[164] Lv D, Li Y, Zhang W, Alvarez AA, Song L, Tang J, et al. TRIM24 is an oncogenic transcriptional co-activator of STAT3 in glioblastoma. Nat Commun 2017;8. doi:10.1038/s41467-017-01731-w.

[165] Yamauchi T, Ueki K, Tobe K, Tamemoto H, Sekine N, Wada M, et al. Tyrosine phosphorylation of the EGF receptor by the kinase Jak2 is induced by growth hormone. Nature 1997;390:91–6. doi:10.1038/36369.

[166] Jiang XW, Ye JZ, Li YT, Li LJ. Hepatitis B reactivation in patients receiving direct-acting antiviral therapy or interferon-based therapy for hepatitis C: A systematic review and meta-analysis. World J Gastroenterol 2018;24:3181–91. doi:10.3748/wjg.v24.i28.3181.

[167] Chen G, Wang C, Chen J, Ji D, Wang Y, Wu V, et al. Hepatitis B reactivation in hepatitis B and C coinfected patients treated with antiviral agents: A systematic review and meta-analysis. Hepatology 2017;66:13–26. doi:10.1002/hep.29109.

[168] Perelló M. C, Fernández-Carrillo C, Londoño MC, Arias-Loste T, Hernández-

Conde M, Llerena S, et al. Reactivation of Herpesvirus in Patients With Hepatitis C Treated With Direct-Acting Antiviral Agents. Clin Gastroenterol Hepatol 2016;14:1662-1666.e1. doi:10.1016/j.cgh.2016.05.016.

[169] Meissner EG, Wu D, Osinusi A, Bon D, Virtaneva K, Sturdevant D, et al. Endogenous intrahepatic IFNs and association with IFN-free HCV treatment outcome. J Clin Invest 2014;124:3352–63. doi:10.1172/JCI75938.

[170] Serti E, Chepa-Lotrea X, Kim YJ, Keane M, Fryzek N, Liang TJ, et al. Successful Interferon-Free Therapy of Chronic Hepatitis C Virus Infection Normalizes Natural Killer Cell Function. Gastroenterology 2015;149:190-200.e2. doi:10.1053/j.gastro.2015.03.004.

[171] Chu P sung, Nakamoto N, Taniki N, Ojiro K, Amiya T, Makita Y, et al. On-treatment decrease of NKG2D correlates to early emergence of clinically evident hepatocellular carcinoma after interferon-free therapy for chronic hepatitis C. PLoS One 2017;12:1–20. doi:10.1371/journal.pone.0179096.

[172] Vantourout P, Willcox C, Turner A, Swanson CM, Haque Y, Sobolev O, et al. Immunological visibility: Posttranscriptional regulation of human NKG2D ligands by the EGF receptor pathway. Sci Transl Med 2014;6:1–14. doi:10.1126/scitranslmed.3007579.

[173] Groh V, Wu J, Yee C, Spies T. Tumour-derived soluble MIC ligands impair expression of NKG2D and T-cell activation. Nature 2002;419:734–8. doi:10.1038/nature01112.

[174] Jinushi M, Takehara T, Tatsumi T, Hiramatsu N, Sakamori R, Yamaguchi S, et al. Impairment of natural killer cell and dendritic cell functions by the soluble form of MHC class I-related chain A in advanced human hepatocellular carcinomas. J Hepatol 2005;43:1013–20. doi:10.1016/j.jhep.2005.05.026.

[175] Pinato DJ, Guerra N, Fessas P, Murphy R, Mineo T, Mauri FA, et al. Immune-based therapies for hepatocellular carcinoma. Oncogene 2020;39:3620–37. doi:10.1038/s41388-020-1249-9.

[176] Aydin Y, Chatterjee A, Chandra PK, Chava S, Chen W, Tandon A, et al. Interferon-alpha-induced hepatitis C virus clearance restores p53 tumor suppressor more than direct-acting antivirals. Hepatol Commun 2017;1:256–69. doi:10.1002/hep4.1025.

[177] El-Serag HB, Kanwal F, Richardson P, Kramer J. Risk of hepatocellular carcinoma after sustained virological response in Veterans with hepatitis C virus infection. Hepatology 2016;64:130–7. doi:10.1002/hep.28535.

[178] Lupberger J, Zeisel MB, Xiao F, Thumann C, Fofana I, Zona L, et al. EGFR and EphA2 are host factors for hepatitis C virus entry and possible targets for antiviral therapy. Nat Med 2011;17:589–95. doi:10.1038/nm.2341.

[179] Zona L, Lupberger J, Sidahmed-Adrar N, Thumann C, Harris HJ, Barnes A, et al. HRas signal transduction promotes hepatitis C virus cell entry by triggering assembly of the host tetraspanin receptor complex. Cell Host Microbe 2013;13:302–13. doi:10.1016/j.chom.2013.02.006.

[180] Baktash Y, Madhav A, Coller KE, Randall G. Single Particle Imaging of Polarized Hepatoma Organoids upon Hepatitis C Virus Infection Reveals an Ordered and Sequential Entry Process. Cell Host Microbe 2018;23:382-394.e5. doi:10.1016/j.chom.2018.02.005.

[181] Diao J, Pantua H, Ngu H, Komuves L, Diehl L, Schaefer G, et al. Hepatitis C Virus Induces Epidermal Growth Factor Receptor Activation via CD81 Binding for Viral Internalization and Entry. J Virol 2012;86:10935–49. doi:10.1128/JVI.00750-12.

[182] Mankouri J, Griffin S, Harris M. The hepatitis C virus non-structural protein NS5A alters the trafficking profile of the epidermal growth factor receptor. Traffic 2008;9:1497–509. doi:10.1111/j.1600-0854.2008.00779.x.

[183] Igloi Z, Kazlauskas A, Saksela K, MacDonald A, Mankouri J, Harris M. Hepatitis C virus NS5A protein blocks epidermal growth factor receptor degradation via a proline motif- dependent interaction. J Gen Virol 2015;96:2133–44. doi:10.1099/vir.0.000145.

[184] Fuchs BC, Hoshida Y, Fujii T, Wei L, Yamada S, Lauwers GY, et al. Epidermal growth factor receptor inhibition attenuates liver fibrosis and development of hepatocellular carcinoma. Hepatology 2014;59:1577–90. doi:10.1002/hep.26898.

[185] Perez S, Kaspi A, Domovitz T, Davidovich A, Lavi-Itzkovitz A, Meirson T, et al. Hepatitis C virus leaves an epigenetic signature post cure of infection by direct-acting antivirals. PLOS Genet 2019;15:e1008181. doi:10.1371/journal.pgen.1008181.

[186] Bardou-Jacquet E, Lorho R, Guyader D. Kinase inhibitors in the treatment of chronic hepatitis C virus. Gut 2011;60:879–80. doi:10.1136/gut.2010.212068.

[187] Thomas MB, Chadha R, Glover K, Wang X, Morris J, Brown T, et al. Phase 2 study of erlotinib in patients with unresectable hepatocellular carcinoma. Cancer 2007;110:1059–67. doi:10.1002/cncr.22886.

[188] Wang J. Fast Identification of Possible Drug Treatment of Coronavirus Disease -19 (COVID-19) Through Computational Drug Repurposing Study. J Chem Inf Model 2020;19. doi:10.1021/acs.jcim.0c00179.

[189] Hoehl S, Rabenau H, Berger A, Kortenbusch M, Cinatl J, Bojkova D, et al. Evidence of SARS-CoV-2 infection in returning travelers from Wuhan, China. N Engl J Med 2020;382:1278–80. doi:10.1056/NEJMc2001899.

[190] Cinatl J, Hoever G, Morgenstern B, Preiser W, Vogel JU, Hofmann WK, et al. Infection of cultured intestinal epithelial cells with severe acute respiratory syndrome coronavirus. Cell Mol Life Sci 2004;61:2100–12. doi:10.1007/s00018-004-4222-9.

[191] Xiao F, Tang M, Zheng X, Liu Y, Li X, Shan H. Evidence for Gastrointestinal Infection of SARS-CoV-2. Gastroenterology 2020;158:1831-1833.e3. doi:10.1053/j.gastro.2020.02.055.

[192] Zhou J, Li C, Liu X, Chiu MC, Zhao X, Wang D, et al. Infection of bat and human intestinal organoids by SARS-CoV-2. Nat Med 2020. doi:10.1038/s41591-020-0912-6.

[193] Lamers MM, Beumer J, van der Vaart J, Knoops K, Puschhof J, Breugem TI, et al. SARS-CoV-2 productively infects human gut enterocytes. Science (80-) 2020;1669:eabc1669. doi:10.1126/science.abc1669.

[194] Wang X, Zhou Y, Jiang N, Zhou Q, Ma WL. Persistence of intestinal SARS-CoV-2 infection in patients with COVID-19 leads to re-admission after pneumonia resolved. Int J Infect Dis 2020;95:433–5. doi:10.1016/j.ijid.2020.04.063.

[195] Klann K, Bojkova D, Tascher G, Ciesek S, Münch C. Growth factor receptor signaling inhibition prevents SARS- CoV-2 replication 2020. doi:10.1101/2020.05.14.095661.

[196] De Meyer S, Bojkova D, Cinatl J, Van Damme E, Meng CB, Van Loock M, et al. Lack of Antiviral Activity of Darunavir against SARS-CoV-2. Int J Infect Dis 2020. doi:10.1016/j.ijid.2020.05.085.

[197] Ellinger B. Identification of inhibitors of SARS-CoV-2 in-vitro cellular toxicity in human (Caco-2) cells using a large scale drug repurposing collection 2020:1–19. doi:10.21203/RS.3.RS-23951/V1.

[198] Klann K, Tascher G, Münch C. Functional Translatome Proteomics Reveal Converging and Dose-Dependent Regulation by mTORC1 and eIF2α. Mol Cell 2019:1–13. doi:10.1016/j.molcel.2019.11.010.

[199] Gordon DE, Jang GM, Bouhaddou M, Xu J, Obernier K, White KM, et al. A SARS-CoV-2 protein interaction map reveals targets for drug repurposing. Nature 2020:1–13. doi:10.1038/s41586-020-2286-9.

[200] Dyall J, Coleman CM, Hart BJ, Venkataraman T, Holbrook MR, Kindrachuk J, et al. Repurposing of clinically developed drugs for treatment of Middle East respiratory syndrome coronavirus infection. Antimicrob Agents Chemother 2014;58:4885–93. doi:10.1128/AAC.03036-14.

[201] Nordor A V., Siwo GH. Predicting Broad-Spectrum Antiviral Drugs against RNA Viruses Using Transcriptional Responses to Exogenous RNA. Preprints 2020:1–20. doi:10.20944/PREPRINTS202003.0437.V1.

[202] Deng C, Lipstein MR, Scotto L, Jirau Serrano XO, Mangone MA, Li S, et al. Silencing c-Myc translation as a therapeutic strategy through targeting PI3Kδ and CK1ε in hematological malignancies. Blood 2017;129:88–99. doi:10.1182/blood-2016-08-731240.

[203] Wang L, Gundelach JH, Bram RJ. Cycloheximide promotes paraptosis induced by inhibition of cyclophilins in glioblastoma multiforme. Cell Death Dis 2017;8:e2807. doi:10.1038/cddis.2017.217.

[204] Emmott E, Munday D, Bickerton E, Britton P, Rodgers MA, Whitehouse A, et al. The Cellular Interactome of the Coronavirus Infectious Bronchitis Virus Nucleocapsid Protein and Functional Implications for Virus Biology. J Virol 2013;87:9486–500. doi:10.1128/jvi.00321-13.

[205] Jourdan SS, Osorio F, Hiscox JA. An interactome map of the nucleocapsid protein from a highly pathogenic North American porcine reproductive and respiratory syndrome virus strain generated using SILAC-based quantitative proteomics. Proteomics 2012;12:1015–23. doi:10.1002/pmic.201100469.

[206] Choi KS, Mizutani A, Lai MMC. SYNCRIP, a Member of the Heterogeneous Nuclear Ribonucleoprotein Family, Is Involved in Mouse Hepatitis Virus RNA Synthesis. J Virol 2004;78:13153–62. doi:10.1128/jvi.78.23.13153-13162.2004.

[207] Luo H, Chen Q, Chen J, Chen K, Shen X, Jiang H. The nucleocapsid protein of SARS coronavirus has a high binding affinity to the human cellular heterogeneous nuclear ribonucleoprotein A1. FEBS Lett 2005;579:2623–8. doi:10.1016/j.febslet.2005.03.080.

[208] Shi ST, Yu G-Y, Lai MMC. Multiple Type A/B Heterogeneous Nuclear Ribonucleoproteins (hnRNPs) Can Replace hnRNP A1 in Mouse Hepatitis Virus RNA Synthesis. J Virol 2003;77:10584–93. doi:10.1128/jvi.77.19.10584-

10593.2003.

[209] Mascarenhas JB, Tchourbanov AY, Danilov SM, Zhou T, Wang T, Garcia JGN. The splicing factor hnRNPA1 regulates alternate splicing of the MYLK gene. Am J Respir Cell Mol Biol 2018;58:604–13. doi:10.1165/rcmb.2017-0141OC.

[210] McArdle J, Schafer XL, Munger J. Inhibition of Calmodulin-Dependent Kinase Kinase Blocks Human Cytomegalovirus-Induced Glycolytic Activation and Severely Attenuates Production of Viral Progeny. J Virol 2011;85:705–14. doi:10.1128/jvi.01557-10.

[211] Gualdoni GA, Mayer KA, Kapsch AM, Kreuzberg K, Puck A, Kienzl P, et al. Rhinovirus induces an anabolic reprogramming in host cell metabolism essential for viral replication. Proc Natl Acad Sci U S A 2018;115:E7158–65. doi:10.1073/pnas.1800525115.

[212] Kilbourne ED. Inhibition of Influenza Virus Multiplication with a Glucose Antimetabolite (2-deoxy-D-glucose). Nature 1959;183:271–2. doi:10.1038/183271b0.

[213] Passalacqua KD, Lu J, Goodfellow I, Kolawole AO, Arche JR, Maddox RJ, et al. Glycolysis is an intrinsic factor for optimal replication of a norovirus. MBio 2019;10:1–18. doi:10.1128/mBio.02175-18.

[214] Cinatl J, Morgenstern B, Bauer G, Chandra P, Rabenau H, Doerr HW. Glycyrrhizin, an active component of liquorice roots, and replication of SARS-associated coronavirus. Lancet 2003;361:2045–6. doi:10.1016/S0140-6736(03)13615-X.

[215] Blanco-Melo D, Nilsson-Payant BE, Liu WC, Uhl S, Hoagland D, Møller R, et al. Imbalanced Host Response to SARS-CoV-2 Drives Development of COVID-19. Cell 2020;181:1036-1045.e9. doi:10.1016/j.cell.2020.04.026.

[216] Donghyuk S, Mukherjee R, Grewe D, Bojkova D, Baek K, Anshu B, et al. Inhibition of papain-like protease PLpro blocks SARS- CoV-2 spread and promotes anti-viral immunity n.d. doi:10.21203/rs.3.rs-27134/v1.

[217] Mantlo E, Bukreyeva N, Maruyama J, Paessler S, Huang C. Antiviral activities of type I interferons to SARS-CoV-2 infection. Antiviral Res 2020;179:104811. doi:10.1016/j.antiviral.2020.104811.

[218] Venkataraman T, Frieman MB. The role of epidermal growth factor receptor (EGFR) signaling in SARS coronavirus-induced pulmonary fibrosis. Antiviral Res 2017;143:142–50. doi:10.1016/j.antiviral.2017.03.022.

Acknowledgments

I would like to thank my supervisor Prof. Dr. Sandra Ciesek for the opportunity to be part of her research group. I am very grateful for her guidance to find my path in research, her patience and kindness through these times.

I would like to acknowledge Prof. Dr. Jindrich Cinatl for his mentoring, advices and all the effort he puts into each project. His hard work is a great inspiration for me.

I would like to thank Dr. Christian Münch, Kevin Klann and Benjamin Koch for their great effort and devotion to accomplish our goals.

To my dear colleague, Sandra,
I could not have wished for a better lab-mate, officemate and occasional roommate. Thank you for everything!

To my long-lost brother, my karaoke partner and my best man, Rui,
thank you!

To Lejla, Benny, Tanja, Candy Andy, Michael, Nicola, Marek and all the other amazing colleagues in Essen and Frankfurt, who helped me, cheered me up and shared all the ups and downs, one big thank you!

To my family and friends in Slovakia and also to my new family and friends in Germany, thank you for all your love and support, you make my life much better!

To my favourite person in the world and my partner in crime, Anna,
I would need to write another dissertation to express how thankful I am to you,
or I will just tell you at home.
Thank you for everything!

Curriculum vitae

The curriculum vitae is not included in the online version for data protection reasons.

Declarations

Declaration:

In accordance with § 6 (para. 2, clause g) of the Regulations Governing the Doctoral Proceedings of the Faculty of Biology for awarding the doctoral degree Dr. rer. nat., I hereby declare that I represent the field to which the topic "Development of antiviral strategies against positive-sense single stranded RNA viruses" is assigned in research and teaching and that I support the application of Denisa Bojkova.

Essen, _____ Prof. Dr. Sandra Ciesek _____

Name of the scientific supervisor/member of the University of Duisburg-Essen

Signature of the supervisor/ member of the University of Duisburg-Essen

Declaration:

In accordance with § 7 (para. 2, clause d and f) of the Regulations Governing the Doctoral Proceedings of the Faculty of Biology for awarding the doctoral degree Dr. rer. nat., I hereby declare that I have written the herewith submitted dissertation independently using only the materials listed, and have cited all sources taken over verbatim or in content as such.

Essen, 8.6.2020 _____

Signature of the doctoral candidate

Declaration:

In accordance with § 7 (para. 2, clause e and g) of the Regulations Governing the Doctoral Proceedings of the Faculty of Biology for awarding the doctoral degree Dr. rer. nat., I hereby declare that I have undertaken no previous attempts to attain a doctoral degree, that the current work has not been rejected by any other faculty, and that I am submitting the dissertation only in this procedure.

Essen, 8.6.2020 _____

Signature of the doctoral candidate